Biological Production Rates in the Southern California Current System

David Russel Munro

A dissertation submitted

in partial fulfillment of the

requirements for the degree of

Doctor of Philosophy

University of Washington

2012

Reading Committee:

Paul D. Quay (Chair)

Allan H. Devol

Steven R. Emerson

Program Authorized to Offer Degree:

School of Oceanography

University of Washington

Abstract

Biological Production Rates in the Southern California Current System

David Russel Munro

Chair of the Supervisory Committee:

Professor Paul D. Quay

School of Oceanography

The isotopic composition of dissolved O_2 ($^{17}\Delta$) and the biological O_2 saturation from O_2:Ar ratios were measured in the surface ocean during six cruises off the coast of Southern California from November 2005 to August 2008 to determine rates of gross oxygen production (GOP), net oxygen production (NOP), and the NOP:GOP ratio (a measure of potential export efficiency). $^{17}\Delta$-GOP and O_2:Ar-NOP estimates were compared to on-deck incubation-based ^{14}C-primary production (^{14}C-PP) and satellite-based PP algorithms for the CalCOFI region. $^{17}\Delta$-GOP estimates were consistently greater than bottle ^{14}C-PP by a factor of 5.6±0.4 and greater than satellite PP estimates by a factor of 3.5±0.3 (mmol O_2:mmol C). The $^{17}\Delta$-GOP to ^{14}C-PP factor was twice the expected factor of 2.7 determined from comparisons of incubation-based ^{18}O-GOP and ^{14}C-PP. The annual mean NOP:GOP ratio was 0.16±0.06 suggesting a potential export efficiency that is surprisingly similar to the open ocean using comparable methods.

The consistent relationship between biological O_2 saturation derived from O_2:Ar dissolved gas ratio measurements and routinely measured O_2 saturation allows estimation of historical potential net community production (NCP) rates from the multi-decadal CalCOFI dataset. NCP rates were also estimated using a nitrate budget approach; historic f-ratio measurements for different regions of the CalCOFI grid coupled with ^{14}C-PP; and the Vertically Generalized Productivity Model (VGPM) of Behrenfeld and Falkowski (1997) coupled with two commonly used export ratio algorithms. The time series of NCP estimates show lower NCP in response to strong El Niño events but an insignificant response to weak El Niño events. NCP estimates show no significant response to La Niña events. Since 2007, all estimates show increases in NCP which correspond to anomalously cool conditions in the northeast Pacific Ocean and stronger equatorward flow in the California Current.

Table of Contents

List of Figures

List of Tables

Dedication

To Val

For supporting and believing in me.

Acknowledgements

I would like to thank my advisor, Paul Quay, for all of his guidance and patience during my time as a graduate student. I am indebted to all of the members of Paul's Stable Isotope Lab who's time at the University of Washington overlapped with mine including Laurie Juranek, Deirdre Lockwood, Hilary Palevsky, Mark Haught, Johnny Stutsman, Dave Wilbur, Cynthia Peacock, and Jackie Leung who all made important contributions to this work. I would like to thank the members of my doctoral committee including Paul, Al Devol, Steve Emerson, Barbara Hickey, and Daniel Schindler for providing valuable guidance; I am especially grateful for the feedback provided by the members of my reading committee, Paul, Al, and Steve, who dramatically improved this thesis.

I would like to acknowledge all technicians and participants in the California Cooperative Oceanic Fisheries Investigations (CalCOFI) program especially David Wolgast and James Wilkinson whose dedication and skill made this work possible and Ralf Goericke who invited my participation in the CalCOFI program. I also thank the captains and crews of the R/V *New Horizon*, R/V *Roger Revelle*, and R/V *David Starr Jordan* for their assistance at sea. Suzanne Dickinson and Kathie Kelly of the Applied Physics Laboratory at the University of Washington processed Quick Scatterometer (QuikSCAT) wind data and computed wind stress for estimates presented in this thesis. This work was supported by a University of Washington Program on Climate Change Graduate Fellowship, a National Defense Science and Engineering Graduate Fellowship, and a NASA Space Grant Fellowship.

Most importantly, I want to thank my friends and family who supported me throughout my graduate career.

Chapter 1: The importance of biological production and carbon cycling in the coastal ocean and overview of research

1.1 Background

The coastal oceans are important both in terms of their contribution to the global carbon cycle and because high biological production in these regions support fisheries which represent a vital fraction of global food supply. Large-scale estimates of coastal carbon fluxes are complicated by the extreme spatial and temporal heterogeneity of coastal environments to such a degree that at present it isn't known whether the coastal seas collectively represent a net source or sink of carbon dioxide to the modern atmosphere (Hales et al. 2008). Accurate estimates of biological production are essential to understanding controls on variability in carbon fluxes between the ocean and atmosphere and between the surface and deep ocean. Understanding relationships between biological production and carbon fluxes will in turn improve predictions of how coastal ecosystems will respond to future climate change.

While satellite-based productivity algorithms provide unmatched spatial and temporal coverage, validation of algorithms with in situ primary production (PP) measurements is essential but lacking for many ocean regions. To date most in situ PP estimates in the coastal ocean have been based on a single method, the ^{14}C incubation approach (^{14}C-PP) (Steemann Nielsen 1952). Because every method for measuring aquatic PP comes with substantial caveats and no benchmark PP standard exists, it is important that validation of satellite-based PP algorithms be performed with multiple PP methods. Together, the $^{17}\Delta$ approach for estimating gross O_2 production ($^{17}\Delta$-GOP) (Luz and Barkan 2000) and the O_2:Ar approach for estimating net O_2 production (O_2:Ar-NOP) (Craig and Hayward 1987; Emerson et al. 1997) provide

significant advantages over traditional incubation-based PP methods in that these estimates are based on in situ measurements and not rates measured inside a bottle. Additionally, the $^{17}\Delta$-GOP and O_2:Ar methods require much less effort at sea than incubation methods allowing for much greater spatial and temporal coverage in dynamic coastal regions.

Eastern Boundary Current (EBC) systems such as the California Current System (CCS) are among the most productive coastal ecosystems; the four major EBC's account for 35% of global wild fish catch despite covering just 1% of the ocean surface area (Kudela et al. 2008). Several studies have suggested that the carbon cycling and ecosystem dynamics in the southern CCS are sensitive to well-known modes of climate variability including the El Niño-Southern Oscillation (ENSO) (Kahru et al. 2002; Chavez et al. 2003), the Pacific Decadal Oscillation (PDO) (Mantua et al. 1997; Chhak and Di Lorenzo 2007), and the North Pacific Gyre Oscillation (NPGO) (Di Lorenzo et al. 2008). The California Cooperative Oceanic Fisheries Investigations (CalCOFI) represents one of the longest coastal time series in existence and provides an excellent opportunity to compare $^{17}\Delta$-GOP and O_2:Ar-NOP estimates to other productivity estimates including ^{14}C-PP. This time series also provides an unparalleled record of interannual variability in biological productivity which can provide some insight into how future climate variability may impact coastal ecosystems.

1.2 Overview of research

The subsequent chapters of this thesis describe application of the $^{17}\Delta$-GOP and O_2:Ar methods at CalCOFI and an analysis of interannual variability in export production in the southern CCS from 1984-2010. Chapter 2 has been submitted for publication in the form

presented here and Chapter 3 will be submitted for publication in a form similar to that presented here.

In Chapter 2 I describe application of the $^{17}\Delta$-GOP and O_2:Ar-NOP methods to the southern CCS based on $^{17}\Delta$ and O_2:Ar measurements collected during six CalCOFI cruises from November 2005 to August 2008. This work represents the most comprehensive application of the $^{17}\Delta$-GOP and O_2:Ar methods in an EBC setting to date (Juranek et al. 2013). $^{17}\Delta$-GOP and O_2:Ar-NOP estimates are compared to traditional incubation-based and satellite-based estimates; the implications of these production estimates to the carbon cycling and ecosystem dynamics of the southern CCS are discussed.

In Chapter 3 I estimate export production using several different approaches for the period from 1984-2010 including an O_2-based estimate which utilizes the consistent relationship between routinely measured O_2 saturation and biological O_2 saturation derived from O_2:Ar measurements observed during five CalCOFI cruises from April 2006 to August 2008. In addition, export production is estimated using a nitrate budget approach, a combination of incubation-based estimates of PP and new production, and two satellite-based approaches. Differences between these estimates and their relationship to well-known indices of climate variability are discussed.

In Chapter 4 I provide a discussion of the advantages and disadvantages of the $^{17}\Delta$ and O_2:Ar methods for estimating biological productivity in the coastal ocean, a summary of all significant conclusions from the research and analysis presented in Chapters 2 and 3, and a description of future work and analysis to be completed.

Chapter 2: Biological production rates off the Southern California coast estimated from triple O_2 isotopes and O_2:Ar gas ratios

2.1 Introduction

The rate of aquatic primary production (PP) is of fundamental importance to understanding of ocean ecosystems, marine biogeochemical cycling, and predictions of how ocean ecosystems will respond to climate change. While satellite sensors and algorithms provide quantitative estimates of ocean chlorophyll and PP at spatial and temporal resolution not achievable with ship-based methods, satellite-based global PP estimates differ by a factor of two and divergence between methods is particularly great in high chlorophyll regions such as the continental margins (Carr et al. 2006). Ultimately, the test of satellite-based PP methods is validation by direct observation. Unfortunately, there is no absolute method to measure aquatic PP, leading to considerable debate regarding the accuracy and interpretation of available PP methods.

Since its introduction over five decades ago, the ^{14}C incubation approach (^{14}C-PP) (Steemann Nielsen 1952) has been the most widely-used PP method in oceanography. The enormous dataset of ^{14}C-PP measurements has contributed greatly to our understanding of oceanic productivity, but fundamental questions remain with regard to its accuracy (Marra 2002). The ^{14}C-PP method, like most PP methods, is an in vitro approach and as such there is inherent uncertainty as to whether rates determined inside a bottle accurately reflect in situ rates. Other specific methodological concerns include differences between on-deck and in situ bottle incubations, duration of incubation (generally 6 to 24 h), recycling of respired CO_2, recycling of labeled organic material, and production of labeled (unmeasured) dissolved organic carbon

(DOC) (Marra 2002). Direct comparisons with O_2-based in vitro approaches including ^{18}O incubations and O_2 light and dark incubations have helped address some of the ^{14}C-PP measurement ambiguity such that under most conditions 24 h ^{14}C-PP incubations are assumed to represent net primary production (NPP) which is also the parameter estimated by satellite-based approaches (Marra 2002). Bottle effects during incubation have been impossible to quantify because of a lack of a PP reference standard.

The triple O_2 isotope method for measuring aquatic gross O_2 production ($^{17}\Delta$-GOP) is based on precise measurement of the natural ^{17}O:^{16}O and ^{18}O:^{16}O ratios of mixed layer dissolved O_2 (Luz and Barkan 2000). The $^{17}\Delta$-GOP method provides several key advantages over traditional PP methods. First, it is based on a mixed layer O_2 budget, and is not an incubation-based approach, thus avoiding the unknowns inherent to in vitro methodologies. Second, very little sample processing is required aboard ship which greatly expands measurement capability. Third, the $^{17}\Delta$-GOP method integrates over the residence time of O_2 in the mixed layer (typically one week in the coastal ocean) which increases the chances of capturing productivity events missed by short-duration incubation experiments. Finally, measurement of the ratio of dissolved O_2 and Ar gases (O_2:Ar) made on the same sample provides a contemporaneous estimate of net O_2 production (NOP), which yields a rate of net carbon production (NCP) which integrates both particulate organic carbon (POC) export and net DOC production. Combining $^{17}\Delta_{diss}$ and O_2:Ar measurements provides a non-incubation-based measure of potential export efficiency (NOP:GOP), where both numerator and denominator are integrated over the same timescale and measured in terms of O_2.

The disadvantages of the $^{17}\Delta$-GOP method include significant uncertainty in GOP estimates due to uncertainty in the gas exchange parameterization and $^{17}\Delta$ measurement

precision. In some situations, the mixed layer budget must include terms for horizontal advection, vertical advection, and mixed layer deepening (i.e., entrainment). The $^{17}\Delta$-GOP and O_2:Ar-NOP methods integrate through the mixed layer and can miss a significant fraction of the productivity when the mixed layer depth is substantially shallower than the photic zone (Luz and Barkan 2009). Another caveat is the ambiguity in relating photosynthetic O_2 production to carbon fixation (Zehr and Kudela 2009). Because all available PP methods come with significant limitations, we emphasize the importance of applying multiple PP methods to a given study region to more accurately characterize PP variability.

Several previous studies have employed the $^{17}\Delta$-GOP method in open ocean environments, including at the Bermuda Atlantic Time-Series (BATS) (Luz and Barkan 2000, 2009), the Hawaii Ocean Time-Series (HOT) (Juranek and Quay 2005; Quay et al. 2010), the subtropical North and South Pacific (Juranek and Quay 2010), the subarctic North Pacific (Juranek et al. 2012), the equatorial Pacific (Hendricks et al. 2005; Juranek and Quay 2010; Stanley et al. 2010), the subarctic North Atlantic (Quay et al. 2012), and the Southern Ocean (Hendricks et al. 2004; Reuer et al. 2007; Hamme et al. 2012). The only previous studies to employ the $^{17}\Delta$-GOP method in the coastal ocean were conducted in Sagami Bay off the coast of Japan (Sarma et al. 2005, 2006, 2008).

Eastern Boundary Current (EBC) systems such as the California Current System (CCS) are among the most biologically productive oceanic environments, accounting for 35% of global annual wild fish catch despite covering just 1% of the ocean surface area (Kudela et al. 2008). Coastal regions, generally, are important for the export of biologically-fixed carbon to the deep ocean and sediments; recent estimates suggest that 30-50% of global carbon export may occur in along continental margins (Laws et al. 2000; Muller-Karger et al. 2005; Dunne et al. 2007). The

CCS is highly sensitive to climate variability with recent studies demonstrating significant physical and ecological responses to both the El Niño-Southern Oscillation (ENSO) (Kahru et al. 2002; Chavez et al. 2003) and the Pacific Decadal Oscillation (PDO) (Mantua et al. 1997; Chhak and Di Lorenzo 2007). Potential effects of future climate change have been hypothesized including intensification of coastal upwelling in response to increased upwelling-favorable wind stress (Bakun 1990; Snyder et al. 2003) and increased stratification associated with surface warming (Di Lorenzo et al. 2005). Over the past decade, PP in the CCS and other EBC systems appears to be increasing (Kahru and Mitchell 2008; Kahru et al. 2009) accompanied in many regions by decreasing O_2 concentrations at depth (Bograd et al. 2008). Clearly, accurate PP measurements are critical to understanding links between PP, climate variability, air-sea CO_2 flux, hypoxia, and productivity at higher trophic levels.

The California Cooperative Oceanic Fisheries Investigations (CalCOFI) program was initiated in 1949 in response to the collapse of the sardine fishery and is one of the longest running oceanographic sampling programs in existence. ^{14}C-PP measurements began in 1984 and represent one of the most extensive oceanic PP datasets available. The CalCOFI program provides an excellent setting in which to apply the $^{17}\Delta$-GOP method because of the opportunity for direct comparison with ^{14}C-PP and regional satellite-based PP estimates (Mitchell and Kahru 1998; Kahru et al. 2009).

The objectives of this study are 1) to determine seasonal and spatial variability in PP and NCP in the CCS using two non-incubation methods ($^{17}\Delta$-GOP and O_2:Ar-NOP), 2) to compare $^{17}\Delta$-GOP and O_2:Ar-NOP estimates with concurrent ^{14}C-PP and satellite-based PP estimates, and 3) to determine variability in the potential export ratio, NOP:GOP, independent of incubation methods. This study represents the most extensive application of the $^{17}\Delta$-GOP and O_2:Ar-NOP

methods in an EBC system to date.

2.2 Methods

Study area

The CalCOFI grid, currently includes 75 stations spread over 6 lines perpendicular to the Southern California coast extending southwest from Point Arguello to San Diego (Fig. 2.1). Station spacing ranges from less than 20 km close to shore to approximately 75 km offshore. Cruises are conducted quarterly (typically in January, April, July or August, and October or November). Individual stations are typically referred to by a line and station number (e.g., 77.100 represents station 100, the outermost station, on line 77, the northernmost line).

Samples for O_2 isotopes and O_2:Ar were collected during six CalCOFI cruises from November 2005 to August 2008. We refer to each cruise using the standard CalCOFI notation, whereby the first two digits refer to the year, the third and fourth digits refer to the month, and the succeeding letters refer to the research vessel (i.e., 0511NH refers to a cruise of the R/V *New Horizon* in November 2005; other vessels include the R/V *Roger Revelle* and the R/V *David Starr Jordan*). We group stations into four regions based on physical setting and historical productivity rates (Fig. 2.1). The North Inshore region (Region 1) encompasses the high historical PP rates associated with the persistent upwelling feature off Point Conception. The South Inshore region (Region 2) includes the Southern California Bight (SCB) which has markedly lower productivity in comparison to other regions inshore of the California Current along the West Coast (Eppley 1992). The California Current region (Region 3) is distinguished by high equatorward transport via the California Current. The Offshore region (Region 4) has historical productivity rates that approach those of the oligotrophic subtropical North Pacific.

$^{17}\Delta$-GOP, O_2:Ar-NCP, and NOP:GOP methods

The details of the $^{17}\Delta$-GOP method have been described previously (Luz and Barkan 2000; Hendricks et al. 2004; Juranek and Quay 2005) and only the fundamentals of the method are summarized here. The method is based on a small but measureable isotopic anomaly which differentiates atmospheric O_2 from O_2 produced during photosynthesis. The O_2 isotopic anomaly is expressed using $^{17}\Delta$ notation (Luz and Barkan 2000; Miller 2002; Angert et al. 2003):

$$^{17}\Delta = (\ln[\delta^{17}O/1000 + 1] - 0.518\times\ln[\delta^{18}O/1000 +1])\times10^6 \quad (1)$$

where $\delta^{17}O$ and $\delta^{18}O$ (in ‰) represents $(R_{sample}/R_{standard} - 1)\times1000$ and R = ^{17}O:^{16}O or ^{18}O:^{16}O for O_2. The value of 0.518 represents the ratio of ^{17}O to ^{18}O fractionation for respiration empirically measured for plankton, microbes, and plants (Luz and Barkan 2005). $^{17}\Delta$ is reported in units of per meg (10^6) rather than per mil relative to atmospheric O_2 (0 per meg). The $^{17}\Delta$ of dissolved O_2 in seawater ($^{17}\Delta_{diss}$) ranges from close to the atmospheric end member to 249±15 per meg for purely photosynthetic O_2 ($^{17}\Delta_p$) on the high end (Luz and Barkan 2000). The $^{17}\Delta$ of atmospheric O_2 dissolved in seawater ($^{17}\Delta_{eq}$) is temperature dependent and has been estimated empirically by Luz and Barkan (2009) ($^{17}\Delta_{eq} = 0.6\times t + 1.8$) where t is temperature in °C.

$^{17}\Delta_{diss}$ is thus a direct measure of the proportion of photosynthetic versus atmospheric O_2. To calculate the GOP rate from measured $^{17}\Delta_{diss}$ requires setting up mixed layer O_2 budgets for each isotopologue of O_2 (mass 32, 33, and 34) as described by Hendricks et al. (2004). Assuming steady state, an equation for GOP integrated through the mixed layer can be derived (Luz and Barkan 2000):

$$GOP = K_g \times C_{sat} \times ({}^{17}\Delta_{diss} - {}^{17}\Delta_{eq}) / ({}^{17}\Delta_{p} - {}^{17}\Delta_{diss}) \quad (2)$$

where K_g (m d^{-1}) is the gas transfer velocity based on an empirically determined function of wind speed specific to O_2, and C_{sat} (mmol m^{-3}) is the concentration of O_2 at saturation. Eq. 2 can be modified to include advective transport terms in regions where horizontal or vertical advection rates are high and/or horizontal or vertical ${}^{17}\Delta_{diss}$ gradients are large (e.g., as done for the equatorial Pacific by Hendricks et al. (2005) and Juranek and Quay (2010), or during periods of mixed layer deepening when subsurface water with high ${}^{17}\Delta_{diss}$ is entrained into the mixed layer (Quay et al. 2010).

Since Ar acts as a biologically inert analog for O_2, the dissolved O_2:Ar gas ratio divided by the O_2:Ar ratio expected at equilibrium with air gives a measure of biological O_2 saturation (i.e., $[O_2:Ar]_{meas} / [O_2:Ar]_{sat}$) (Craig and Hayward 1987). Mixed layer steady state O_2 and Ar budgets have been used to derive an expression for NOP (Emerson et al. 1997):

$$NOP = K_g \times C_{sat} \times ([(O_2:Ar)_{meas} / (O_2:Ar)_{sat}] - 1) \quad (3)$$

where $(O_2:Ar)_{sat}$ depends on measured temperature and salinity (Garcia and Gordon 1992; Hamme and Emerson 2004). This expression, like Eq. 2, ignores advective transport terms.

The NOP:GOP ratio, a measure of biological production efficiency, results from the combination of Eqs. 2 and 3 to yield:

$$NOP:GOP = ([(O_2:Ar)_{meas} / (O_2:Ar)_{sat}] - 1) \times ({}^{17}\Delta_{diss} - {}^{17}\Delta_{p}) / ({}^{17}\Delta_{eq} - {}^{17}\Delta_{diss}) \quad (4)$$

again assuming steady state and ignoring advective terms. Importantly, NOP:GOP is essentially independent of gas exchange and its associated uncertainty. In addition, both numerator and denominator are measured in units of O_2 and integrated over the same time period, avoiding the uncertainty of converting measurements in different units that integrate over different time and space scales.

GOP and NOP including advection

Mixed layer budgets for the two stable isotopologues of O_2 of interest (i.e., $^{16}O^{17}O$ and $^{16}O^{18}O$) are constructed following Hendricks et al. (2004):

$$h\times d(C_{ml}\times X_{ml})/dt = GOP\times X_p - R\times\alpha_r\times X_{ml} + K_g\times\alpha_g(C_{sat}\times X_{air}\times\alpha_{sol} - C_{ml}\times X_{ml}) + h\times(u/L_x)\times(C_x\times X_x - C_{ml}\times X_{ml}) + h\times(v/L_y)\times(C_y\times X_y - C_{ml}\times X_{ml}) + w\times(C_z\times X_z - C_{ml}\times X_{ml}) \quad (5)$$

where h (m) is the mixed layer depth; R is the respiration rate (mmol O_2 m^{-2} d^{-1}); u and v represent zonal and alongshore velocities (m d^{-1}); w represents upwelling rate (m d^{-1}); C_{ml} represents the mixed layer O_2 concentration (mmol O_2 m^{-3}); C_x and C_y represent the upstream O_2 concentrations for zonal and alongshore transports (mmol O_2 m^{-3}); C_z represents the O_2 concentration below the mixed layer (mmol O_2 m^{-3}); L_x and L_y represent the horizontal length scales over which the gradients in O_2 are considered (m); X_{ml} represents the isotope ratio ^{17}O:^{16}O or ^{18}O:^{16}O of mixed layer O_2; X_p represents the isotopic composition of photosynthetic O_2; X_x, X_y, and X_z represent the isotopic composition of upstream O_2 and O_2 below the mixed layer; α_r

and α_g represent the kinetic fractionation effects due to respiration and gas exchange, respectively, and α_{sol} is the O_2 solubility equilibrium fractionation effect. $d(C_{ml} \times X_{ml})/dt$ is the rate of change for an O_2 isotopologue in the mixed layer (equal to zero at steady state) (mmol O_2 m^{-3} d^{-1}); Horizontal gradients were calculated between the four regions in the CalCOFI grid described above (Fig. 2.1). Combining the equations for $^{16}O^{17}O$ and $^{16}O^{18}O$ expressed in terms of $^{17}\Delta$ and solving for GOP (assuming that respiration has no effect on mixed layer $^{17}\Delta_{diss}$ as discussed above) yields:

$$GOP = [K_g \times C_{sat} \times (^{17}\Delta_{diss} - {}^{17}\Delta_{eq}) + h \times (u/L_x) \times (^{17}\Delta_{diss} - {}^{17}\Delta_x) + h \times (v/L_y) \times (^{17}\Delta_{diss} - {}^{17}\Delta_y) + w \times (^{17}\Delta_z - {}^{17}\Delta_{eq})] / (^{17}\Delta_p - {}^{17}\Delta_{diss}) \quad (6)$$

Recently, the equation to calculate GOP rates from dissolved O_2 isotope measurements has been improved to allow direct calculation from the ^{18}O:^{16}O and ^{17}O:^{16}O ratios rather than in terms of $^{17}\Delta$ (Luz and Barkan 2011; Prokopenko et al. 2011). We use the revised approach outlined by Luz and Barkan (2011) with additional terms for horizontal and vertical advection as included in Eqs. 5 and 6; for this study the revised approach yields GOP rates that are within five percent (for individual regions) of rates calculated using Eq. 6.

Similarly, the expression for NOP can be modified to include horizontal and vertical advection terms as follows:

$$NOP = K_g \times C_{sat} \times ((O_2{:}Ar)_{bio\_ml} - 1) + h \times (u/L_x) \times C_x \times (((O_2{:}Ar)_{bio\_ml} / (O_2{:}Ar)_{bio\_x}) - 1) + h \times (v/L_y) \times C_y \times (((O_2{:}Ar)_{bio\_ml} / (O_2{:}Ar)_{bio\_y}) - 1) +$$

$$w \times C_z \times (((O_2{:}Ar)_{bio\_ml} / (O_2{:}Ar)_{bio\_z}) - 1) \quad (7)$$

where $(O_2{:}Ar)_{bio}$ represents the biological O_2 saturation in the mixed layer (ml) and for water transported zonally (x), alongshore (y), and via upwelling (z).

To determine the likelihood that steady state conditions were met for the GOP and NOP calculation, we compared surface water residence times to the dissolved O_2 residence times in the four regions described above. For all regions the O_2 replenishment time due to air-sea exchange was 4 to 7 days, which was a result of mixed layer depths of 25 to 35 m divided by a K_g of 3 to 6 m d^{-1}. In comparison, for the North Inshore region the average water residence time was 11 days based on an average current velocity of 15 cm s^{-1} calculated from geostrophic and Ekman transports. Similar calculations yielded water residence times of 26, 17, and 26 days for the South Inshore, California Current, and Offshore regions, respectively. For all regions, residence times for water are 2 to 5x greater than residence times for O_2, suggesting that mixed layer O_2, $^{17}\Delta_{diss}$, and O_2:Ar approach a steady state balance between biological production, air-sea gas exchange, and advection within each region.

PP terminology and conversions

The terminology used to describe PP rates can be confusing due in part to differences in what various methods actually measure. For clarity, we define the following terms. Gross O_2 production (GOP) refers to the amount of O_2 production during photosynthesis and is typically expressed as a vertically integrated daily rate (mmol O_2 m^{-2} d^{-1}). GOP can be determined by both $^{17}\Delta$ measurements as reported here, or by $H_2{}^{18}O$ incubation experiments (^{18}O-GOP).

Estimates from two commonly used satellite-based PP models, the Vertically Generalized

Productivity Model (VGPM) (Behrenfeld and Falkowski 1997) and the Carbon based Productivity Model (CbPM) (Westberry et al. 2008) were acquired from the Ocean Productivity Group at Oregon State University (http://web.science.oregonstate.edu/ocean.productivity/custom.php) for comparison to $^{17}\Delta$-GOP and ^{14}C-PP measurements. Although ^{14}C-PP and most satellite methods are assumed to approximate net autotrophic primary production (NPP), we use the method name to define the measured rate (e.g., ^{14}C-PP, VGPM-PP for the Vertically Generalized Productivity Model, and CbPM-PP for the Carbon based Productivity Model). Rates estimated using triple O_2 isotope composition will similarly be defined by $^{17}\Delta$-GOP. Since $^{17}\Delta$-GOP is estimated using a mixed layer budget for O_2 and O_2 isotopologues, we determine the mixed layer fraction of ^{14}C-PP for comparisons between methods. The ^{14}C-PP mixed layer fraction can also be used to extrapolate mixed layer $^{17}\Delta$-GOP estimates to the photic zone, where it exceeds the mixed layer depth (i.e., by dividing mixed layer $^{17}\Delta$-GOP by the mean mixed layer fraction of ^{14}C-PP for each region and cruise).

Lastly, net O_2 production (NOP) equals GOP minus community respiration and at steady state is equal to the amount of PP available for export (mmol O_2 m^{-2} d^{-1}) whether by sinking flux, conversion to dissolved organic matter (DOM), or transfer to higher trophic levels. NOP is converted to net carbon production or NCP (mg C m^{-2} d^{-1}) using a photosynthetic quotient (PQ) for new production of 1.4 (Laws 1991). As mentioned above, our NCP rates integrate both POC export and net DOC production. The NOP:GOP ratio can be related to the ratio of new production to NPP (i.e., the f-ratio) by assuming a photosynthetic quotient of 1.4 for new production and assuming a constant ratio of GOP to NPP of 2.7 as determined from comparisons of ^{14}C-PP and ^{18}O-GOP (Marra 2002).

^{14}C-PP measurement

A detailed sampling procedure for CalCOFI ^{14}C-PP and other hydrographic sampling techniques is described on the CalCOFI website (http://www.calcofi.org/field-program/rosette-sampling.html) and in Mantyla et al. (1995); several important aspects of the procedure are relevant for this study. ^{14}C-PP samples are collected from a mid-morning cast each day at six depths determined by the photic zone depth and depth of the chlorophyll maximum. The deepest ^{14}C-PP depth receives 0.2% to 0.5% of the surface irradiance. Incubations are conducted over half a light cycle from local apparent noon (LAN) to sunset in on-deck incubators cooled with surface seawater and with neutral density screens to simulate in situ light conditions at each depth. Eppley (1992) used comparisons of concurrent ^{14}C-PP$_{24h}$ to half-day ^{14}C-PP$_{6h}$ conducted by CalCOFI and the Southern California Bight (SCB) study to estimate a scaling factor of 1.81 (i.e., multiplying ^{14}C-PP$_{6h}$ by 1.81 provides an estimate of ^{14}C-PP$_{24h}$). ^{14}C-PP rates reported by CalCOFI were multiplied by 1.81 to estimate ^{14}C-PP$_{24h}$ and to provide a more useful comparison with other PP estimates.

Estimating rates of gas exchange and advection

To calculate K_g necessary for GOP and NOP estimates, we used wind speed data (referenced to a height of 10 m) from the SeaWinds instrument on the QuikSCAT satellite processed daily on 0.5° × 0.5° fields. K_g was calculated using the parameterization of Nightingale et al. (2000) which is a mid-range approach compared to parameterizations of Wanninkhof (1992) and Liss and Merlivat (1986) and very similar to the recent parameterization of Ho et al. (2006). The daily weighting approach of Reuer et al. (2007) was used to calculate

averaged K_g values representative of the residence time of O_2 in the mixed layer.

Upwelling due to wind stress curl (curl-driven upwelling) can be comparable to coastal upwelling as a source of nutrients in the CalCOFI region (Rykaczewski and Checkley 2008). QuikSCAT wind stress was calculated using the equations of Large et al. (1994) and used to calculate curl-driven upwelling rates (w_{curl}) for every region sampled for O_2 isotopic composition and O_2:Ar.

Coastal upwelling rates (w_{coast}) for the nearshore regions of Regions 1 and 2 were calculated using the offshore Ekman transport from National Data Buoy Center (NDBC) winds; buoys 46023 and 46063 were used for the North Inshore region and buoy 46025 was used for the South Inshore region. Upwelling rates based on buoy winds agree closely with estimates based on QuikSCAT winds.

Horizontal current velocities were determined from calculations of geostrophic velocities (relative to 500 m) using dynamic height data (http://www.calcofi.org/data/x-btldata.html); surface layer Ekman velocities were calculated from QuikSCAT wind stress. Geostrophic velocities were extrapolated into depths shallower than 500 m using the approach of Reid and Mantyla (1976). A rotated coordinate system was used such that 'u' represents velocity parallel to CalCOFI lines 77 through 93 and 'v' represents velocity perpendicular to the CalCOFI lines (Fig. 2.1).

Sample collection and analytical methods for O_2 isotope and O_2:Ar measurements

Samples for $^{17}\Delta_{diss}$ and O_2:Ar were collected from Niskin bottles within the mixed layer (typically <25 m) at 15 to 50 stations per cruise. Depth profiles (four to seven depths) were collected at three to five stations per cruise to characterize the photic zone and upper aphotic

zone.

For O_2 isotope and O_2:Ar samples, 150 to 250 mL of seawater was collected in preevacuated bottles (300 to 500 mL) poisoned with 200 μL of saturated $HgCl_2$ solution following the protocol of Juranek and Quay (2005). In the lab, samples were equilibrated at room temperature for 12 to 24 h and afterwards seawater was removed by vacuum. After equilibration, samples were typically stored for several weeks (never more than six months) before mass spectrometer analysis. Bottle sidearms were filled with seawater at the time of collection and then with CO_2 after equilibration to limit air contamination.

Mass spectrometer measurement procedure has been described in Juranek and Quay (2005). Internal precision based on standard error of the mean (SEM) of 75 paired measurements is as follows: ±7 per meg for $^{17}\Delta$, 0.003‰ for $\delta^{18}O$, and 0.007‰ for $\delta^{17}O$. $^{17}\Delta_{diss}$ of each sample was corrected for variation in O_2:Ar. Final $^{17}\Delta_{diss}$ and O_2:Ar values are reported versus air using a lab gas standard calibrated daily against air. The overall measurement uncertainty was calculated from 39 replicate sample pairs collected from the same Niskin bottle where the mean standard deviation (SD) for all replicates was ±9 per meg for $^{17}\Delta_{diss}$ and ±0.1% for biological O_2 saturation.

2.3 Results

$^{17}\Delta$-GOP estimates

Mean mixed layer $^{17}\Delta_{diss}$ for each of the four regions calculated for each cruise ranged from 24±3 to 108±12 per meg (Table 2.1) where uncertainty represents the SEM of all mixed layer samples collected in a given region during each cruise. Depth profiles typically show $^{17}\Delta_{diss}$ maxima (up to 139 per meg) beneath the mixed layer within the photic zone that are most

pronounced during summer and fall (Fig. 2.2) in oligotrophic regions of the CalCOFI grid including the Southern California Bight and; in the aphotic zone, $^{17}\Delta_{diss}$ decreases to a mean of 74±13 per meg (n = 5) at 200 to 300 m. Depth profiles for regions of active upwelling show little vertical variability (Fig. 2.2). Mixed layer $^{17}\Delta_{diss}$ was highest in the North Inshore region (annual mean = 87±7 per meg) and lowest in the Offshore region (annual mean = 34±4 per meg) (Table 2.1; Fig. 2.3). Uncertainty in the annual mean represents the mean SEM in each region for all cruises. Seasonal variability for $^{17}\Delta_{diss}$ was greatest in the North Inshore region with a range from 68±6 per meg in October 2006 to 108±12 per meg in July 2006 and least in the Offshore region with a range from 24±3 per meg during July 2006 to 43±7 per meg during January 2007 (Table 2.1; Fig. 2.3). The mean annual spatially-weighted mixed layer $^{17}\Delta_{diss}$ for the entire CalCOFI grid was 53±5 per meg (Table 2.1).

Mixed layer $^{17}\Delta$-GOP rates were calculated using the approach outlined in Luz and Barkan (2011) and Prokopenko et al. (2011) with terms added for horizontal and vertical advection as in Eqs. 5 and 6; horizontal advection terms were neglected for the Offshore region because horizontal surface $^{17}\Delta_{diss}$ gradients were typically less than the uncertainty of mixed layer $^{17}\Delta_{diss}$. $^{17}\Delta$-GOP rates were not calculated during the January cruise (0701JD) due to winter entrainment of high $^{17}\Delta_{diss}$ water beneath the mixed layer (mixed layer depths during January 2007 were typically 2x those observed during the previous October). $^{17}\Delta$-GOP rates were also not calculated for the South Inshore region for the fall 2005 cruise (i.e., 0511NH) because mixed layer samples were taken at only one station within the region and during the summer 2008 cruise (i.e., 0808NH) because the mixed layer fraction of productivity based on ^{14}C-PP was less than 40% indicating that $^{17}\Delta$-GOP mixed layer budgets missed the majority of depth integrated production. Annual mean mixed layer productivity was greatest in the North Inshore region

(326±120 mmol O_2 m^{-2} d^{-1}) and least in the Offshore region (83±39 mmol O_2 m^{-2} d^{-1}) (Table 2.2). Temporal variability in $^{17}\Delta$-GOP was greatest in the North Inshore region with a range from 234±85 to 533±185 mmol O_2 m^{-2} d^{-1} and least in the Offshore region with a range from 49±23 to 121±40 mmol O_2 m^{-2} d^{-1} (Table 2.3).

The effect of advection on $^{17}\Delta$-GOP estimates varied markedly from inshore regions moving offshore. The most significant corrections were applied to the California Current region where the July 2006 $^{17}\Delta$-GOP values were reduced by 36%, from 98 mmol O_2 m^{-2} d^{-1} using the unapproximated version of Eq. 2 to 62 mmol O_2 m^{-2} d^{-1} including all advection terms (i.e., as in Eqs. 5 and 6). This was a result of high $^{17}\Delta_{diss}$ water from nearshore regions being advected offshore via Ekman transport. Advection corrections reduced mean annual $^{17}\Delta$-GOP rates by 12% in the California Current region and by negligible amounts for the North and South Inshore and Offshore regions. Advection reduced uncorrected mean annual $^{17}\Delta$-GOP estimates for the entire CalCOFI grid by 4% from 156 to 151 mmol O_2 m^{-2} d^{-1}.

O_2:Ar-NOP estimates

Mean mixed layer biological O_2 saturation based on measured O_2:Ar ranged from 1.008±0.001 to 1.127±0.024 for the four regions where uncertainties represent one SEM for each region (Table 2.1). Depth profiles show small biological O_2 saturation maxima associated with subsurface cholophyll maxima and a consistent decrease with depth below the photic zone (Fig. 2.2). Annual mean biological O_2 saturation was highest in the North Inshore region (1.069±0.012) and lowest in the Offshore region (1.013±0.002) (Table 2.1; Fig. 2.4). Seasonal variability was greatest in the North Inshore region with a range from 1.037±0.005 during October 2006 to 1.127±0.024 during July 2006 and least in the Offshore region with a range

from 1.008±0.001 in January 2007 to 1.017±0.001 in October 2006 (Table 2.1; Fig. 2.4). Notably, biological O_2 saturation exceeded 1.000 for 297 of 310 (96%) individual mixed layer samples. The mean annual biological O_2 saturation for the CalCOFI grid was 1.028±0.005 (Table 2.1).

Mixed layer O_2:Ar-NOP was calculated using Eq. 7, which accounted for horizontal advection terms. Advection terms were negligible for the Offshore region. Annual O_2:Ar-NOP was greatest in the North Inshore region (65±18 mmol of O_2 m^{-2} d^{-1}) and least in the Offshore region (13±4 mmol O_2 m^{-2} d^{-1}) (Table 2.2). Temporal variability in O_2:Ar-NOP was greatest in the North Inshore region with a range from 18±9 to 135±31 mmol O_2 m^{-2} d^{-1} and least in the Offshore region with a range from 10±3 to 16±4 mmol O_2 m^{-2} d^{-1} (Table 2.3).

The effect of advection on O_2:Ar-NOP estimates was greatest for the two inshore regions with up to a 2x increase from 4 to 8 mmol O_2 m^{-2} d^{-1} for the South Inshore region in January of 2007 due to upwelling of water with significant biological undersaturation. Advection increased mean annual O_2:Ar-NOP estimates by 44% and 57% in the North and South Inshore regions, respectively, and reduced rates by 6% and 3% in the California Current and Offshore regions, respectively. Advection increased the mean annual O_2:Ar-NOP estimate for the CalCOFI grid by 21% from 20 to 25 mmol O_2 m^{-2} d^{-1}.

NOP:GOP

NOP:GOP ratios for the mixed layer were calculated by dividing O_2:Ar-NOP (Eq. 7) by $^{17}\Delta$-GOP (Eq. 5) for all cruises and regions except the January 2007 cruise (0701JD) due to the $^{17}\Delta_{diss}$ entrainment bias discussed above; estimates were also not calculated for the South Inshore region during August 2008 due to the low fraction of mixed layer primary production as

discussed above. Annual means for NOP:GOP for the four regions ranged from 0.14±0.07 in the California Current region to 0.20±0.06 in the North Inshore region (Table 2.2). Temporal variability was similar for all regions. The seasonal range was largest for the California Current region (from 0.08±0.03 to 0.33±0.23) and least for the North Inshore region (from 0.15±0.07 to 0.29±0.05) (Table 2.3). The annual mean for the entire CalCOFI grid was 0.16±0.06 (Table 2.2).

Error analysis

Uncertainty in $^{17}\Delta$-GOP, O_2:Ar-NOP, and NOP:GOP was estimated using a Monte Carlo analysis similar to the approach described in Juranek and Quay (2005). A mean value and error (±1 SD) was assigned to each term in Eqs. 6 and 7, a value for each term was randomly selected assuming a normal distribution, and $^{17}\Delta$-GOP, O_2:Ar-NOP, or NOP:GOP calculated. The random selection process and calculations were repeated 1000 times and the uncertainty was calculated as ±1 SD for all 1000 values.

Assigned errors (±1 SD) for the parameters in Eqs. 6 and 7 applied in the Monte Carlo analysis are as follows: 25% for K_g (i.e., the range in K_g for different gas exchange parameterizations); 0.2% for C_{sat}; 15 per meg for $^{17}\Delta_p$ and 2 per meg for $^{17}\Delta_{eq}$ (Luz and Barkan 2000); 4 to 7 per meg for $^{17}\Delta_{diss}$ (i.e., the SEM of all mixed layer values within each region as given in Table 2.1); 10 per meg for $^{17}\Delta_z$ (i.e., the SD of the vertical gradient in $^{17}\Delta_{diss}$); 0.2% to 1.2% for $(O_2:Ar)_{bio\_ml}$ (i.e., the SEM of all mixed layer values within each region as given in Table 2.1); 1.5% for $(O_2:Ar)_{bio\_z}$ (i.e., the SD of the vertical gradient in biological O_2 saturation); 7 mmol m^{-3} for C_{ml} (i.e., the typical SD of all mixed layer estimates within each region); 7 cm s^{-1} for geostrophic current velocities and 0.2 cm s^{-1} for Ekman velocities (i.e., the typical SD of all velocity estimates across a given boundary); 0.5 m d^{-1} for w_{coast} in the two inshore regions (i.e.,

the SD of simultaneous w_{coast} estimates for two buoys within the North Inshore region); 0.02 m d^{-1} for w_{curl} in all regions (i.e., the typical SD of individual w_{curl} estimates within a given region). Note that the sensitivity of GOP to $^{17}\Delta_{diss}$ increases as $^{17}\Delta_{diss}$ approaches $^{17}\Delta_{eq}$ whereas the fractional uncertainty in K_g remains constant for all GOP and NOP estimates.

Time and space integration of different PP methods

Comparisons between different productivity methods are complicated by the different integration times of each method. The ^{14}C-PP method represents a snapshot of the period of hours over which incubation experiments are conducted (i.e., six hours for ^{14}C-PP experiments conducted during CalCOFI cruises). The $^{17}\Delta$-GOP and O_2:Ar-NOP methods integrate over the residence time of O_2 in the mixed layer which is typically four to seven days in the CalCOFI region. To account for the different integration periods of the two methods, we average ^{14}C-PP both temporally and spatially as done for $^{17}\Delta$ and O_2:Ar measurements. The ^{14}C-PP calculated for each region (Fig. 2.1) and cruise represents the mean of three to five different ^{14}C-PP incubations conducted over five to ten days which is close to the residence time of O_2 in the mixed layer. We also determine the fraction of ^{14}C-PP occurring in the mixed layer relative to the photic zone for each station where incubations were conducted; the mean of the mixed layer fraction of ^{14}C-PP for all stations within a given region is then used to extrapolate the mixed layer $^{17}\Delta$-GOP rate to a photic zone rate. The satellite-based productivity estimates are also averaged temporally and spatially to provide a more meaningful comparison; VGPM and CbPM estimates represent 16-day composites on a 10 km spatial scale during which ship-based productivity measurements were conducted. The regional estimate for VGPM-PP and CbPM-PP represents the mean of all individual observations (typically several hundred) within each region.

Annual means for all productivity estimates (Table 2.2) were calculated by first averaging cruise estimates seasonally over three month intervals (i.e., January to March, April to June, July to September, and October to December). $^{17}\Delta$-GOP for each region during the January to March interval was estimated using the regional mean $^{17}\Delta$-GOP:^{14}C-PP slope for the five other cruises (i.e., cruises which took place in spring, summer, and autumn) and measured ^{14}C-PP. Annual means presented in Table 2.2 for ^{14}C-PP, VGPM-PP, and CbPM-PP are within 15% of long-term annual means calculated for the period from 2000 to 2009 for all regions except the North Inshore region where the annual ^{14}C-PP was approximately 30% lower than the long-term annual mean. The low annual ^{14}C-PP for the North Inshore region may be due to undersampling of high productivity stations in the North Inshore region during cruises also sampled for $^{17}\Delta$ and O_2:Ar as the annual VGPM-PP estimate for this region (Table 2.2) was 10% above the long-term mean. The $^{17}\Delta$-GOP:^{14}C-PP relationship determined on a station by station basis for all stations not influenced by significant advection transports is nearly the same as the relationship determined using the seasonal and regional averaging scheme described above (i.e., the $^{17}\Delta$-GOP:^{14}C-PP slope for the station by station analysis was 5.4 compared to the slope of 5.6 presented in Fig. 2.5).

2.4 Discussion

Spatial and seasonal trends in $^{17}\Delta$-GOP, ^{14}C-PP, and satellite-based PP

The spatial and seasonal range in photic zone $^{17}\Delta$-GOP for all four regions reported here (71 to 958 mmol O_2 m^{-2} d^{-1}) is similar to the range in $^{17}\Delta$-GOP reported by Sarma et al. (2008) for Sagami Bay off the coast of Japan in May 2006 (34 to 963 mmol O_2 m^{-2} d^{-1}) which is the only other location where $^{17}\Delta$-GOP rates have been reported for the coastal ocean. Annual photic

zone $^{17}\Delta$-GOP for the entire CalCOFI region (235±88 mmol O_2 m^{-2} d^{-1}) is more than 2.2x mean annual $^{17}\Delta$-GOP in the subtropical North Pacific at HOT (105±41 mmol O_2 m^{-2} d^{-1}) (Quay et al. 2010) and 1.2x the highest $^{17}\Delta$-GOP reported from May to October of 2000 in the subtropical North Atlantic at BATS (150 to 192 mmol O_2 m^{-2} d^{-1}) (Luz and Barkan 2009). Annual mean $^{17}\Delta$-GOP for the Offshore region at CalCOFI (122±53 mmol O_2 m^{-2} d^{-1}) is comparable to rates observed in the oligotrophic ocean at HOT and BATS (Table 2.2).

Spatially, annual $^{17}\Delta$-GOP and ^{14}C-PP_{24h} exhibited similar variability between regions; annual $^{17}\Delta$-GOP and ^{14}C-PP_{24h} for the North Inshore region were 3.9x and 4.1x, respectively, annual rates in the Offshore region (Table 2.2). Spatial variability of VGPM-PP was similar to that of $^{17}\Delta$-GOP while CbPM-PP was less variable between regions (Table 2.2). Annual mean VGPM-PP and CbPM-PP for the North Inshore region were 4.2x and 2.5x rates in the Offshore region, respectively (Table 2.2). Seasonal variability for all methods was largest in the North Inshore region (Table 2.3); summer photic zone $^{17}\Delta$-GOP was 2.9x rates observed during fall (winter $^{17}\Delta$-GOP rates are not reported due to the entrainment bias). The Offshore region was least variable from cruise to cruise for all PP methods except $^{17}\Delta$-GOP which was least variable in the South Inshore region (Table 2.3). The uncertainty in $^{17}\Delta$-GOP estimates makes the seasonal range difficult to distinguish in oligotrophic regions of the North Pacific as noted by Quay et al. (2010).

Comparisons of $^{17}\Delta$-GOP with ^{14}C-PP

Annual mean $^{17}\Delta$-GOP (mmol O_2 m^{-2} d^{-1}) estimated for each region was 4 to 6x bottle ^{14}C-PP_{24h} (mmol C m^{-2} d^{-1}) (Table 2.2; Fig. 2.5). The mixed layer $^{17}\Delta$-GOP:^{14}C-PP_{24h} was more variable on a seasonal basis (Table 2.3) with ratios greater than 9 observed in spring (April 2006)

for the California Current and Offshore regions and in summer (July 2006) for the inshore regions; the lowest ratio (near 3.1) was observed in the Offshore region during July 2006 (Table 2.3). The seasonal range of $^{17}\Delta$-GOP:^{14}C-PP$_{24h}$ for the CalCOFI grid of 3.1 to 9.4 (Table 2.3) is similar to the range observed at BATS (4.4 to 9.9) by Luz and Barkan (2009) but significantly higher than the range observed at HOT (2.6 to 3.4) by Quay et al. (2010) (Table 2.2). It should be noted that some of the variability in the $^{17}\Delta$-GOP:^{14}C-PP results from the conversion of shorter duration ^{14}C-PP incubation experiments at CalCOFI (6 h), BATS (12 h), and HOT (12 h) to 24 h rates as described above and from the uncertainty in $^{17}\Delta$-GOP (± 30%) (Table 2.2). We explore several possible explanations for the variation in $^{17}\Delta$-GOP:^{14}C-PP$_{24h}$ ratios observed at CalCOFI, HOT, and BATS: 1) variability in the O_2 production:carbon fixation ratio 2) entrainment of high $^{17}\Delta$ water from the deep photic zone into the mixed layer, and 3) ^{14}C-PP methodological effects.

In a study of Lake Kinneret, Luz et al. (2002) observed ^{18}O-GOP:^{14}C-PP ratios of 1.9 for non-bloom conditions and 7.5 for bloom conditions, comparable to the seasonal range observed during our study (3.1 to 9.4). Robinson et al. (2009) observed ^{18}O-GOP:^{14}C-PP ratios >5 at a diatom-dominated station in the Celtic Sea. One possible explanation for these high ^{18}O-GOP:^{14}C-PP ratios is that the O_2 production to carbon fixation ratio increases under high light conditions, as discussed in Zehr and Kudela (2009). While variability in light conditions may contribute to the high seasonal variability in $^{17}\Delta$-GOP:^{14}C-PP$_{24h}$ ratios at CalCOFI and BATS relative to HOT, it does not seem likely that variability in light conditions can explain the disparity between the annual mean $^{17}\Delta$-GOP:^{14}C-PP$_{24h}$ ratio of ~3 at HOT (Quay et al. 2010) and ~6 for the Offshore region at CalCOFI given that both sites are located in the oligotrophic subtropical North Pacific (Table 2.2). In any case, a better understanding of the variability in rates of photosynthetic O_2 production and corresponding carbon fixation for different plankton

species under different light and nutrient conditions is clearly needed.

Entrainment of high $^{17}\Delta$ water beneath the mixed layer (Fig. 2.2) can inflate $^{17}\Delta$-GOP rates which could also lead to higher than expected $^{17}\Delta$-GOP:^{14}C-PP$_{24h}$ ratios. Nicholson et al. (2012) demonstrated using a one-dimensional model that high mixed layer ratios observed at BATS (Luz and Barkan 2009) were likely due to entrainment of high $^{17}\Delta$ water from the deep photic zone. We note that $^{17}\Delta$ depth profiles at CalCOFI typically display smaller subsurface maxima than at BATS where a large fraction of the photic zone is beneath the mixed layer during the summer and fall. At CalCOFI, the South Inshore region which includes the sheltered Southern California Bight develops strong subsurface maxima in $^{17}\Delta$ in the late summer and early fall which could lead to significant entrainment bias. We have excluded $^{17}\Delta$-GOP estimates for this region for the August 2008 cruise where less than 40% of ^{14}C-PP occurred within the mixed layer because mixed layer budgets missed a large fraction of the total photic zone production and because of the potential for entrainment bias (Table 2.3). In contrast, vertical profiles in high productivity inshore regions show no identifiable maximum in the deep photic zone which suggests entrainment bias in these regions is negligible (Fig. 2.2). Although we cannot rule out the potential for entrainment bias in other regions, we note that on average annual $^{17}\Delta$-GOP:^{14}C-PP$_{24h}$ ratios are consistent for all four regions (Table 2.2) and that during the most productive times of year, the bulk of ^{14}C-PP (>80%) occurs in the mixed layer which, combined with high vertical velocities due to coastal and curl-driven upwelling, limits the development of large sub-mixed layer $^{17}\Delta$ maxima characteristic of more stratified oligotrophic regions.

Another possible explanation for high $^{17}\Delta$-GOP:^{14}C-PP$_{24h}$ rates observed during CalCOFI cruises is that ^{14}C-PP increasingly underestimates PP at high productivity rates. Effects which could be responsible for ^{14}C-PP underestimation include high rates of DO^{14}C excretion,

heterotrophic recycling of ^{14}C during incubations, and internal recycling of unlabeled CO_2 (Marra 2002). Karl et al. (1998) measured $DO^{14}C$ excretion rates at HOT that accounted for up to 30% of $PO^{14}C$ uptake. Additionally, the importance of heterotrophic recycling of $PO^{14}C$ and internal recycling of unlabeled CO_2 could increase as the PP rate increases yielding greater underestimates of $PO^{14}C$ production at high rates of PP. Given that annual $^{17}\Delta$-GOP:^{14}C-PP_{24h} ratios were similar in the lower productivity Offshore region (6.0±0.9) and the high productivity North Inshore region (5.9±0.8) and that the $^{17}\Delta$-GOP:^{14}C-PP_{24h} ratio itself did not increase at greater ^{14}C-PP rates (Fig. 2.5), it does not seem likely that effects related to increasing PP rates can account for differences in $^{17}\Delta$-GOP:^{14}C-PP_{24h} ratios between HOT and CalCOFI. High rates of $DO^{14}C$ excretion, on the other hand, could contribute to consistently higher $^{17}\Delta$-GOP:^{14}C-PP_{24h} ratios at CalCOFI. While rates of $DO^{14}C$ excretion were not determined on CalCOFI cruises, if we assume that $DO^{14}C$ accounted for 30% of $PO^{14}C$ uptake at CalCOFI, the annual $^{17}\Delta$-GOP:^{14}C-PP_{24h} ratio for the Offshore region is reduced from 6.0±0.9 to 4.2±0.6 which is still outside the range of ratios observed at HOT (2.6-3.4) (Table 2).

Another methodological issue which could contribute to differences between the long-term mean ^{14}C-PP_{24h} at HOT (400 mg C m^{-2} d^{-1}) (Karl et al. 1998) and the annual mean for the CalCOFI Offshore region (235±40 mg C m^{-2} d^{-1}) may be systematic differences between on-deck simulated in situ (SIS) and in situ (IS) bottle incubation (in contrast, $^{17}\Delta$-GOP estimates for the two studies were based on $^{17}\Delta$ measurements made by the same research group using similar calculation procedures). The ^{14}C-PP method at HOT utilizes in situ bottle incubation at five depths from 5 to 125 m between dawn and dusk, whereas the CalCOFI ^{14}C-PP method utilizes on-deck incubation for 6 h where on-deck incubators are temperature-regulated with surface seawater and in situ light conditions simulated using neutral density screens. Grande et al. (1989)

observed greater ^{18}O-GOP$_{SIS}$:^{14}C-PP$_{SIS}$ (on-deck) ratios (2.2) relative to ^{18}O-GOP$_{IS}$:^{14}C-PP$_{IS}$ (in situ) ratios (1.4) which they attributed to differences in the spectral composition of light filtered through neutral density screens compared to light in situ. Other studies observed suppression of ^{14}C assimilation using on-deck incubators possibly due to photoinhibition (Marra 1980; Harris 1984). If we assume that on-deck methodology contributed to underestimation of ^{14}C-PP$_{24h}$ by 35% as suggested by Grande et al. (1989), the annual $^{17}\Delta$-GOP:^{14}C-PP$_{24h}$ ratio for the Offshore region is reduced from 6.0 to 4.4. Recent ^{14}C-PP estimates for the CalCOFI region using the same 24 h in situ methodology employed at HOT also suggest that on-deck incubations underestimate ^{14}C-PP. Stukel et al. (2011) measured ^{14}C-PP within the Offshore region (i.e., Region 4 of this study) of 520 mg C m^{-2} d^{-1} during a CCE-LTER cruise in May and June 2006; the ^{14}C-PP estimate for the Offshore region during the April 2006 CalCOFI cruise was 200 mg C m^{-2} d^{-1} (where the CalCOFI ^{14}C-PP has been scaled to a 24 h rate using the factor of 1.81 discussed above). We also note that recent comparisons of mixed layer $^{17}\Delta$-GOP and ^{14}C-PP off the central California coast (D. Munro unpubl. data) yielded $^{17}\Delta$-GOP:^{14}C-PP ratios between two and three which agrees with comparisons of incubation-based ^{18}O-GOP and ^{14}C-PP (Marra 2002) and also suggests methodological biases in ^{14}C-PP at CalCOFI. It is possible that the combined effects of DO^{14}C excretion and on-deck incubation could account for the 2x higher $^{17}\Delta$-GOP:^{14}C-PP$_{24h}$ ratios observed at CalCOFI compared to HOT.

Comparisons of $^{17}\Delta$-GOP and ^{14}C-PP with satellite PP

The mean ^{14}C-PP$_{24h}$:VGPM-PP and ^{14}C-PP$_{24h}$:CbPM-PP ratios (PP estimates in mg C m^{-2} d^{-1}) for all stations and cruises were 0.62±0.03 and 0.90±0.07, respectively. The ^{14}C-PP$_{24h}$:VGPM-PP relationship is consistent with previous results for the CalCOFI region and has

been assumed to indicate an overestimation of PP by the VGPM in the coastal ocean (Kahru et al. 2009). More recent productivity models including the CbPM estimate significantly lower PP for high productivity regions such as the North Inshore region in this study (Table 2.2). Kahru et al. (2009) presented an empirically-derived modification of the VGPM algorithm ($VGPM_{cal}$) based on comparisons with CalCOFI ^{14}C-PP which reduces VGPM-PP estimates by 36% (Table 2.2). At HOT, $^{14}C\text{-}PP_{24h}$:VGPM-PP ratio was 1.38 (P. Quay unpubl. data), where $^{14}C\text{-}PP_{12h}$ was converted to $^{14}C\text{-}PP_{24h}$ as described above and in Table 2.2. That the $^{14}C\text{-}PP_{24h}$:VGPM of 0.6 in the Offshore region of CalCOFI is only half that observed at HOT is surprising and may be related to the ^{14}C-PP methodological issues at CalCOFI discussed above rather than overestimation of PP by the VGPM.

At CalCOFI, the $^{17}\Delta$-GOP:VGPM-PP and $^{17}\Delta$-GOP:CbPM-PP ratios using the photic zone GOP estimates described above were 3.5±0.3 and 4.8±0.5 which are close to previous estimates using the $^{17}\Delta$ method. At HOT, the $^{17}\Delta$-GOP:VGPM-PP ratio was 4.5 (P. Quay unpubl. data). For further comparison, Juranek and Quay (2010) report $^{17}\Delta$-GOP:VGPM-PP and $^{17}\Delta$-GOP:CbPM-PP ratios for the equatorial Pacific of 7.0 and 4.6, respectively, and Reuer et al. (2007) observed a $^{17}\Delta$-GOP:VGPM-PP of 5.4 in the Southern Ocean. The significant disparity between $^{17}\Delta$-GOP, ^{14}C-PP, and satellite PP for different regions highlights the substantial uncertainty of each PP method and emphasizes the need to utilize multiple approaches whenever possible.

Net carbon production (NCP) and NOP:GOP

The annual rate of NCP (equivalent to organic carbon export at steady state) estimated from O_2:Ar ranged from 109 mg C m^{-2} d^{-1} (3.3 mol C m^{-2} yr^{-1}) for the Offshore region to 560 mg

C m^{-2} d^{-1} (17.0 mol C m^{-2} yr^{-1}) for the North Inshore region; the spatially-weighted annual rate for the entire CalCOFI grid was 210 mg C m^{-2} d^{-1} (6.4 mol C m^{-2} yr^{-1}). The conversion from O_2 to carbon units assumed a photosynthetic quotient of 1.4 as described above. Previous NCP estimates for different regions within the CalCOFI grid are presented in Table 2.4. Our O_2:Ar-NCP estimates agree closely with new production estimates based on f-ratios from ^{15}N uptake experiments and ^{14}C-PP_{24h} in the CalCOFI region (204 mg C m^{-2} d^{-1}) (Dugdale and Wilkerson 1992; Eppley 1992), and are more than 2x greater than particulate organic carbon (POC) flux estimates based on sediment trap (Landry et al. 1992) and ^{234}Th (Stukel et al. 2011; Huh and Beasley 1987) measurements within the North and South Inshore regions (Table 2.4). That POC export estimates are significantly lower than O_2:Ar-NCP is expected due to potentially large differences in the spatial integration scale of these measurements and the contribution of the DOC component of the export flux, as observed at HOT by Emerson et al. (1997).

NOP:GOP ratios determined by measurements of $^{17}\Delta_{diss}$ and O_2:Ar during CalCOFI ranged from 0.08±0.03 to 0.33±0.23 (Table 2.3). NOP:GOP increased only slightly with increasing productivity (Fig. 2.5). For comparison, the range in NOP:GOP based on O_2:Ar and $^{17}\Delta_{diss}$ measurements reported by Sarma et al. (2008) for Sagami Bay off Japan was -0.49 to 0.28 where the negative values were confined to a small spatial region near the outflow of the Sakawa River. Estimated NOP:GOP at CalCOFI is strikingly similar to estimates at open ocean sites where contemporaneous O_2:Ar and $^{17}\Delta_{diss}$ measurements have been made. At HOT, Quay et al. (2010) reported a winter mean of 0.13±0.05 and summer mean of 0.22±0.06 similar to the range reported by Luz and Barkan (2009) at BATS (0.08 to 0.21). For further comparison, Hendricks et al. (2005) and Stanley et al. (2010) reported mean NOP:GOP ratios of 0.06±0.05 and 0.06±0.02, respectively, in the equatorial Pacific; and Reuer et al. (2007) reported a mean of 0.13 in the

Southern Ocean.

Previous estimates of organic carbon export efficiency in the CalCOFI region have been based on an f-ratio determined from incubation measurements. For example, Eppley et al. (1979) and Eppley (1992) reported f-ratios based on $^{15}NO_3$-uptake based estimates of NCP and ^{14}C-PP of 0.36 and 0.33 for the Southern California Bight (comparable to the South Inshore region), respectively. Dugdale and Wilkerson (1992) reported an f-ratio based on $^{15}NO_3$ and $^{15}NH_4$ uptake of 0.57 in the upwelling region near Point Conception, with values >0.8 during the height of bloom conditions. We estimated an equivalent f-ratio by converting NOP to NCP (as described above) and dividing by ^{14}C-PP_{24h}. This calculation yielded a mean annual f-ratio (in carbon units) for the CalCOFI grid, North Inshore, South Inshore, California Current, and Offshore regions of 0.40, 0.58, 0.33, 0.33, and 0.46, respectively. Alternately, f-ratios were calculated by converting our NOP:GOP ratio to NCP:^{14}C-PP_{24h} where O_2:Ar-NOP was divided by 1.4 to yield NCP and $^{17}\Delta$-GOP was divided by 2.7 (Marra 2002) to yield ^{14}C-PP, as described above. This calculation yields mean annual f-ratios for the CalCOFI grid, North Inshore, South Inshore, California Current, and Offshore regions of 0.32, 0.39, 0.31, 0.28, and 0.29, respectively. Differences may result from variability in the relationship between O_2 production and carbon fixation and/or underestimation of ^{14}C uptake by on-board incubation methods as discussed above. It is important to recognize that the NOP:GOP ratio determined from O_2:Ar and $^{17}\Delta_{diss}$ represents a new gauge of potential export efficiency that should not necessarily be expected to agree with incubation-based approaches. In any case, NOP:GOP estimates based on O_2:Ar and $^{17}\Delta_{diss}$ suggest potential export efficiency (~0.15) throughout the CalCOFI region remarkably close to efficiencies of open ocean environments determined using the same method (Table 2.2).

Export production in the California Current Ecosystem

Several studies based on both in situ (Stukel et al. 2011; Thunell 1998) and modeling (Olivieri and Chavez 2000) approaches suggest that particulate organic carbon (POC) export may be inversely related to primary production in the California Current Ecosystem. These studies also suggest that much of the organic material fixed in high productivity regions inshore of the California Current may be advected offshore in the Ekman layer. Our results of potential export efficiency based on the NOP:GOP ratio indicate lower efficiency in the productive North Inshore region compared to estimates of the f-ratio based on incubation experiments (Dugdale and Wilkerson 1992). Additionally, our results yield much higher estimates of NCP in the North Inshore region compared to past estimates of POC export (Table 2.4) indicating that a large fraction (up to 75%) of the organic material produced in the high productivity regions inshore of the California Current does not sink out of the surface ocean within the inshore regions.

Comparison of our estimates with other budget estimates for the entire CalCOFI grid provides some indication about the fate of the organic material registered as NCP using the O_2:Ar approach. Our mean O_2:Ar-NCP estimate (210 mg C m^{-2} d^{-1}) for the CalCOFI grid is within the interannual variability of estimates determined for 1984-1987 by Roemmich (1989) (annual mean of 240 mg C m^{-2} d^{-1}) and for 1984-1997 by Bograd et al. (2001) (annual mean of 327 mg C m^{-2} d^{-1}) who both estimated NCP based on a nutrient (NO_3^- and PO_4^{3-}) budget (assuming Redfield stoichiometry of 106:16:1 in relating C:N:P) for a control volume (bounded by CalCOFI line 77 to the north, line 93 to the south, station 100 to the west, and extending to a depth of 500 m) utilizing measured nutrient concentrations and geostrophic and Ekman transport estimates. The NCP estimates of Roemmich (1989) and Bograd et al. (2001) are potentially

lower than NCP in the mixed layer because some of the exported NCP is remineralized within the control volume (which extends to 500 m). Agreement between our O_2:Ar-NCP rates and the nutrient budget-based estimates of Roemmich (1989) and Bograd et al. (2001) has three important implications: 1) that organic carbon export in the CalCOFI region is supported almost entirely by nutrients supplied from outside the control volume (i.e., non-local sources); 2) that respiration between the mixed layer and 500 m is low within the CalCOFI grid; and 3) that most of the NCP which occurs within the control volume is advected horizontally out of the control volume in the Ekman layer. This final conclusion is based on sediment trap studies in the central CCS (Knauer and Martin 1981) that indicated very low POC flux at 500 m and the assumption that POC export to the narrow shelf in this region accounted for a relatively small fraction of NCP for the entire CalCOFI grid. With regard to the suggestion that the respiration rate is low between the mixed layer and 500 m, the uncertainties in both methods complicate accurate estimation of the deep respiration rate. We note that the study of Bograd et al. (2001) indicates significant interannual variability in NCP with annual rates from 1993-1997 more than 2.7x rates observed from 1988-1992. We believe that it is unlikely that the O_2:Ar-NCP estimate is biased low given agreement between our estimate presented here and estimates of potential new production (an upper limit on export production) based on nitrate supply for the CalCOFI region (Messié et al. 2009) and carbon budgets for other upwelling regions of the CCS (Pennington et al. 2010) (Table 2.4). We also note that our O_2:Ar NCP estimates are within 10% of O_2-based NCP estimates from a more extensive analysis of the CalCOFI dataset (i.e., from 1984 to 2010) (D. Munro unpubl. manuscript).

[17]Δ-GOP and O_2:Ar-NOP productivity estimates in the California Current Ecosystem

We highlight the following five observations and implications of the productivity estimates presented here.

1. PP as determined by the $^{17}\Delta$-GOP, ^{14}C-PP, and VGPM methods increases by a factor of four from regions inshore of the California Current to the subtropical North Pacific.

2. The ratio of $^{17}\Delta$-GOP:^{14}C-PP is twice that expected from previous comparisons of incubation experiments (i.e., ^{18}O-GOP:^{14}C-PP) which may result from methodological issues with ^{14}C-PP measurement and/or biases in the $^{17}\Delta$-GOP method including variable ratios of O_2:C production.

3. The photic zone $^{17}\Delta$-GOP:VGPM-PP ratios of 4-5 are the same as found at HOT using the same methods. Ratios of ^{14}C-PP:VGPM-PP of 0.6 in the CalCOFI region may be a result of methodological problems with ^{14}C-PP rather than overestimation by the VGPM.

4. The potential e-ratio in O_2 units (i.e., O_2:Ar-NOP: $^{17}\Delta$-GOP) of 0.16 is surprisingly similar to measurements made in the subtropical North Pacific at HOT using the same methods which implies efficiency of organic carbon production in coastal oceans similar to that in the open oligotrophic ocean.

5. O_2:Ar-NCP estimates are much higher than sediment trap and ^{234}Th estimates of POC flux which implies either methodological biases in approaches or that DOC is an important component of the export flux. Agreement between O_2:Ar-NCP and nitrate budget estimates of NCP implies little respiration of 'exportable' organic carbon beneath the mixed layer within the

coastal ocean. This result is consistent with a recent study by Deutsch et al. (2011) that suggests recent observations of lower O_2 concentrations at depth in the CalCOFI region (Bograd et al. 2008) may be a result of transport of low O_2 waters into the CCS rather than an increase in respiration beneath the mixed layer. Accurate estimation of the deep respiration rate is complicated by uncertainties in the mixed layer NCP estimates presented here and NCP estimates integrating to 500 m (Bograd et al. 2001).

In sum, $^{17}\Delta$-GOP and O_2:Ar-NOP non-incubation results provide a significantly different view of PP and NCP in the CalCOFI region compared with results based on incubation and satellite-based methods. Thus, the recommendation from this and similar recent studies (Juranek and Quay 2005; Robinson et al. 2009; Quay et al. 2010) is to adopt a multi-pronged approach to PP and NCP measurement utilizing a suite of methods, each with their own biases, that in combination should better constrain biological productivity rates in the coastal ocean.

Table 2.1: Seasonal range and annual mean values of mixed layer $^{17}\Delta_{diss}$ and biological O_2 saturation for each region; $^{17}\Delta_{diss}$ is relative to atmospheric O_2. Uncertainty is calculated as the standard error of the mean (SEM) for all mixed layer values in a given region during each cruise (i.e., SD / (*n*^0.5)). Uncertainty in the annual mean represents the mean SEM for each region for all cruises.

	Seasonal range $^{17}\Delta_{diss}$ (in per meg)	Annual mean $^{17}\Delta_{diss}$ (in per meg)	Seasonal range biological O_2 saturation	Annual mean biological O_2 saturation
Region 1: North Inshore	68±6 to 108±12	87±7	1.037±0.005 to 1.127±0.024	1.069±0.012
Region 2: South Inshore	58±5 to 91±2	68±5	1.013±0.005 to 1.062±0.006	1.038±0.007
Region 3: California Current	33±2 to 55±16	44±5	1.008±0.002 to 1.030±0.002	1.019±0.003
Region 4: Offshore	24±3 to 43±7	34±4	1.008±0.001 to 1.017±0.001	1.013±0.002
CalCOFI grid	44±3 to 60±3	53±5	1.016±0.002 to 1.040±0.005	1.028±0.005

Table 2.2: Annual production rates and ratios based on $^{17}\Delta_{diss}$, O_2:Ar, ^{14}C incubations, and satellite measurements. nc – not calculated.

	Mixed layer $^{17}\Delta$-GOP (mmol O_2 m^{-2} d^{-1})	Photic zone $^{17}\Delta$-GOP (mmol O_2 m^{-2} d^{-1})	^{14}C-PP_{24h}[a] (mg C m^{-2} d^{-1})	O_2:Ar-NOP (mmol O_2 m^{-2} d^{-1})	O_2:Ar-NCP[b] (mg C m^{-2} d^{-1})	VGPM-PP[c] (mg C m^{-2} d^{-1})	$VGPM_{cal}$-PP[d] (mg C m^{-2} d^{-1})	CbPM-PP[e] (mg C m^{-2} d^{-1})	Mixed layer $^{17}\Delta$-GOP: ^{14}C-PP_{24h}	Photic zone $^{17}\Delta$-GOP: VGPM-PP	Mixed layer O_2:Ar-NOP: $^{17}\Delta$-GOP
Region 1: North Nearshore	326±120	439±162	969±195	65±18	560±157	1738±356	1116±228	1029±184	5.9±0.8	3.4±0.6	0.20±0.06
Region 2: South Nearshore	183±54	353±100	775±139	30±8	256±71	1017±128	653±82	790±128	5.4±1.0	3.9±0.5	0.16±0.06
Region 3: California Current	116±55	182±81	430±60	17±6	143±50	665±64	427±41	567±82	4.3±0.8	3.1±0.6	0.14±0.07
Region 4: Offshore	83±39	122±53	235±40	13±4	109±33	416±21	267±14	405±44	6.0±0.9	4.2±0.5	0.15±0.06
CalCOFI grid:	151±59	235±88	529±90	25±8	210±64	820±113	527±73	638±96	5.7±0.3	3.6±0.1	0.16±0.06
Other studies: HOT[e]	nc	105±41	387±64	14±4	170±40	280±35	nc	nc	2.6-3.4	4.5	0.2±0.1
BATS[f] Seasonal range (May-Oct)	29-103	150-192	288-516	6-8	137-206	nc	nc	nc	4.4-9.9	nc	0.08 to 0.21

[a]CalCOFI ^{14}C-PP is converted from a 6 to 24 h rate using the Eppley (1992) scaling factor of 1.81; HOT ^{14}C-PP is converted from a 12 to 24 h rate assuming ^{14}C-$PP_{24h} = 0.85 \times {}^{14}C\text{-}PP_{12h}$ (Karl et al. 1996).

[b]NOP is converted to NCP using a PQ of 1.4 (Laws 1991).

[c]Satellite-based estimates, VGPM-PP (Behrenfeld and Falkowski 1997) and CbPM-PP (Westberry et al. 2008), were obtained from the Ocean Productivity Group (Oregon State University).

[d]$VGPM_{cal}$-PP is an empirically-derived algorithm based on comparisons between CalCOFI ^{14}C-PP and VGPM-PP: $VGPM_{cal}\text{-}PP = 10^{\log(VGPM) - 0.1924}$ (Kahru et al. 2009).

[e]Estimates from Quay et al. (2010) and P. Quay (unpubl. data).

[f]Estimates from Luz and Barkan (2009); ^{14}C-PP converted from a 12 to 24 h rate using the formula determined for HOT by Karl et al. (1996).

Table 2.3: Seasonal variability in production rates and ratios based on $^{17}\Delta_{diss}$, O_2:Ar, ^{14}C incubations, and satellite observations. nc – not calculated.

	Mixed layer $^{17}\Delta$-GOP (mmol O_2 m^{-2} d^{-1})	Photic zone $^{17}\Delta$-GOP (mmol O_2 m^{-2} d^{-1})	O_2:Ar-NOP (mmol O_2 m^{-2} d^{-1})	Mixed layer $^{17}\Delta$-GOP: ^{14}C-PP_{24h}	Photic zone $^{17}\Delta$-GOP: VGPM-PP	O_2:Ar-NOP: $^{17}\Delta$-GOP
Region 1: North Inshore						
0511NH(Nov 2005)	399±137	nc	60±21	nc	nc	0.15±0.07
0604NH (Apr 2006)	309±100	415±135	88±20	5.0	2.2	0.29±0.05
0607NH (Jul 2006)	533±185	958±332	135±31	8.1	4.8	0.25±0.05
0610RR (Oct 2006)	234±85	334±121	38±15	6.8	3.6	0.16±0.12
0701JD (Jan 2007)	nc	nc	18±9	nc	nc	nc
0808NH (Aug 2008)	391±115	468±138	78±20	4.8	2.9	0.20±0.05
Region 2: South Inshore						
0511NH(Nov 2005)	nc	nc	nc	nc	nc	nc
0604NH (Apr 2006)	197±60	365±111	55±11	4.5	3.1	0.28±0.06
0607NH (Jul 2006)	188±56	466±138	50±11	8.1	4.3	0.26±0.10
0610RR (Oct 2006)	132±42	301±96	17±6	6.6	5.2	0.13±0.05
0701JD (Jan 2007)	nc	nc	8±6	nc	nc	nc
0808NH (Aug 2008)	nc	nc	27±7	nc	nc	nc
Region 3: California Current						
0511NH(Nov 2005)	133±52	160±63	11±5	3.4	2.8	0.08±0.03
0604NH (Apr 2006)	133±45	273±92	16±6	9.4	6.2	0.12±0.05
0607NH (Jul 2006)	62±40	146±93	20±8	3.3	2.0	0.33±0.23
0610RR (Oct 2006)	82±36	155±68	11±4	5.5	3.6	0.13±0.10
0701JD (Jan 2007)	nc	nc	17±6	nc	nc	nc
0808NH (Aug 2008)	134±50	196±73	26±7	4.8	3.0	0.19±0.05
Region 4: Offshore						
0511NH(Nov 2005)	121±40	160±52	10±4	6.9	4.9	0.08±0.03
0604NH (Apr 2006)	91±32	146±51	13±4	9.1	4.5	0.14±0.06
0607NH (Jul 2006)	49±23	71±33	12±3	3.1	2.3	0.23±0.20
0610RR (Oct 2006)	105±34	158±51	10±3	6.7	5.1	0.09±0.04
0701JD (Jan 2007)	nc	nc	14±4	nc	nc	nc
0808NH (Aug 2008)	78±29	164±60	16±4	5.7	4.2	0.21±0.09
CalCOFI Grid:						
0511NH(Nov 2005)	181±62	247±84	14±7	nc	3.6	0.08±0.04
0604NH (Apr 2006)	159±52	279±91	34±8	6.1	3.6	0.21±0.05
0607NH (Jul 2006)	150±58	307±118	40±10	5.9	3.5	0.26±0.17
0610RR (Oct 2006)	120±43	214±77	16±6	6.4	4.3	0.13±0.07
0701JD (Jan 2007)	nc	nc	14±6	nc	nc	nc
0808NH (Aug 2008)	144±49	246±86	30±8	5.0	3.4	0.21±0.06

Table 2.4: Comparison of export production estimates from different studies in the California Current System.

Authors	Method	Region	Estimated carbon export (mg C m^{-2} d^{-1})	Estimated carbon export (mol C m^{-2} yr^{-1})
This study	O_2:Ar-NCP mixed layer	North Inshore	560	17.0
		South Inshore	256	7.8
		California Current	143	4.3
		Offshore	109	3.3
		CalCOFI grid	210	6.4
Dugdale and Wilkerson 1992 Eppley 1992	^{15}N uptake based f-ratio × ^{14}C-PP[a] photic zone	North Inshore	553	16.8
		South Inshore	256	7.8
		California Current	142	4.3
		Offshore	77	2.3
		CalCOFI grid	205	6.2
Landry et al. 1992	sediment trap 110-135 m	Santa Monica Basin	121	3.7
Huh and Beasley 1987	^{234}Th POC export	Southern California Bight	130	4.0
Stukel et al. 2011	^{234}Th POC export[b]	North Inshore	123	3.7
		California Current	72	2.2
		Offshore	76	2.3
Roemmich 1989	nutrient budget	CalCOFI grid	240	7.3
Bograd et al. 2001	nutrient budget	CalCOFI grid	327	9.9
Messié et al. 2009	nutrient budget	North Inshore (32.9 – 35 N)	622	18.9
Pennington et al. 2010	nutrient budget	Coastal Upwelling Region off Monterey Bay (comparable to North Inshore)	559	17.0

[a]New production calculated from f-ratios based on ^{15}N uptake experiments for the Point Conception region (f = 0.57) reported by Dugdale and Wilkerson (1992) and for the Southern California Bight (f = 0.33) reported by Eppley (1992) multiplied by ^{14}C-PP from the six cruises where $^{17}\Delta_{diss}$ and O_2:Ar were also measured.
[b]^{234}Th particulate organic carbon export estimates were made for three regions within the southern California Current System comparable to regions discussed in this study. Two measurements were made in the region inshore of the California Current (comparable to our North Inshore region); these estimates are averaged.

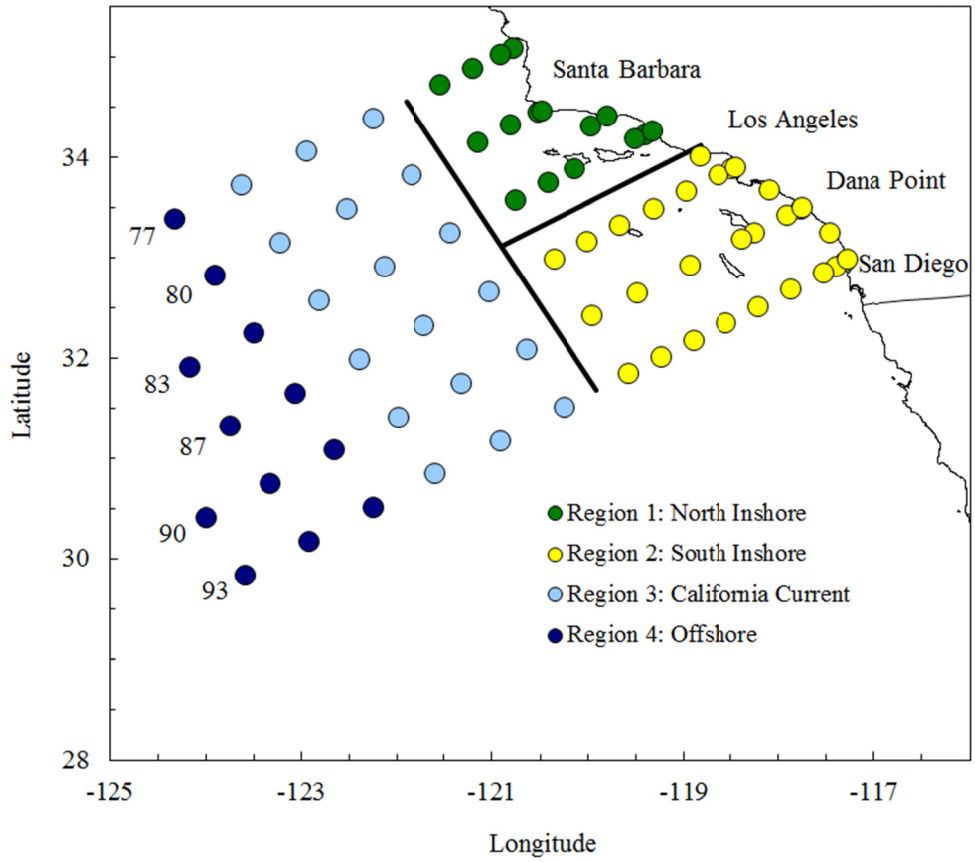

Figure 2.1: CalCOFI station positions with locations of standard stations and Southern California Coastal Ocean Observing System (SCCOOS) stations (circles). Region 1 (North Inshore) is green. Region 2 (South Inshore) is yellow. Region 3 (California Current) is light blue. Region 4 (Offshore) is dark blue. Alongshore transports were calculated across the line separating CalCOFI lines 83 and 87 between Regions 1 and 2. Offshore and onshore transports were calculated across the line separating stations 60 and 70 between Regions 1, 3 and Regions 2, 3.

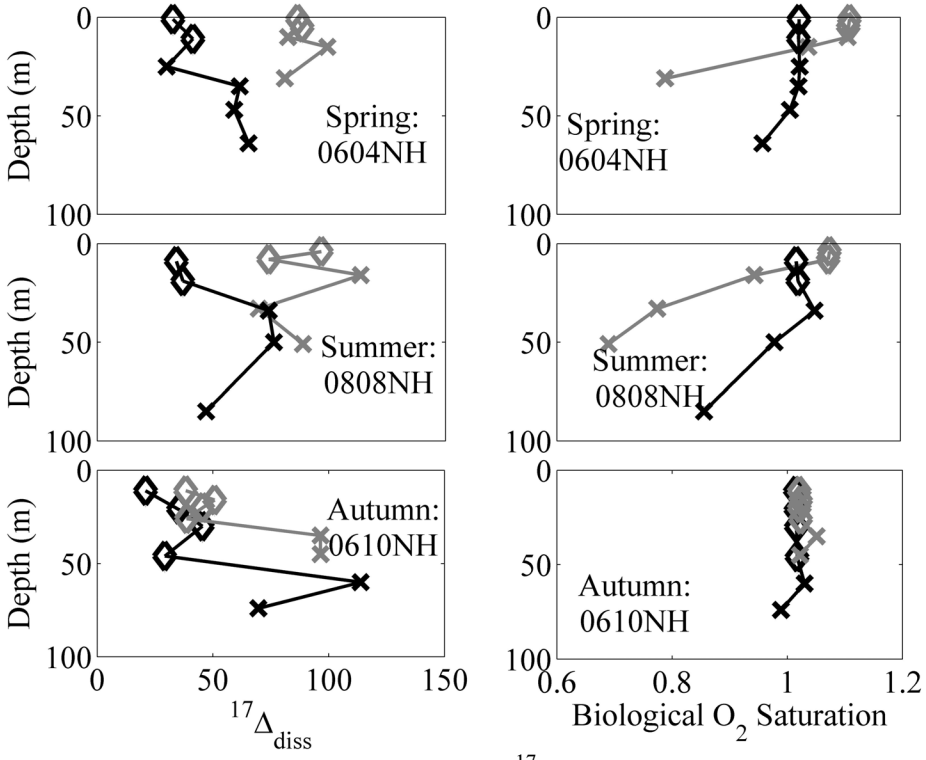

Figure 2.2: Representative depth profiles of $^{17}\Delta_{diss}$ in parts per meg relative to air, and biological O_2 saturation [$(O_2{:}Ar)_{meas}$ / $(O_2{:}Ar)_{sat}$]. Diamonds denote samples within the mixed layer. Xs denote samples beneath the mixed layer. Gray lines indicate profiles located within the North and South Inshore regions; black lines indicate profiles located within the California Current and Offshore regions.

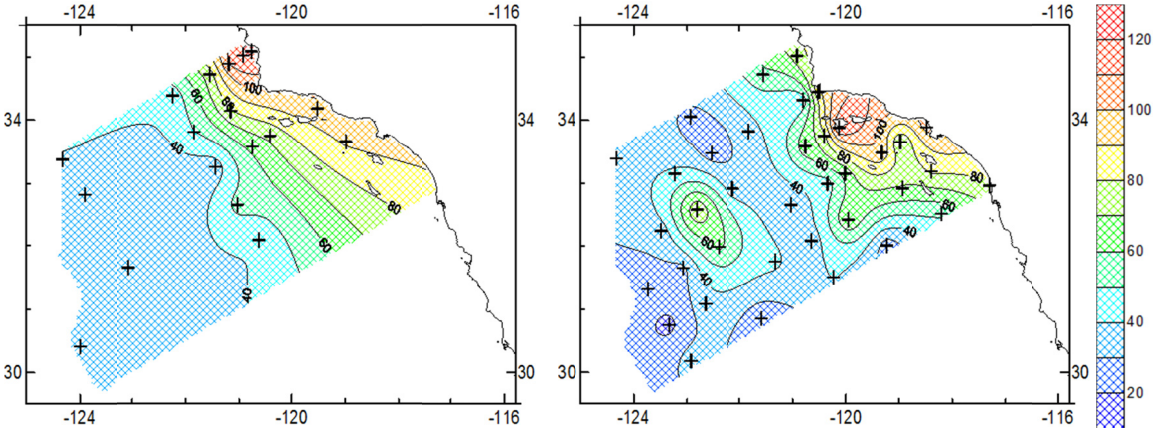

CalCOFI Cruise 0511NH

CalCOFI Cruise 0604NH

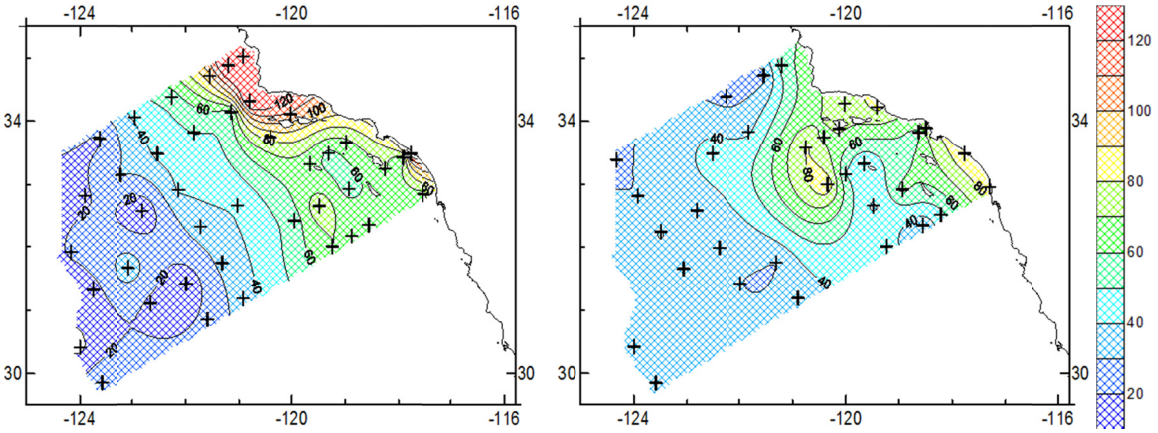

CalCOFI Cruise 0607NH

CalCOFI Cruise 0610RR

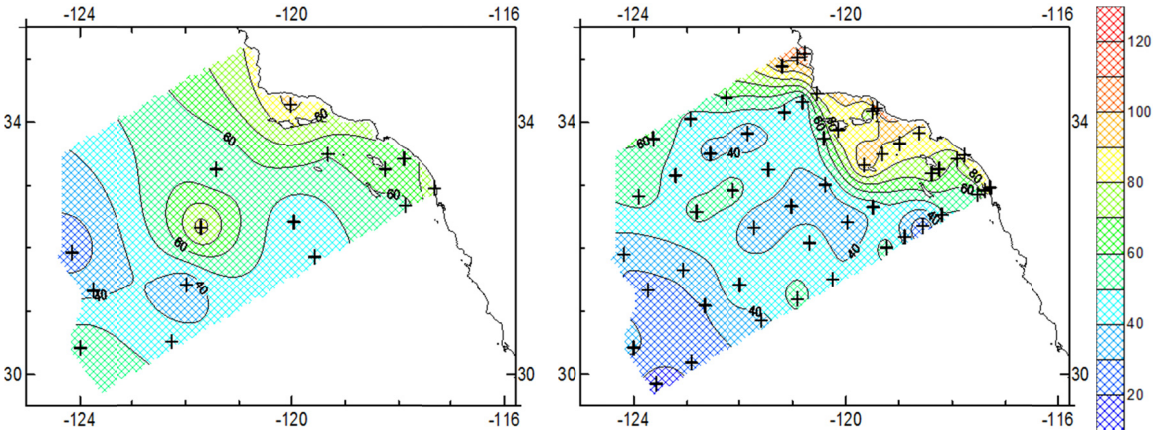

CalCOFI Cruise 0701JD

CalCOFI Cruise 0808NH

Figure 2.3: Contour maps of mixed layer $^{17}\Delta_{diss}$ in parts per meg for all six CalCOFI cruises.

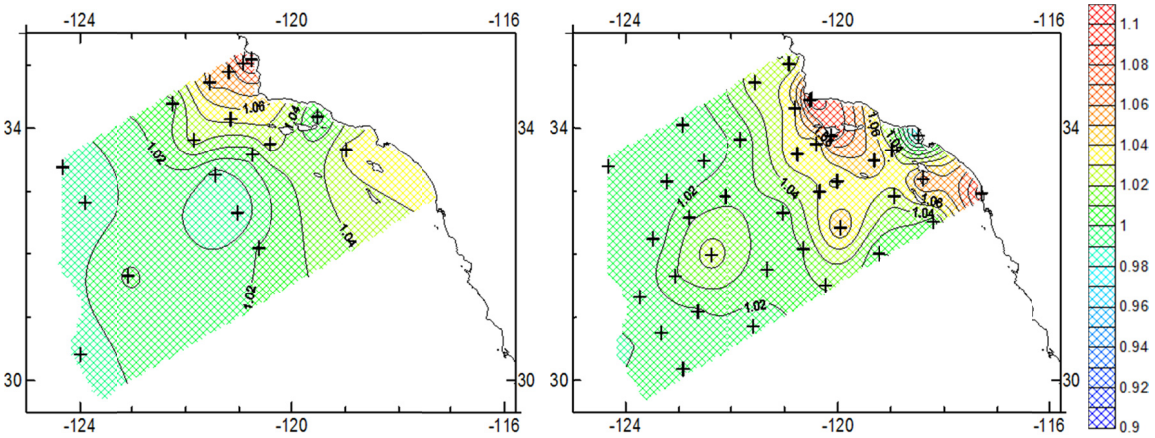

CalCOFI Cruise 0511NH

CalCOFI Cruise 0604NH

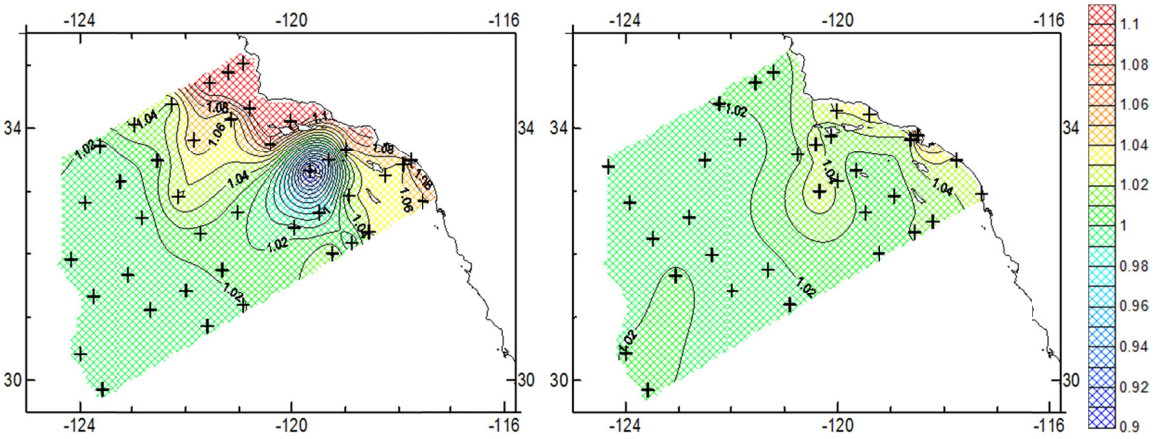

CalCOFI Cruise 0607NH

CalCOFI Cruise 0610RR

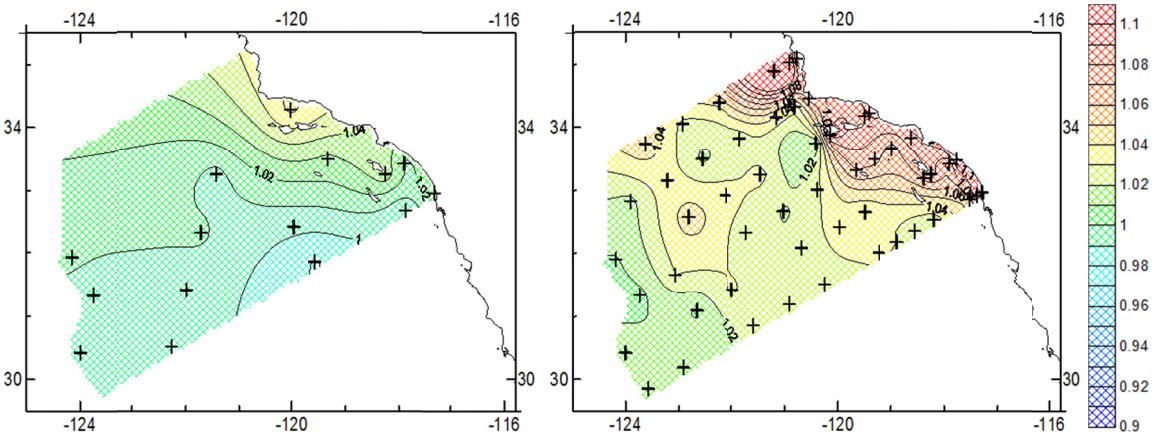

CalCOFI Cruise 0701JD

CalCOFI Cruise 0808NH

Figure 2.4: Contour maps of mixed layer biological O_2 saturation for all six CalCOFI cruises.

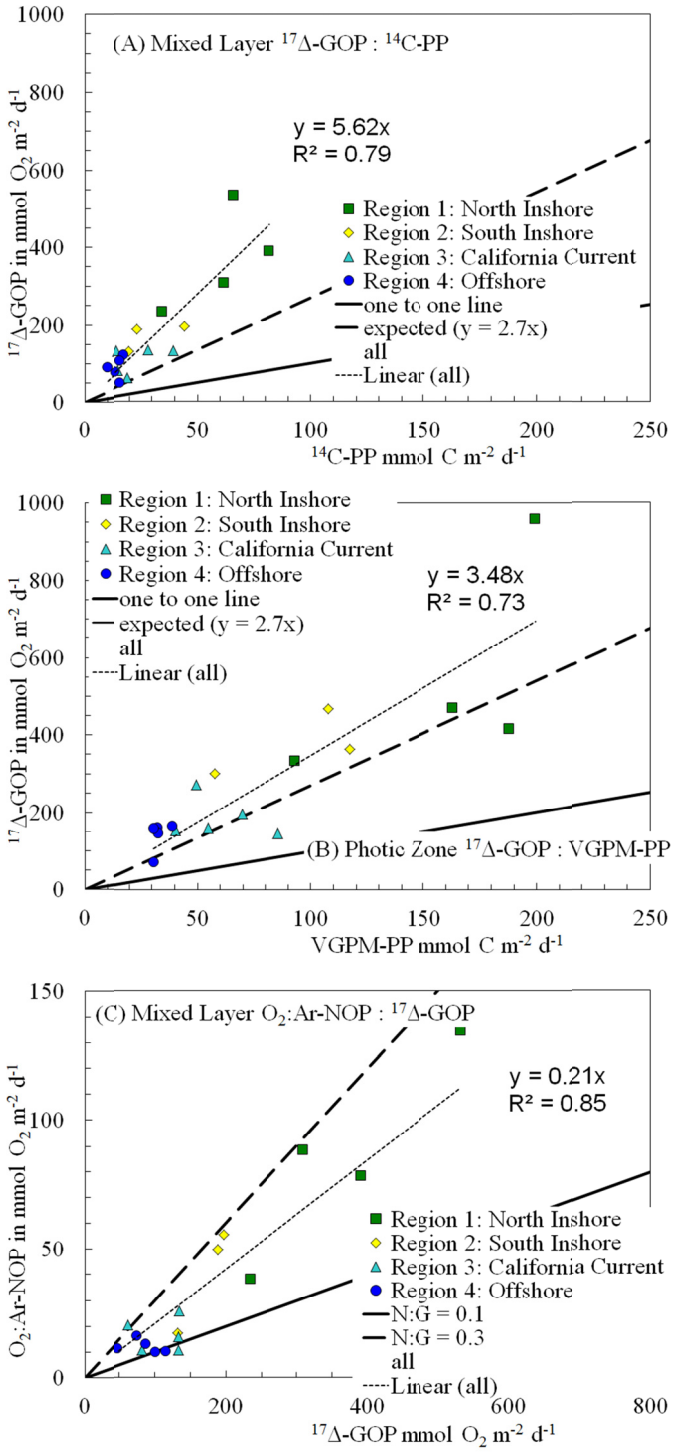

Figure 2.5: The relationship between (A) mixed layer $^{17}\Delta$-GOP and mixed layer $^{14}C\text{-}PP_{24h}$; (B) photic zone $^{17}\Delta$-GOP and photic zone VGPM-PP; and (C) mixed layer O_2:Ar-NOP and mixed layer $^{17}\Delta$-GOP for all cruises except 0701JD. Productivity calculations were not made for the January cruise 0701JD due to the entrainment bias discussed in the text. N:G – the ratio of net O_2 production to gross O_2 production.

Chapter 3: Multi-decadal records of net biological production rates in the southern California Current System based on dissolved oxygen and nitrate budgets

3.1 Introduction

Recent estimates suggest that 30-50% of global carbon export to the deep ocean may occur along continental margins (Dunne et al. 2007; Muller-Karger et al. 2005; Laws et al. 2000). The extreme spatial and temporal heterogeneity of continental margin ecosystems complicates efforts to estimate large-scale biogeochemical fluxes. For this reason, most global estimates of carbon export to the deep ocean rely on a series of algorithms to estimate both net autotrophic production and the fraction of production exported to the deep ocean (Dunne et al. 2007; Muller-Karger et al. 2005). While satellite estimates provide unmatched spatial and temporal resolution, validation of satellite and export algorithms using direct measurements of biological productivity and carbon export over a range of ecosystems is essential, but lacking.

The heterogeneity of continental margin environments also complicates efforts to estimate the air-sea CO_2 flux to the point that it is currently not known whether the coastal seas collectively represent a net source or sink to the atmosphere (Hales et al. 2008). Recent studies suggest that there is a strong latitudinal dependence on annual CO_2 flux such that many mesotrophic and eutrophic high latitude coastal environments are strong CO_2 sinks (Thomas et al. 2004; Hales et al. 2005) and many low latitude environments are sources of CO_2 to the atmosphere (Cai et al. 2006). Even within particular biogeochemical provinces there appears to be a large degree of variability in terms of air-sea CO_2 exchange. Along the West Coast of North America estimates of CO_2 flux off the Oregon Coast suggest that this region represents a sink of atmospheric CO_2 (Hales et al. 2005) whereas estimates further north off the Washington Coast

(Ianson and Allen 2002) and south off the central California Coast (Pennington et al. 2010) are much closer to neutral in terms of annual CO_2 exchange. The variability of biogeochemical estimates is undoubtedly due to the dynamic nature of upwelling systems, a lack of observations, and sensitivity to climate variability.

Eastern Boundary Current (EBC) systems such as the California Current System (CCS) are important both in terms of their contribution to global biogeochemical fluxes and because these productive systems support an enormous fraction of the global fisheries. EBC systems account for 35% of global annual wild fish catch (Kudela et al. 2008) and 11% of global export production (Chavez and Toggweiler 1995) despite covering just 1% of the ocean surface area. The CCS is sensitive to both the El Niño-Southern Oscillation (ENSO) (Kahru et al. 2002; Chavez et al. 2003) and the Pacific Decadal Oscillation (PDO) (Mantua et al. 1997; Chhak and Di Lorenzo 2007); climate variability has also been shown to have important ramifications for air-sea CO_2 exchange (Friederich et al. 2002), O_2 concentrations at depth (Deutsch et al. 2011), and fisheries (Rykaczewski et al. 2008). Globally, stratification resulting from warming may be driving a decline in marine productivity (Boyce et al. 2010) although in situ records from ocean time series sites suggest the opposite trend (Chavez et al. 2011). The response of EBC systems to climate change is uncertain; although stratification may be increasing (Di Lorenzo et al. 2005), it has been hypothesized that intensification of coastal upwelling in response to increased upwelling-favorable wind stress (Bakun 1990; Snyder et al. 2003) may increase primary production. Satellite observations suggest that primary production (PP) in the CCS and other EBC systems is increasing (Kahru and Mitchell 2008; Kahru et al. 2009) accompanied in many regions by decreasing O_2 concentrations at depth (Bograd et al. 2008; McClatchie et al. 2010). Clearly, accurate estimates of biological production and carbon export are critical to

understanding links between biological productivity, climate variability, air-sea CO_2 flux, hypoxia, and the health of coastal fisheries.

The California Cooperative Oceanic Fisheries Investigations (CalCOFI) program is one of the longest ongoing oceanographic sampling programs. The current sampling grid (Fig. 3.1) has been sampled regularly since 1984; the extensive hydrographic and PP datasets provide an unparalleled record of interannual and decadal trends in the CCS. O_2:Ar measurements collected on five CalCOFI cruises from 2006 to 2008 have shown that the O_2 saturation state largely reflects net biological productivity (D. Munro unpubl. manuscript). This relationship allows us to use the historical CalCOFI O_2 dataset to investigate interannual and decadal variability in net community production (NCP) in the southern CCS and compare results from this relatively new approach to past estimates using nutrient budgets (Bograd et al. 2001; Roemmich 1989), estimates of particle export (Stukel et al. 2011) and more recent approaches which utilize algorithms to estimate both PP (Behrenfeld and Falkowski 1997) and the fraction of productivity exported to the deep ocean (Dunne et al. 2007; Laws et al. 2000; Muller-Karger et al. 2005). The objectives of this study are 1) to determine temporal and spatial variability in NCP in the CCS utilizing budgets for nitrate and dissolved O_2 and 2) to compare budget-based estimates with concurrent satellite-based approaches and an estimate which utilizes the CalCOFI ^{14}C-based PP (^{14}C-PP) dataset.

3.2 Study Region

The CalCOFI grid has been regularly sampled since 1984 and includes 66 standard stations spread over 6 lines perpendicular to the Southern California coast extending southwest from Point Arguello to San Diego (Fig. 3.1). Station spacing ranges from less than 20 km close

to shore to approximately 75 km offshore. Cruises are conducted quarterly (typically in January, April, July or August, and October or November). We group stations into four regions based on physical setting and historical productivity rates (Fig. 3.1) as done by Munro et al. (submitted). The North Inshore region (Region 1) encompasses the high historical PP rates associated with the persistent upwelling feature off Point Conception. The South Inshore region (Region 2) includes the Southern California Bight (SCB) which has markedly lower productivity in comparison to other regions inshore of the California Current along the West Coast (Eppley 1992). The California Current region (Region 3) is distinguished by high equatorward transport via the California Current. The Offshore region (Region 4) has historical productivity rates that approach those of the oligotrophic subtropical North Pacific. Over the time interval of our investigation 1984-2010 there were 106 CalCOFI cruises.

3.3 Data Records

CalCOFI hydrographic data

A detailed sampling procedure for CalCOFI hydrographic and productivity sampling techniques is described on the CalCOFI website (http://www.calcofi.org/field-program/rosette-sampling.html) and in Mantyla et al. (1995); here we highlight several aspects relevant to this study. Hydrocasts are typically conducted to 515 m using a 24 Niskin rosette; ten to twelve depths are routinely sampled in the top 100 m for offshore regions with greater vertical resolution over the shelf and slope regions. The amount of dissolved O_2 in seawater is measured using the Carpenter modification (Carpenter 1965) of the Winkler method. Concentrations of macronutrients (nitrate, nitrite, silicate, phosphate, and ammonium) are measured using a Seal Analytical continuous-flow AutoAnalyzer 3 (AA3). ^{14}C-PP samples are collected from a mid-

morning cast each day at six depths determined by the photic zone depth (based on Secchi disk observations) and depth of the chlorophyll maximum. ^{14}C-PP experiments are conducted in on-board incubators from local apparent noon (LAN) to dusk; half-day productivities are converted to a 24 h rate using a factor of 1.81 (Eppley 1992). Approximately sixteen productivity measurements are conducted each cruise such that ^{14}C-PP experiments are conducted at three to five stations within each region.

Wind products

We used wind speed data (referenced to a height of 10 m) from the SeaWinds instrument on the QuikSCAT satellite processed daily on 0.5° × 0.5° fields for the period from 1998 to 2008 for all calculations of gas exchange rates, Ekman transports, and curl of the wind stress. QuikSCAT winds used for coastal upwelling calculations represent the grid points closest to shore but at least 25 km from the coast (NASA 2002) and no further than 50 km from the coast. For the periods from 1984-1998 and 2008-2010 ECMWF wind data processed daily on 0.5° × 0.5° fields was used for all calculations; for consistency, ECMWF winds were correlated to QuikSCAT wind speeds for each region. Both QuikSCAT and ECMWF winds were well correlated with NDBC buoy winds in Regions 1 and 2. All wind speeds used in gas exchange parameterizations were averaged using a ten day mean of the root mean square (the approximate residence time of O_2 in the mixed layer) ending on the last day hydrocasts were collected in a region. Similarly, Ekman transports were calculated by averaging over a ten day interval ending on the last day of sampling in a given region. Wind stress was calculated using the parameterization of Large et al. (1994).

Estimation of coastal upwelling, alongshore and offshore Ekman transports, and curl-driven upwelling

Coastal upwelling rates for Regions 1 and 2 were estimated by determining the offshore movement of water in response to the alongshore wind stress:

$$T = \frac{\tau_a}{\rho_w f} \quad (1)$$

Where T is equivalent to the volume of water upwelled in $m^3\ s^{-1}$ per m of coastline, τ_a represents the alongshore wind stress averaged spatially within 50 km of the coast for Regions 1 and 2 and temporally over the ten days prior to the last sampling day in a given region, ρ_w is the density of seawater upwelling into the surface layer ($kg\ m^{-3}$), and f is the Coriolis parameter (s^{-1}). An upwelling rate ($m\ s^{-1}$) for the nearshore zone can be calculated as follows:

$$w_{coast} = \frac{T}{R_d} \quad (2)$$

where R_d is the Rossby radius (m). A R_d of 25 km was used in this study consistent with past studies in the CalCOFI region (Checkley and Barth 2009; Pickett and Schwing 2006). It is important to note that the choice of R_d does not influence the magnitude of the coastal upwelling term which is dependent on the volume of water upwelled. The choice of R_d does however affect the relative proportion of the two inshore regions influenced by the curl-driven upwelling term described below.

Cross-shore Ekman transports were calculated by taking the ten day mean ending on the last day stations were occupied for the regions considered; transports were calculated parallel to

the lines of the CalCOFI grid for the boundaries separating Regions 1 and 3 and Regions 2 and 3 (Fig. 3.1). Alongshore Ekman transports were calculated for the boundary between Regions 1 and 2 (Fig. 3.1). Spatially, both zonal and alongshore transports are averages of all grid points within 25 km of the boundaries depicted in Fig. 3.1.

The rate of upwelling due to the curl of the wind stress was calculated as follows:

$$w_{curl} = \nabla \times \tau \frac{1}{\rho_w f} \quad (3)$$

where w_{curl} is the upwelling rate in m s^{-1} and $\nabla \times \tau$ is the curl of the wind stress field. As with Ekman transport, w_{curl} rates represent ten day averages ending with last day samples were taken in a region. Spatially, all grid points within each region were averaged except for points closest to shore in Regions 1 and 2 which were used to calculate the volume of water upwelled at the coast.

3.4 Methods: Estimating net community production

Nitrate budget approach

Net carbon production based on nitrate utilization for the two regions inshore of the California Current (Regions 1 and 2) was estimated by calculating the loss of nitrate that occurred between the time water was upwelled into the mixed layer and exported offshore into the region of the California Current (Region 3). Budgets for nitrate also include cross-shore Ekman transport terms for cruises where there was a shoreward Ekman transport from Region 3 to Regions 1 or 2. Alongshore Ekman transport was also calculated between Regions 1 and 2. The following nitrate budget was constructed to calculate NCP in terms of N for the surface

mixed layer:

$$h \times \Delta[NO_3^-]_{surface} / \Delta t = h \times (u/L_x) \times ([NO_3^-]_{surface\_x} - [NO_3^-]_{surface}) +$$
$$h \times (v/L_y) \times ([NO_3^-]_{surface\_y} - [NO_3^-]_{surface}) +$$
$$w_{coast} \times f_{coast} \times ([NO_3^-]_{up\_nearshore} - [NO_3^-]_{surface\_stn60}) +$$
$$w_{curl} \times f_{curl} \times ([NO_3^-]_{up\_offshore} - [NO_3^-]_{surface\_stn60}) -$$
$$NCP \quad (4)$$

where h (m) is the mixed layer depth; u and v represent cross-shore and alongshore velocities (m d^{-1}); w_{coast} is the upwelling rate (m d^{-1}) for f_{coast}, the fraction of the surface area of the region supplied by coastal upwelling; w_{curl} is the upwelling rate (m d^{-1}) for f_{curl}, the fraction of the surface area supplied by curl driven upwelling; $[NO_3^-]_{surface}$ (mmol m^{-3}) represents the surface layer nitrate concentration; $[NO_3^-]_{surface\_x}$ and $[NO_3^-]_{surface\_y}$ represent the upstream nitrate concentrations for cross-shore and alongshore transports; $[NO_3^-]_{up\_nearshore}$ represents the average nitrate concentration upwelled into the surface layer within the nearshore zone of an inshore region (i.e., within one Rossby radius, or 25 km, of the coast); $[NO_3^-]_{up\_offshore}$ represents the average nitrate concentration upwelled into the surface layer within the offshore zone of an inshore region (i.e., the fraction of an inshore region not included within the narrow coastal zone); $[NO_3^-]_{surface\_stn60}$ represents the average nitrate concentration for offshore stations in Regions 1 and 2 (i.e., stations west of the narrow coastal zone); L_x and L_y represent the horizontal length scales (m) over which the gradients in nitrate are considered (i.e., the cross-shore and alongshore dimensions of Regions 1 and 2); and NCP is a vertically integrated daily rate (mmol m^{-2} d^{-1}) in terms of N; NCP was converted to C assuming Redfield stoichiometry

(i.e., using a ratio of 106:16).

Nitrate budgets were also constructed for Regions 3 and 4 (i.e., the California Current and Offshore region) with several modifications. Alongshore transports in both regions were neglected since alongshore gradients in nitrate were small; likewise, cross-shore transport between Regions 3 and 4 was neglected because nitrate gradients were negligible. Cross-shore Ekman transports were included between Regions 1 and 3 and Regions 2 and 3. The depth of the water upwelled into the mixed layer via coastal upwelling and wind stress curl-driven upwelling was based on the depth of the Ekman layer for each region which was typically between 30 and 40 m for all regions. The nitrate concentration was averaged over the ten meters directly beneath the Ekman layer. The depth of the Ekman layer, De, was calculated as follows:

$$De = W \times \frac{3.2}{\sqrt{sin\theta}} \quad (5)$$

where W is the wind speed in m s^{-1}; θ is the latitude; and 3.2 is a constant in units of seconds which is a function of the density of air and water the wind drag coefficient and the rotation of the Earth (Messié et al. 2009).

O_2 budget approach

NCP based on net O_2 production within the mixed layer can be estimated using a budget based approach for dissolved O_2 similar to that for nitrate with an additional term for gas exchange. In addition, corrections must be made for the physical processes which influence the solubility of O_2 in the surface ocean, including warming/cooling and bubble injection. Since Ar acts as a biologically inert analog for O_2, the O_2:Ar saturation state, which equals the measured

dissolved O_2:Ar gas ratio divided by the O_2:Ar ratio expected at equilibrium with air (i.e., $[O_2:Ar]_{meas}$ / $[O_2:Ar]_{sat}$) (Craig and Hayward 1987), represents the portion of the O_2 saturation state that is biologically produced and a value greater than one represents net autotrophy and a value less than one represents net heterotrophy. The relationship between the O_2 saturation state and the biological O_2 saturation state has been determined for each region and season from measured O_2:Ar ratios during five CalCOFI cruises from 2006 to 2008 (Fig. 3.2) (D. Munro unpubl. manuscript) and used to estimate the biological O_2 saturation state for the extensive CalCOFI dataset. A budget for O_2 which includes the O_2:Ar correction can be constructed as follows:

$$
\begin{aligned}
h\times\Delta(C_{sat}\times(O_2:Ar)_{bio\_ml}) / \Delta t = {} & K_g\times C_{sat}\times(1 - (O_2:Ar)_{bio\_ml}) + \\
& h\times(u/L_x)\times C_x\times(1 - ((O_2:Ar)_{bio\_ml} / (O_2:Ar)_{bio\_x})) + \\
& h\times(v/L_y)\times C_y\times(1 - ((O_2:Ar)_{bio\_ml} / (O_2:Ar)_{bio\_y})) + \\
& w_{coast}\times f_{coast}\times C_{z\_nearshore}\times(1 - ((O_2:Ar)_{bio\_stn60} / (O_2:Ar)_{bio\_z\_nearshore})) + \\
& w_{curl}\times f_{curl}\times C_{z\_offshore}\times(1 - ((O_2:Ar)_{bio\_stn60} / (O_2:Ar)_{bio\_z\_offshore})) + \\
& NCP \qquad (6)
\end{aligned}
$$

where h is the mixed layer depth, K_g (m d^{-1}) is the gas transfer velocity based on an empirically determined function of wind speed specific to O_2; C_{ml} represents the mixed layer O_2 concentration (mmol m^{-3}); C_x and C_y represent the upstream O_2 concentrations for cross-shore and alongshore transports; $C_{z\_nearshore}$ and $C_{z\_offshore}$ represent the O_2 concentration below the mixed layer in the nearshore and offshore zones of an inshore region, respectively; and $(O_2:Ar)_{bio}$ represents the biological O_2 saturation in the mixed layer (ml) and for water transported cross-

shore (x), alongshore (y), via coastal upwelling (z_nearshore) and via curl-driven upwelling (z_offshore). NCP is vertically integrated through the mixed layer and converted from net O_2 to net carbon production using a photosynthetic quotient (PQ) of 1.4 (Laws 1991).

The gas transfer velocity, K_g, was calculated using the parameterization of Nightingale et al. (2000) which is a mid-range approach compared to the parameterizations of Wanninkhof (1992) and Liss and Merlivat (1986) and yields K_g values that are close to the estimates of Ho et al. (2006) for wind speeds typical of the CalCOFI region. The depth of water upwelled into the mixed layer (i.e., water from the 10 m beneath the Ekman layer) is the same as used for the nitrate budget above. Cross-shore advective transports for the two inshore regions (i.e., Regions 1 and 2), are included for the infrequent cruises where there is onshore Ekman transport from the California Current region to inshore regions. As with the nitrate budget approach, modifications are required for Regions 3 and 4 such that only cross-shore Ekman transports are included for Region 3 and no horizontal advective transports are included for Region 4 due to negligible gradients in biological O_2 saturation.

Ekman transports were considered in both nitrate and O_2 budget approaches described above but geostrophic transports were omitted. Geostrophic transports are primarily alongshore in the CalCOFI region where gradients in biogeochemical parameters typically are much smaller than in the cross-shore. Neglecting geostrophic transports led to a less than 5% underestimation/overestimation of annual nitrate and O_2-based NCP rates in Region 3 and negligible underestimation/overestimation in all other regions.

To confirm the assumption that steady state conditions were met for the NCP calculation, we compared surface water residence times to the dissolved O_2 residence times in the four regions described above by dividing the mean mixed layer depth by the mean gas exchange rate

as done by D. Munro (unpubl. manuscript). This represents a low-end estimate of the residence time for O_2 in the surface layer since horizontal and vertical advection are both significant terms in the O_2 budget, particularly for inshore regions. For Regions 1, 2, 3, and 4 the O_2 replenishment time due to air-sea exchange was 6, 7, 10, and 13 days, respectively. In comparison, for Region 1 the average water residence time was 11 days based on an average current velocity of 15 cm s^{-1} calculated from surface geostrophic and Ekman transports. Water residence times of 26, 17, and 26 days were determined for Regions 2, 3, and 4, respectively. For all regions, residence times for water were at least 2 to 4x greater than residence times for O_2, suggesting that mixed layer O_2, $^{17}\Delta_{diss}$, and O_2:Ar likely approached a steady state balance between biological production, air-sea gas exchange, and advection within each region.

During strong upwelling events, high offshore Ekman transport and steep sea surface height gradients decrease the residence time of water for regions inshore of the California Current such that the mixed layer O_2 saturation may not have time to reach steady state before it is advected offshore into the California Current region. During these conditions, the O_2 budget approach is no longer valid and will give unreasonably low NCP estimates due to large negative gas exchange terms. This condition only occurred in the Point Conception upwelling region (i.e., Region 1) during spring due to its smaller horizontal dimensions and high coastal upwelling rates and was identified when surface O_2 saturation was less than 95% (i.e., biological O_2 saturation of ~0.95). This condition occurred for only 3 out of the 106 cruises over the length of the time series (i.e., for the April 1995, 2007, and 2008 cruises). For all other regions, this condition was never met and O_2-NCP estimates assumed valid for all 106 cruises.

Satellite-based estimates of NCP

NCP was estimated from a satellite-based net primary production (NPP) model and combined with two commonly used algorithms of export efficiency (Dunne et al. 2007; Laws et al. 2000). The Vertically Generalized Productivity Model (VGPM) used to estimate NPP (Behrenfeld and Falkowski 1997) was acquired from the Ocean Productivity Group at Oregon State University (http://web.science.oregonstate.edu/ocean.productivity/custom.php)). Export efficiency was estimated following the Dunne et al. (2007) algorithm which is a function of sea surface temperature and surface chlorophyll concentration and the Laws et al. (2000) algorithm which is a function of sea surface temperature and (NPP). Multiplying the VGPM-based NPP by the export efficiency yields an estimate of NCP. For clarity, we will refer to each NCP estimate by identifying the export efficiency model used; NCP07 represents the VGPM coupled with the Dunne et al. (2007) algorithm and NCP00 represents the VGPM coupled with the Laws et al. (2000) algorithm. The VGPM model was chosen for this study because it has been used by many recent studies of the CCS (e.g., Kahru et al. 2009; Chavez and Messié 2009; Messié et al. 2009; Chavez et al. 2011).

NCP estimates based on ^{15}N uptake experiments and ^{14}C-PP

NCP was also estimated using the historical CalCOFI ^{14}C-PP dataset and f-ratios estimated for different regions of the CalCOFI grid by $^{15}NO_3^-$ and $^{15}NH_4^+$ uptake experiments. To calculate NCP we multiply the mean ^{14}C-PP for each region and cruise by an f-ratio (here equal to $^{15}NO_3^-$ uptake / ($^{15}NO_3^-$ +$^{15}NH_4^+$ uptake) or $^{15}NO_3^-$ uptake / ^{14}C-PP) representative for each region. The f-ratio represents a mean estimate based on uptake experiments conducted in each region; a value of 0.57 is used for the Point Conception upwelling region during the spring and summer based on the work of Dugdale and Wilkerson (1992), 0.36 is used for the South

Inshore region and for Region 1 during the fall and winter based on estimates by Eppley (1992), and 0.33 is used for the California Current and Offshore regions (Eppley 1992). For Regions 2, 3, and 4 the same f-ratio is used for all cruises and so the seasonality of this estimate is based entirely on variability in ^{14}C-PP. For clarity, we will refer to NCP estimated using ^{15}N and ^{14}C uptake experiments as ^{15}N^{14}C-NCP from hereon.

In closing our discussion of NCP methods, we emphasize an important difference between budget-based NCP estimates and the satellite-based and ^{15}N^{14}C-NCP approaches. NCP measured by budget-based approaches is equal to the amount of PP available for export whether by sinking flux as particulate organic matter (POM), conversion to dissolved organic matter (DOM), or transfer to higher trophic levels. In contrast, the satellite-based approaches and the ^{15}N^{14}C-NCP approach just estimate the particulate fraction of NCP (i.e., both the export production data incorporated into the NCP07 pe-ratio algorithm and the model represented by the NCP00 algorithm estimate particle export; in addition, $^{15}NO_3^-$ uptake includes just the particulate fraction filtered during uptake experiments). As a result, in regions where DOM and/or transfer to upper trophic levels are major components of NCP, budget estimates should be expected to exceed satellite-based and ^{15}N^{14}C-NCP estimates.

Previous O_2:Ar-NCP estimates for the CalCOFI region

Previous application of the O_2:Ar method for the CalCOFI region during 2005-08 by D. Munro (unpubl. manuscript) yielded annual O_2:Ar-NCP rates for the North Inshore region (560 ±157 mg of C m^{-2} d^{-1}) that were 5x rates in the Offshore region (109±33 mg C m^{-2} d^{-1}). Annual mean O_2:Ar-NCP for the CalCOFI grid of 210±64 mg C m^{-2} d^{-1} (6.4±2.0 mol C m^{-2} yr^{-1}) agreed within uncertainty with past nutrient budget based estimates of 240 and 327 mg C m^{-2} d^{-1}

(Roemmich et al. 1989; Bograd et al. 2001). In contrast, the O_2:Ar-NCP for the CalCOFI region during 2005-08 was 4x higher than ^{234}Th-based estimates of POC (123 mg C m^{-2} d^{-1}) for regions inshore of the California Current (Stukel et al. 2011). D. Munro (unpubl. manuscript) suggest several explanations for this disagreement between methods including 1) that organic material fixed in regions inshore of the California Current is advected horizontally into the California Current region, and 2) DOC represents an important part of the total organic carbon export flux. Agreement between surface mixed layer O_2:Ar-based (D. Munro unpubl. manuscript) and water column integrated (i.e., to a depth of 500 m) nutrient budget based NCP estimates of Roemmich (1989) and Bograd et al. (2001) implies little respiration of NCP exported out of the mixed layer within the coastal ocean or methodological biases.

3.5 Results

Major characteristics of multidecadal records used in nitrate and O_2-NCP estimates

Surface O_2 saturation – Mean annual surface O_2 saturation state was highest within inshore Region 2 (105.4%) and slightly higher than inshore Region 1 (104.5%) (Table 3.1). If we remove the influence of upwelling events in these two inshore regions by eliminating O_2 saturation measurements at stations where surface nitrate concentrations were greater than 0.5 mmol m^{-3} (20<% of stations), the mean O_2 supersaturation increases to 108.7% and 106.2 % for Regions 1 and 2, respectively. Surface O_2 saturations were significantly lower further offshore in Regions 3 (102.9%) and 4 (102.3%) (Table 3.1). The mean surface O_2 supersaturation (area weighted) for the entire CalCOFI grid was 103.5% (Table 3.1).

The seasonal range in O_2 saturation state (Fig. 3.3) was greatest in Region 1 with mean supersaturation for all summer cruises (108.6%) more than 5x mean winter supersaturation

(101.6%). Mean surface O_2 was undersaturated for 12 of 108 cruises for Region 1 and only observed during winter and spring cruises with the greatest O_2 undersaturation occurring during the strongest upwelling events in the spring. Region 4 exhibited the smallest range in O_2 saturation state with a winter mean of 101.5% and a summer mean of 102.6%. Notably, Regions 2, 3, and 4 were supersaturated with respect to O_2 all year round for all 106 cruises of the time series (Fig. 3.3).

Gas Exchange Velocity (K_g) – Mean annual K_g was highest for Region 1 (3.1 m d^{-1}) and lowest for Region 2 (2.5 m d^{-1}) which includes the sheltered Southern California Bight. The mean annual K_g for the entire CalCOFI grid was 2.8 m d^{-1}. Region 2 exhibited the greatest seasonal variability (Fig. 3.3) with a range in mean K_g from 1.9 m d^{-1} during fall cruises to 3.1 m d^{-1} in spring. Seasonal variability in K_g was smallest in Region 4 with a range from 2.6 m d^{-1} in fall to 3.3 m d^{-1} in spring. Seasonal mean K_g for all regions was highest during spring and minimums occurred during fall for Regions 2 and 4 and winter for Regions 1 and 3.

Coastal upwelling due to offshore Ekman transport – Mean annual offshore Ekman transport for Region 1 (91 metric tonnes of water upwelled s^{-1} per 100 m of coastline) was nearly 2x the mean for Region 2 (52 metric tonnes s^{-1} per 100 m of coastline). The seasonal range in offshore Ekman transport was similar in both regions with the maximum typically in spring and the minimum most often in winter for Region 1 and fall for Region 2.

O_2 % saturation at 40m for the nearshore zone of Regions 1 and 2 – The annual mean O_2 % saturation at 40 m for the nearshore zone (i.e., standard CalCOFI stations within 25 km of the coast) of Regions 1 and 2 was similar at 76.7% and 79.4%, respectively. The seasonal range was similar for both regions with lowest saturations in spring (mean of all spring cruises of 62.9% and 64.0% in Regions 1 and 2, respectively) and highest saturations in fall (85.0% and 89.8% for

Regions 1 and 2, respectively).

40 m nitrate concentration for the nearshore zone of Regions 1 and 2 – Annual mean 40 m nitrate concentration for the nearshore zones of Regions 1 and 2 was 10.7 and 8.5 mmol m^{-3}, respectively. Seasonal variability was similar for both regions; lowest nitrate occurred in winter (winter cruise mean of 7.1 and 5.2 mmol m^{-3} for Regions 1 and 2, respectively) and highest in spring (17.3 and 14.3 mmol m^{-3} for Regions 1 and 2, respectively).

Seasonal and spatial variability of multidecadal nitrate, O_2, satellite, and $^{15}N^{14}C$-based NCP estimates

Nitrate-based NCP

Annual mean nitrate-NCP for Region 1 (456±64 mg C m^{-2} d^{-1}) was nearly 3.5x nitrate-NCP in Region 2 (131±24 mg C m^{-2} d^{-1}) (Table 3.2; Fig. 3.4) and more than an order of magnitude greater than Region 3 (30±10 mg C m^{-2} d^{-1}) and Region 4 (<1 mg C m^{-2} d^{-1}) estimates (Table 2). The annual mean for the entire CalCOFI grid was 101±14 mg C m^{-2} d^{-1} (3.1±0.4 mol C m^{-2} yr^{-1}) where the uncertainty represents the 95% confidence interval as determined by 2x the standard error for all annual means over the length of the time series as discussed below. Nitrate-NCP was lowest in winter and highest during spring for all regions (Table 3.2; Fig. 3.5); rates during spring cruises were 8.9, 13.5, 73, and 11.3x rates during winter cruises for Regions 1, 2, 3, and the entire CalCOFI grid, respectively.

O_2-based NCP

Annual mean O_2-NCP in Region 1 (616±65 mg C m^{-2} d^{-1}) was 1.8, 4.2, and 5.5x rates in Regions 2, 3, and 4, respectively (Table 3.2; Fig. 3.4) where uncertainty was calculated in the

same way as for nitrate-NCP. The annual mean for the CalCOFI grid was 240±19 mg C m^{-2} d^{-1} (7.3±0.6 mol C m^{-2} yr^{-1}). Minimum O_2-NCP occurred in winter for Region 1 (205±74 mg C m^{-2} d^{-1}), fall for Region 2 (176±29 mg C m^{-2} d^{-1}), and summer for Regions 3 and 4 (112±24 and 59±15 mg C m^{-2} d^{-1}, respectively) (Table 3.2; Fig. 3.5). Maximum O_2-NCP occurred in spring for all regions except Region 4 where winter rates and spring rates were nearly equivalent (Table 3.2; Fig. 3.4). Seasonal variability was greatest in the two inshore regions; spring rates were greater than winter rates by 4.7 and 3.6x in Regions 1 and 2, respectively, compared to 1.2 and 0.9x in Region 3 and 4, respectively (Table 3.2). For the CalCOFI grid, area-weighted O_2-NCP during spring was 2.3x winter rates (Fig. 3.5).

Satellite-based NCP

NCP07 and NCP00 were calculated monthly for the period from late 1997 to early 2009 using VGPM data provided by the OSU Ocean Productivity website and the Dunne et al. (2007) and Laws et al. (2000) export efficiency algorithms as described above. Annual mean NCP07 in Region 1 (484±70 mg C m^{-2} d^{-1}) was 2.1, 3.9, and 9.3x rates in Regions 2, 3, and 4, respectively (Table 3.1) where uncertainty was calculated in the same way as for nitrate and O_2-NCP. Annual mean Dunne et al. (2007) pe-ratios for Regions 1, 2, 3, and 4 were 0.32, 0.25, 0.20, and 0.14, respectively; the mean pe-ratio for the entire grid was 0.19 (Table 3.5). The annual mean NCP07 for the CalCOFI grid was 171±20 mg C m^{-2} d^{-1} (5.2±0.6 mol C m^{-2} yr^{-1}) (Table 3.2). Annual mean NCP00 in Region 1 (585±58 mg C m^{-2} d^{-1}) was 2.1, 3.5, and 7.9x rates in Regions 2, 3, and 4, respectively. Laws et al. (2000) pe-ratios for Regions 1, 2, 3, and 4 were 0.38, 0.28, 0.26, and 0.18, respectively; the mean pe-ratio for the CalCOFI grid was 0.26.

NCP07 was highest in spring for regions inshore of the California Current; NCP07

estimates for Region 3 were highest in spring and summer and Region 4 estimates were highest in winter and spring (Table 3.2; Fig. 3.5) similar to the seasonality in O_2-based NCP. NCP07 was lowest in fall and winter for all regions except Region 4 with the differences between these two seasons typically within estimate uncertainties (Table 3.2); seasonality was mainly a result of variability in satellite chlorophyll (Table 3.5). Seasonal variability was greatest in Regions 1 and 2; spring rates were 2.5x winter rates in Region 1 and 2.4x fall rates in Region 2 (Fig. 3.4). Seasonal patterns were similar for the NCP00 with a similar seasonal range in the two inshore regions and consistent NCP throughout the year in the offshore regions (Table 3.2; Fig. 3.5). For the CalCOFI grid, area-weighted NCP07 and NCP00 during spring were 1.8 and 1.9x fall rates, respectively.

$^{15}N^{14}C$-based NCP

Annual mean $^{15}N^{14}C$-NCP for Region 1 (750±54 mg C m^{-2} d^{-1}) was 2.4, 5.5, and 9.3x rates in Regions 2, 3, and 4, respectively (Table 3.1) where uncertainty was calculated in the same way as for nitrate-NCP. The annual $^{15}N^{14}C$-NCP mean for the CalCOFI grid (244±12 mg C m^{-2} d^{-1} (7.4±0.4 mol C m^{-2} y^{-1}) was within the uncertainty of the O_2-NCP estimate (Table 3.2). $^{15}N^{14}C$-NCP was lowest in fall and winter and highest in spring for all regions except Region 4 where seasonality was not distinguishable (Table 3.2; Fig. 3.5). As with all other methods, seasonality was greatest in Regions 1 and 2; spring rates were 4.4, 2.1, and 1.3x winter rates in Regions 1, 2, and 3, respectively. Unlike the NCP07 and NCP00 estimates where seasonality is a function of both variability in the pe-ratio and VGPM-PP, seasonality in $^{15}N^{14}C$-PP is entirely dependent on variability in the ^{14}C-PP estimate as seasonally averaged f-ratios were not available except for Region 1 where an f-ratio 0.57 was used for spring/summer and 0.36 for fall and

winter. For the CalCOFI grid, area-weighted $^{15}N^{14}C$-NCP during spring was 1.9x winter rates (Fig. 3.5).

Error analysis

Uncertainty in O_2-based and nitrate-based NCP for individual cruises and regions was estimated using a Monte Carlo analysis similar to the approach described in Juranek and Quay (2005). A mean value and error (±1 SD) was assigned to each term in Eqs. 4 and 6, a value for each term was randomly selected assuming a normal distribution, and O_2-NCP and nitrate-NCP calculated. The random selection process and calculations were repeated 1000 times and the uncertainty was calculated as ±1 SD for all 1000 values.

Assigned errors (±1 SD) for the parameters in Eqs. 4 and 6 applied in the Monte Carlo analysis are as follows: 25% for K_g (i.e., the range in K_g for different gas exchange parameterizations); 0.2% for C_{sat}; 0.3% to 1.5% for $(O_2{:}Ar)_{bio\_ml}$ (i.e., a combination of the error in the slope used to calculate biological O_2 saturation from surface O_2 saturation shown in Fig. 3.2 and the typical standard error of all mixed layer values averaged for each region and cruise); 10% for $(O_2{:}Ar)_{bio\_z}$ (i.e., the range of different estimates for $(O_2{:}Ar)_{bio\_z}$ depending on the depth upwelled into the mixed layer); 7 mmol m^{-3} for the mixed layer O_2 concentrations (i.e., the typical SD of all mixed layer O_2 measurements within each region); 30 mmol m^{-3} for C_z for both coastal and curl-driven vertical transports (i.e., the range of different estimates for C_z depending on the depth upwelled into the mixed layer); 0.2 mmol m^{-3} for $[NO_3^-]_{surface}$ (i.e., the typical SD of all mixed layer estimates within each region); 6 mmol m^{-3} for $[NO_3^-]_{up}$ for both coastal and curl-driven vertical transports (i.e., the range of different estimates for $[NO_3^-]_{up}$ depending on the depth upwelled into the mixed layer); 15% for all Ekman transports (i.e., the typical SD of all

transport estimates across a given boundary); and 0.02 m d^{-1} for w_{curl} in all regions (i.e., the typical SD of individual w_{curl} estimates within a given region).

Application of the Monte Carlo method described above yielded median uncertainties of individual O_2-NCP estimates of ±239, ±94, ±52, and ±37 mg C m^{-2} d^{-1} for Regions 1, 2, 3, and 4, respectively; median uncertainties for individual nitrate-NCP estimates was ±272, ±107, ±42, and ±32 mg C m^{-2} d^{-1} for Regions 1, 2, 3, and 4, respectively. As mentioned above, uncertainty in seasonal and annual means was estimated for all productivity estimates at the 95% confidence interval using 2x the standard error for all estimates over the length of the time series (Table 3.2). Uncertainty in the seasonal and annual means calculated using the 2x the standard error approach was typically much smaller than uncertainty in individual estimates (e.g., uncertainty in annual O_2-NCP is less than one third the median estimate for individual cruises). This result is due in part to the fact that our uncertainty calculation for individual estimates takes into account systematic errors which affect the accuracy of our estimates including the range of gas exchange parameterizations used to estimate the rate of K_g and the range of estimates of the depth of water upwelled into the mixed layer via coastal and curl-driven upwelling.

The depth of upwelling used in O_2 and nitrate budgets represents one of the greatest sources of systematic error in budget-based approaches particularly for regions inshore of the California Current (i.e., the uncertainty in the concentration of O_2 and nitrate upwelled into the mixed layer represents 45% and 80% of the uncertainty for individual O_2-NCP and nitrate-NCP estimates in Region 1, respectively). This uncertainty is due to high temporal and spatial variability in the depth of upwelling (Chhak and Di Lorenzo 2007; Messié and Chavez 2009) and other factors which influence the depth of upwelling such as deviations in bottom topography and the shape of the coastline (Hickey and Banas 2008). The uncertainty of the upwelling depth

is most dramatic for the nitrate budget due to the dominance of upwelling term as discussed below.

Magnitude of terms in O_2 and nitrate budgets

A summary of the magnitude of terms in the O_2 and nitrate budgets used to estimate NCP rates is presented in Table 3.3. As described above, the notable difference in these two budget approaches is that gas exchange represents a major term in the O_2 approach. The importance of the gas exchange term relative to total O_2-NCP increased moving offshore; gas exchange represented 39, 68, 97, and 91% of annual O_2-NCP in Regions 1, 2, 3, and 4, respectively. The coastal upwelling term represented 58 and 24% of annual O_2-NCP in Regions 1 and 2, respectively. All other terms (i.e., curl-driven upwelling, horizontal advection, and time rate of change) represented less than 10% of annual O_2-NCP in all regions (Table 3.3). In contrast, coastal upwelling accounted for nearly all of nitrate-NCP in Region 1 with all other terms accounting for less than 5% of annual nitrate-NCP. Coastal upwelling accounted for 76% of nitrate-NCP in Region 2 with curl-driven upwelling accounting for nearly all of the remainder. Horizontal transports from regions inshore of the California Current accounted for 97% of all nitrate-NCP in Region 3. Curl-driven upwelling of nitrate into the mixed layer was insignificant in both Regions 3 and 4 (Table 3.3).

The dominance of the coastal upwelling term in the nitrate budget approach makes the nitrate-NCP approach inherently less accurate than the O_2-NCP approach because we can estimate air-sea O_2 gas flux more accurately than nitrate transport. As an example of the sensitivity of nitrate-NCP to the depth of upwelled water, we calculate O_2-NCP and nitrate-NCP assuming a depth of upwelling of 60 m as used by Messié and Chavez (2009) and compare this

result to our Ekman layer based estimate. Using this deeper upwelling depth increases O_2-NCP for the CalCOFI grid by 28% (from 240 to 307 mg C m^{-2} d^{-1}) and nitrate-NCP by 82% (from 101 to 184 mg C m^{-2} d^{-1}). Because the CalCOFI grid extends well into the oligotrophic North Pacific where the gas exchange term dominates the O_2 budget, we believe the O_2-NCP approach provides a more accurate estimate of NCP for the entire grid as discussed below.

3.6 Discussion

Comparison of NCP approaches

The strong correlation between NCP results for O_2-based, nitrate-based, and $^{15}N^{14}C$-NCP approaches for Region 1 (Fig. 3.6) indicates that all approaches identify strong seasonal variability of NCP in upwelling regions inshore of the California Current. High spring O_2-based and nitrate-based NCP in regions inshore of the California Current results from high upwelling rates and high subsurface nitrate (low O_2) (Table 3.1; Table 3.3). However, the highest $^{15}N^{14}C$-NCP also occurs in spring which is independent of upwelling rate and supports seasonal trends in the O_2 and nitrate budget based NCP estimates (Fig. 3.5).

We acknowledge that the significant correlation between O_2 and nitrate-based NCP for Regions 1 and 2 (Fig. 3.6) is due in part to the importance of upwelling terms in common to both budgets as discussed above. However, we can demonstrate the independence of agreement between the two approaches by estimating NCP using an alternate O_2 budget where we estimate NCP from the gas exchange term only, neglecting transport and upwelling terms from Eq. 6. In this modified budget we eliminate the influence of upwelling on the O_2 budget by dropping from spatial averages all stations which exhibit characteristics of recently upwelled water (i.e., stations where the surface concentration of nitrate exceeds 0.5 mmol m^{-3}). Recently upwelled water

typically has nitrate concentrations greater than 10 mmol m^{-3}, thus we assume that stations where nitrate is less than 0.5 mmol m^{-3} have been at the surface for at least 5 to 7 days (i.e., close to the residence time of O_2 in the mixed layer for Region 1) allowing the O_2 budget to be represented by a balance between gas exchange and NOP. Annual NCP calculated using this alternate O_2 approach agrees with the rigorous O_2 budget estimates for Region 1 and the CalCOFI grid within the uncertainty of both methods (i.e., alternate approach yields annual NCP of 548±62 and 213±15 mg C m^{-2} d^{-1} for Region 1 and the CalCOFI grid, respectively, compared to 616±65 and 240±19 mg C m^{-2} d^{-1}, respectively, for the approach used in Eq. 6). This result is relatively insensitive to the nitrate concentration used to identify recently upwelled water (i.e., we achieve similar results by excluding all stations with nitrate greater than 1 or 2 mmol m^{-3} instead of 0.5 mmol m^{-3}) The estimates presented here also agree well with previous nutrient-based approaches for upwelling regions of the CCS (Messié et al. 2009; Pennington et al. 2010) (Table 3.2).

For Regions 2, 3, and 4, O_2-NCP and $^{15}N^{14}C$-NCP are considerably higher than nitrate-NCP. Annual O_2-NCP and $^{15}N^{14}C$-NCP are 2.6 and 2.4x annual nitrate NCP in Region 2 and 4.8 and 4.5x annual nitrate-NCP in Region 3, respectively. Horizontal transport from Regions 1 and 2 accounts for nearly all nitrate-NCP for Region 3 and the supply of nitrate to the mixed layer via curl-driven upwelling is insignificant in both Regions 3 and 4. Certainly, our low nitrate-NCP estimates in regions offshore of the California Current result in part from Ekman layer depths which are much shallower than typical photic zone depths (i.e., the Ekman layer depth is typically around 30 m and the photic zone depth around 80 m in Region 4) meaning that nitrate is depleted to a much deeper depth compared to regions inshore of the California Current. Even if we increase the depth of nitrate upwelled into the photic zone via curl-driven upwelling to 100 m, which is more than three times the typical Ekman layer depth, nitrate-NCP in Region 4 is still

less than 25% of O_2 and $^{15}N^{14}C$-NCP estimates (i.e., nitrate-NCP of 19±6 compared to O_2-NCP and $^{15}N^{14}C$-NCP estimates of 113±9 mg C m^{-2} d^{-1} and 81±6 mg C m^{-2} d^{-1}, respectively). In contrast, the gas exchange term is dominant in the O_2-based approach for Regions 2, 3, and 4 (Table 3.3).

We believe that the O_2-budget approach, which is dominated by the gas exchange term, provides a more accurate estimate of NCP for Regions 2, 3, and 4 than the nitrate budget approach due to the difficulty of quantifying all sources of imported N into the surface layer. We note that our O_2-budget estimate for Region 4 agrees with previous estimates for the subtropical North Pacific including a rigorous O_2-budget estimate at the Hawaii Ocean Time Series (HOT) by Emerson et al. (2008) (135±62 mg C m^{-2} d^{-1}) and O_2:Ar-NCP estimates for HOT by Quay et al. (2010) (120±35 mg C m^{-2} d^{-1}). Our annual O_2-NCP estimates are also within 20% of rates estimated using budgets for dissolved inorganic carbon (DIC) and $DI^{13}C$ for the oligotrophic Pacific Ocean by Quay et al. (2009) (85 mg C m^{-2} d^{-1}). This result indicates that sources other than Ekman pumping must be responsible for supplying a significant fraction of new N to the photic zone in Regions 2, 3, and 4. This result is consistent with previous studies which suggest that sources other than diffusive transport and Ekman pumping must be important sources of new N in the oligotrophic North Pacific at HOT (Chavez et al. 2011) which is similar in setting to the offshore regions of the CalCOFI grid. In oligotrophic regions of the North Pacific, eddy-pumping (McGillicuddy et al. 2007), vertical migration of phytoplankton (Letelier et al. 1996; Johnson et al. 2010), and N_2-fixation (Zehr and Paerl 2008) may all be important to supporting PP and NCP. In addition, geostrophic transports from outside the CalCOFI region and winter convection may be important sources of new N as suggested by Mantyla et al. (2008).

Budget based approaches versus satellite estimates

The two satellite-based NCP methods presented here, NCP07 and NCP00, yield annual rates for the CalCOFI grid which are closer to the O_2-NCP (and $^{15}N^{14}C$-NCP estimates) than the nitrate-NCP estimate (Table 3.2). Annual NCP00 for the CalCOFI grid (223±23 mg C m^{-2} d^{-1}) is within the uncertainty of both annual O_2-NCP (240±19 mg C m^{-2} d^{-1}) and $^{15}N^{14}C$-NCP (244±12). In contrast, annual NCP07 (171±20 mg C m^{-2} d^{-1}) was ~30% below annual O_2-NCP (and $^{15}N^{14}C$-NCP) for the CalCOFI grid (Table 3.2). Regional comparisons of satellite and budget based approaches indicate more significant differences (Fig. 3.4). Annual O_2-NCP, $^{15}N^{14}C$-NCP, and NCP00 were 2.3, 1.7, and 1.5x NCP07 (49±6 mg C m^{-2} d^{-1}) for Region 4, respectively (Table 3.2). The NCP07 estimate is low in comparison to NCP00, O_2-NCP, and $^{15}N^{14}C$-NCP for Region 4 due in part to a pe-ratio estimate for this region which is significantly lower than the NCP00 estimate (Table 3.5). In contrast, O_2-NCP, $^{15}N^{14}C$-NCP, and NCP00 for Region 1 were 1.3, 1.5, and 1.2x NCP07 (484±70 mg C m^{-2} d^{-1}) for Region 1, respectively. The $^{15}N^{14}C$-NCP approach was highest for Region 1 due in part to a spring and summer f-ratio estimate for that region of 0.57 (Dugdale and Wilkerson 1992) which is significantly greater than the pe-ratio predicted by both the Dunne et al. (2007) and Laws et al. (2000) algorithms. The estimate of 0.57 may be an overestimate for Region 1 due to lack of spatial and temporal coverage of the ^{15}N uptake experiments surrounding the upwelling center off Point Conception. For Region 1, annual NCP00 agrees with O_2-NCP and annual NCP07 agrees with annual nitrate-NCP within the estimate uncertainty (Table 3.2). Even so, this comparison suggests that either the VGPM may increasingly underestimate net autotrophic production moving into less productive offshore regions or the Dunne et al. (2007) algorithm increasingly underestimates the pe-ratio moving offshore.

Although uncertainties remain with regard to the accuracy of the VGPM in the CalCOFI region, comparison of O_2-NCP to the VGPM provides an estimate of export efficiency which we can compare to the export efficiency estimates predicted by Dunne et al. (2007) and Laws et al. (2000) (Table 3.5). The O_2-NCP:VGPM ratio yields estimates for Region 4 that are 2.2 and 1.4x higher than ratios predicted by the Dunne et al. (2007) and Laws et al. (2000) algorithms, respectively (we do not calculate an e-ratio estimate for the nitrate-based approach for this region because we assume that significant inputs of new N to the photic zone in the oligotrophic North Pacific are missing from our budget as discussed above). While it is possible that our O_2 approach overestimates NCP, we note that our O_2-NCP estimates for Region 4 are close to rigorous budget estimates for the oligotrophic North Pacific as mentioned above. More likely, the O_2-NCP:VGPM e-ratio estimate is higher because it includes both the dissolved and particulate components of the export flux whereas the Dunne et al. (2007) and Laws et al. (2000) algorithms only include the particulate fraction of the export flux. It is worth noting that the annual NCP00 for Region 4 is nearly identical to the ^{234}Th-POC export estimates of Stukel et al. (2011) for the region offshore of the California Current (Table 3.2). At HOT, the fraction of organic carbon export as DOC has been estimated at 15-33 % (Emerson et al. 1997; Hansell et al. 1998; Benitez-Nelson et al. 2001). Agreement between O_2-NCP and POC estimates for Region 4 would require the DOC fraction to be larger: 57% for NCP07 and 35% for NCP00.

Decadal variability in NCP estimates

Comparisons of budget-based and in situ NCP estimates to well-established climate indices such as the Multivariate ENSO Index (MEI; Wolter and Timlin 1998), the Pacific Decadal Oscillation (PDO; Mantua et al. 1997), and the North Pacific Gyre Oscillation (NPGO;

Di Lorenzo et al. 2008) are complicated by event-scale variability and limited temporal coverage of CalCOFI cruises (i.e., the MBARI time series conducts 18-24 cruises per year in comparison to 4 cruises per year at CalCOFI), particularly during the productive spring and summer months. During some years, the spring and summer cruises coincided with strong upwelling events which may not be representative of the entire upwelling season while at times cruises coincided with relaxation events. To evaluate interannual and decadal variability, anomalies for O_2, nitrate, $^{15}N^{14}C$ and satellite based NCP were calculated on quarterly intervals using monthly time series means (Fig. 3.6) by differencing each cruise estimate from the time series mean (1984-2010) for that month (Fig. 3.7), which follows the approach applied to the MBARI time series by Chavez et al. (2011). Records of NCP anomalies were then compared to climate indices (Fig. 3.8) for the same interval. All NCP records show similar deviations over the length of the time series with several trends worthy of discussion.

ENSO events clearly have a strong impact on NCP in the CCS as noted by previous studies including Chavez et al. (2002) and Kahru and Mitchell (2002). The 1998 El Niño event coincides with negative NCP anomalies in all methods with O_2-NCP and NCP00 showing the largest deviations. Other significant El Niño events also coincide with negative NCP anomalies including the 1987 and 1992 El Niño events. The correlation between the negative NCP anomalies from 1991-94 and the consistently positive MEI index is remarkable (Fig. 3.7; Fig. 3.8). This period is also characterized by a positive PDO signal indicating warm conditions in the northeast Pacific and a consistent and strongly negative NPGO signal indicating weaker than normal equatorward flow in the California Current (Fig. 3.7; Fig. 3.8). The most likely explanation for reduced NCP estimates is a reduction in annual mean nitrate at a depth of 40 m in the nearshore zones of Region 1 and 2 during these El Niño events (Fig. 3.3). The nitrate

concentration at 40 m decreased from the record-long (1984-2010) mean by 35-50% in Regions 1 and 2, respectively, during the El Niño events in 1991-1992 and 1998. Upwelling rates were also depressed during these events, particularly during 1991-92. The correlation between strong El Niño events and low NCP is consistent with the nutrient-budget result of Bograd et al. (2001) who found that non-ENSO years were 70% more productive than El Niño years from 1984-97. The NCP response to weaker El Niño events typical of the last decade is less clear. For example, the most recent El Niño event in 2009-10 coincided with positive NCP anomalies for all methods. Although the PDO index was also weakly positive during this event, the NPGO was strongly positive indicating strong equatorward flow in the California Current almost continuously since the late 1990's (Fig. 3.8). The NCP response to La Niña events appears to be insignificant over most of the time series with the exception of the strong 2008 event which coincided with significant positive NCP anomalies in all methods.

Chavez et al. (2011) and others have suggested that a significant transition in the CCS may have occurred following the strong 1997-98 El Niño event. This transition coincides with a shift in the PDO towards more negative values marked by cooler conditions in the northeast Pacific and a shift in the NPGO toward more positive values marked stronger equatorward flow in the California Current (Fig. 3.8) (Bjorkstedt et al. 2011). Chavez et al. (2011) note that this transition also coincides with dramatic increases in the concentration of nitrate at 60 m, surface chlorophyll concentrations, and ^{14}C-PP at the MBARI time series off central California particularly from 2005-2010. In comparison, mean O_2 and nitrate-NCP for the CalCOFI grid estimated for 1999-2010 was not significantly different than the mean value for 1984-1998 (Table 3.4), whereas the mean $^{15}N^{14}C$-NCP since 1998 was slightly (15%), but significantly,

higher than before 1998 (Table 3.4). Thus the NCP estimates at CalCOFI don't consistently support a significant regime shift in the CCS since 1998.

The most recent portion of the record since 2007 exhibits the longest stretch of positive NCP anomalies in the time series with deviations of similar magnitude for all NCP methods (Fig. 3.7). This period coincides with high nitrate concentrations at depth, strong winds and strong upwelling particularly in the Point Conception upwelling region (Region 1) (Fig. 3.3). The current interval of consistently positive NCP anomalies coincides with a negative phase in the PDO, a positive phase of the NPGO, and only one El Niño event. It will be interesting to see how long these conditions persist.

Significance of decadal records of export production in the southern CCS

We highlight several observations and implications regarding the NCP estimates presented here.

1. Annual O_2-NCP, nitrate-NCP, $^{15}N^{14}C$-NCP, NCP07, and NCP00 estimates vary by 5-10x from the productive regions inshore of the California Current to the oligotrophic portion of the CalCOFI grid.

2. Seasonality of the NCP estimates generally was greatest in regions inshore of the California Current. Spatially-weighted NCP for the CalCOFI grid generally were highest in spring and decreased by half during winter.

3. Regional O_2-NCP estimates and the surface O_2 saturation state suggest that the CalCOFI grid is autotrophic year round with no large-scale regions of net heterotrophy observed during any

cruises from 1984-2010.

4. O_2-NCP rates provide a more accurate estimate of NCP compared to the nitrate-based approach for the CalCOFI grid because of the uncertainty in estimating the depth and rate of upwelling which dominates the nitrate-based NCP estimates; in contrast, the gas exchange term dominates the O_2-based NCP estimates. For Regions 3 and 4 the nitrate approach significantly underestimates NCP compared to all other methods because processes other than curl-driven upwelling and horizontal advection are important in supporting new production.

5. O_2-NCP estimates are significantly greater than satellite-based NCP estimates for the offshore oligotrophic region of the CalCOFI grid (i.e., Region 4) most likely due to one or a combination of the following: the importance of DOC as a significant fraction of NCP, VGPM underestimation of NPP, and/or that commonly used algorithms underestimate the e-ratio in the oligotrophic North Pacific.

6. The time series of budget-based NCP estimates clearly shows lower NCP in response to strong El Niño events (e.g., 1992, 1998) but an insignificant response to weaker El Niño events. The NCP anomalies for La Niña events are generally indistinguishable from non-ENSO years. Although positive NCP anomalies occur more frequently for the period of the record since 1999 compared to prior to 1999, which is similar to the ^{14}C-PP trend for the MBARI time series observed by Chavez et al. (2011), mean NCP was not significantly different between the two intervals.

7. Since 2007, all NCP methods indicate consistently positive anomalies which correspond to negative MEI and PDO indices indicating cool conditions in the northeast Pacific and a positive NPGO index indicating strong equatorward flow in the California Current.

Table 3.1: Multi-decadal records of biological and physical parameters for the CalCOFI region for the period 1984-2010.

Parameter	Unit	Region	Winter	Spring	Summer	Fall	Annual
Surface O_2 saturation	%	R1	101.5	102.7	108.6	104.6	104.4
		R2	102.4	106.4	107.8	104.9	105.5
		R3	101.8	103.0	103.6	102.7	102.8
		R4	101.5	102.5	102.6	102.2	102.2
		CalCOFI grid	101.8	103.6	105.0	103.3	103.5
K_g (gas exchange velocity)	m d^{-1}	R1	2.6	3.8	2.9	2.8	3.1
		R2	2.3	3.1	2.5	1.9	2.5
		R3	2.5	3.6	2.9	2.6	2.9
		R4	2.6	3.3	2.9	2.6	2.9
		CalCOFI grid	2.5	3.4	2.8	2.5	2.8
Offshore Ekman transport	Metric tons s^{-1} per 100m of coastline	R1 Nearshore[a]	58	126	91	82	91
		R2 Nearshore[a]	37	82	49	36	52
Nearshore 40m O_2 saturation	%	R1 Nearshore[a]	87.0	63.8	74.4	85.0	76.7
		R2 Nearshore[a]	87.3	66.8	76.8	89.8	79.4
Nearshore 40m $[NO_3^-]$	mmol m^{-3}	R1 Nearshore[a]	6.1	16.7	11.6	7.0	10.7
		R2 Nearshore[a]	5.1	13.1	10.0	4.6	8.5

[a]The nearshore zone of Regions 1 and 2 is within 25 km of the coast.

Table 3.2: Seasonality of export production estimates. Uncertainty represents 2x the standard error of time series means.

Authors	Method	Region	Export rate (mg C m^{-2} d^{-1}) Winter	Spring	Summer	Fall	Annual
This study	O_2-NCP	R1	205±74	958±160	855±166	388±92	616±65
		R2	179±32	635±114	331±71	176±29	346±42
		R3	150±20	183±27	112±24	133±26	145±13
		R4	146±17	134±21	59±15	118±23	113±9
		CalCOFI grid	163±22	370±48	246±43	172±27	240±19
This study	Nitrate-NCP	R1	96±69	851±190	537±131	238±82	456±64
		R2	22±12	297±74	134±36	32±10	131±24
		R3	1±10	73±36	26±13	11±4	30±10
		R4	-1±2	1±2	0±1	0±1	0±0
		CalCOFI grid	18±13	208±41	111±26	42±12	101±14
Behrenfeld and Falkowski (1997) Dunne et al. (2007)	NCP07 VGPM × pe-ratio	R1	288±54	714±80	543±79	369±50	484±70
		R2	194±15	345±31	223±40	144±17	229±34
		R3	119±10	135±15	124±15	111±14	121±17
		R4	61±10	56±5	43±4	46±7	49±6
		CalCOFI grid	142±14	235±16	177±24	133±13	171±20
Behrenfeld and Falkowski (1997) Laws et al. (2000)	NCP00 VGPM × pe-ratio	R1	389±62	867±64	623±68	442±44	585±58
		R2	251±23	459±36	240±39	154±18	279±38
		R3	154±14	199±24	182±22	143±17	168±25
		R4	80±12	83±6	76±4	68±7	74±7
		CalCOFI grid	188±18	316±19	224±25	164±13	223±23
Dugdale and Wilkerson (1992) Eppley (1992)	^{15}N uptake f-ratio × ^{14}C-PP[a]	R1	275±39	1214±136	1038±142	298±38	750±54
		R2	191±17	395±50	342±44	211±16	317±21
		R3	126±13	160±26	149±15	127±20	136±9
		R4	76±10	79±10	88±10	81±10	81±6
		CalCOFI grid	176±15	335±27	285±29	185±16	244±12
Bograd et al. (2001)	Nutrient budget	CalCOFI grid	203	579	364	193	327
Messié et al. (2009)	Nutrient Budget	32.9 – 35 N					620
		34.4 – 40.5 N					1190
Pennington et al. (2010)	Nutrient Budget	Coastal Upwelling Zone Monterey Bay					560
Stukel et al. (2011)	^{234}Th POC export	CCE LTER (~35 N)					
		Aged upwelled					120
		California Current					70
		Offshore					80

[a]New production calculated from f-ratios based on ^{15}N uptake experiments for the Point Conception region (f = 0.57) reported by Dugdale and Wilkerson (1992) and for the Southern California Bight and offshore regions (f = 0.36 and f = 0.33, respectively) reported by Eppley (1992) multiplied by 24 h ^{14}C-PP.

Table 3.3: Magnitude of terms for budget-based export production estimates in mg C m^{-2} d^{-1}. Values represent annual means; uncertainty represents 2x the standard error of annual means; nc – not calculated.

Method	Region	Gas exchange	Coastal upwelling	Curl-driven upwelling	Horizontal advection	Time rate of change	Annual
O_2-NCP	R1	241±36	357±55	15±4	-2±2	2±3	616±65
	R2	236±27	82±17	22±6	0±0	6±2	346±42
	R3	141±10	nc	0±0	-3±3	7±3	145±13
	R4	103±8	nc	-1±0	nc	11±3	113±9
Nitrate-NCP	R1	nc	463±68	19±5	-16±6	-9±5	456±64
	R2	nc	99±21	34±8	-1±0	-2±1	131±24
	R3	nc	nc	3±1	29±10	-2±1	30±10
	R4	nc	nc	0±0	nc	0±0	0±0

Table 3.4: Interannual variability of export production estimates. All estimates are in mg C m^{-2} d^{-1}. Uncertainty represents 2x the standard error of annual means. Too reduce the impact of weak or short duration events, only strong El Niño and La Niña events are considered (i.e., the four years with an MEI >1 or < -0.8 during the winter and spring of the calendar year). EN years include 1987, 1991-92, and 1998; LN years include 1989, 1999, and 2008.

Region	Interval	O_2-NCP	Nitrate-NCP	$^{15}N^{14}C$-NCP
Region 1:	1984-2010	616±65	456±64	750±54
Point Conception	1984-1998	587±86	439±86	703±68
Upwelling	1999-2010	651±99	477±100	805±78
	El Niño	493±67	402±92	679±102
	La Niña	567±93	470±24	737±181
Region 2:	1984-2010	346±42	131±24	317±21
Southern California	1984-1998	311±49	114±32	292±26
Bight	1999-2010	386±66	150±36	346±25
	El Niño	267±137	68±43	302±66
	La Niña	357±53	149±46	324±25
Region 3:	1984-2010	145±13	30±10	136±9
California Current	1984-1998	143±13	18±8	127±9
	1999-2010	148±23	44±18	147±13
	El Niño	124±27	5±5	124±10
	La Niña	173±36	57±64	174±25
Region 4:	1984-2010	113±9	0±0	81±6
Offshore	1984-1998	120±11	0±1	78±7
	1999-2010	105±12	0±1	84±10
	El Niño	102±21	0±1	80±13
	La Niña	132±6	1±2	99±14
CalCOFI grid	1984-2010	240±19	101±14	244±12
	1984-1998	230±26	91±18	228±14
	1999-2010	251±29	114±22	263±14
	El Niño	198±37	70±13	227±26
	La Niña	236±39	117±28	262±27

Table 3.5 Satellite data and export ratio comparisons.

Method	Unit	Region	Winter	Spring	Summer	Fall	Annual
SeaWiFS chlorophyll	mg m^{-3}	R1	1.15	1.97	1.28	1.01	1.34
		R2	0.74	0.88	0.58	0.55	0.68
		R3	0.35	0.32	0.27	0.33	0.32
		R4	0.17	0.14	0.11	0.15	0.14
		CalCOFI grid	0.50	0.62	0.43	0.42	0.49
AVHRR sea surface temperature	°C	R1	15.21	16.31	20.04	17.92	17.38
		R2	16.30	19.02	24.56	20.64	20.14
		R3	15.95	16.57	19.72	18.59	17.73
		R4	16.63	17.19	20.03	19.28	18.30
		CalCOFI grid	16.12	17.28	21.00	19.18	18.41
VGPM	mg m^{-2} d^{-1}	R1	959	1943	1887	1301	1528
		R2	744	1192	1153	740	962
		R3	559	661	743	627	648
		R4	394	413	448	405	416
		CalCOFI grid	610	887	910	682	774
O_2-based NCP :VGPM		R1	0.19	0.47	0.48	0.35	0.42
		R2	0.27	0.51	0.29	0.23	0.33
		R3	0.23	0.23	0.15	0.20	0.20
		R4	0.30	0.27	0.15	0.30	0.26
		CalCOFI grid	0.26	0.38	0.27	0.26	0.29
pe-ratio Dunne et al. (2007)		R1	0.30	0.34	0.27	0.27	0.30
		R2	0.26	0.26	0.18	0.21	0.23
		R3	0.21	0.19	0.16	0.18	0.18
		R4	0.15	0.12	0.09	0.12	0.12
		CalCOFI grid	0.23	0.24	0.18	0.20	0.21
pe-ratio Laws et al. (2000)		R1	0.40	0.45	0.33	0.34	0.38
		R2	0.33	0.38	0.20	0.21	0.28
		R3	0.27	0.29	0.24	0.22	0.26
		R4	0.20	0.20	0.17	0.17	0.18
		CalCOFI grid	0.28	0.31	0.22	0.22	0.26

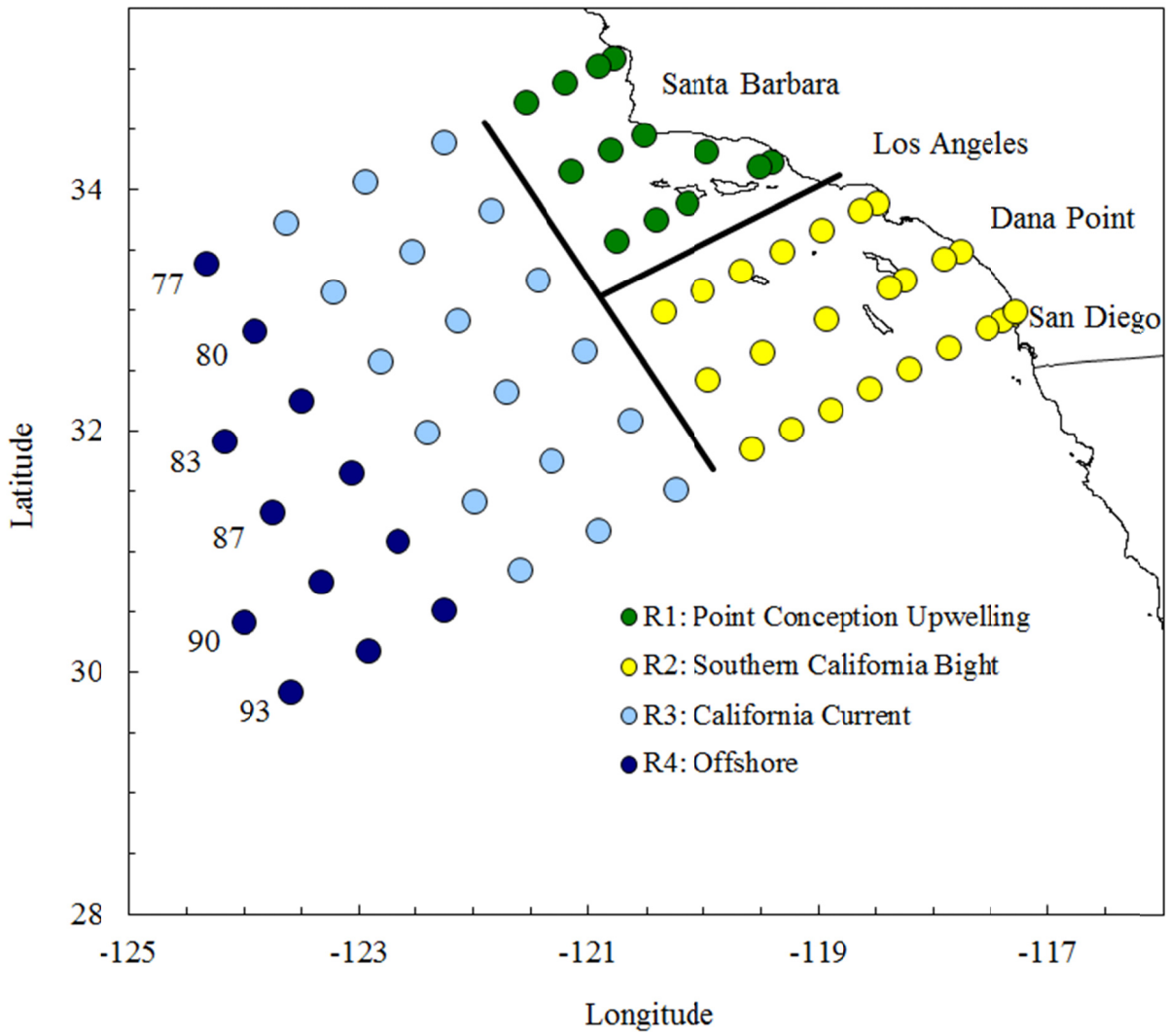

Figure 3.1. CalCOFI station positions with locations of standard stations (circles). Region 1 (Point Conception Upwelling) is green. Region 2 (Southern California Bight) is yellow. Region 3 (California Current) is light blue. Region 4 (Offshore) is dark blue. Alongshore transports were calculated across the line separating CalCOFI lines 83 and 87 between Regions 1 and 2. Offshore and onshore transports were calculated across the line separating stations 60 and 70 between Regions 1, 3 and Regions 2, 3.

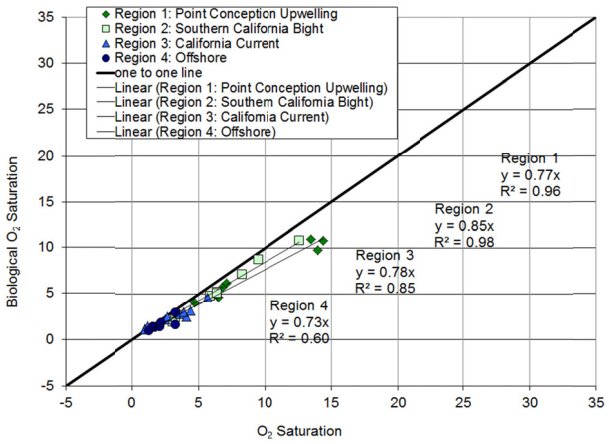

April 2006

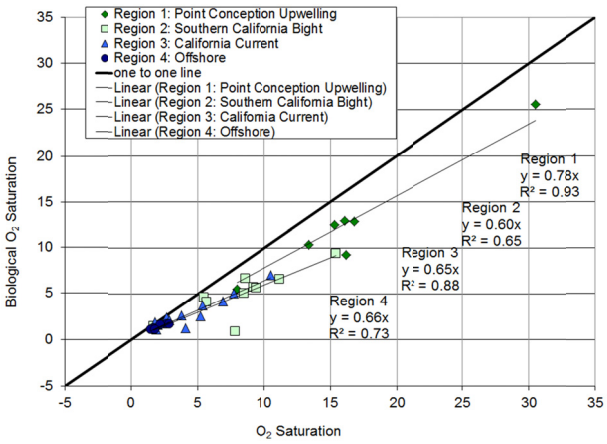

July 2006

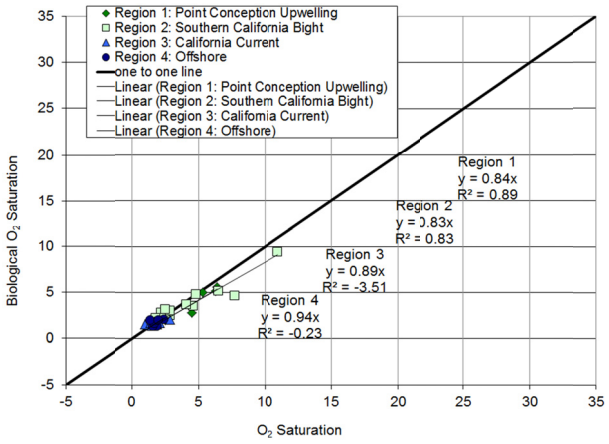

October 2006

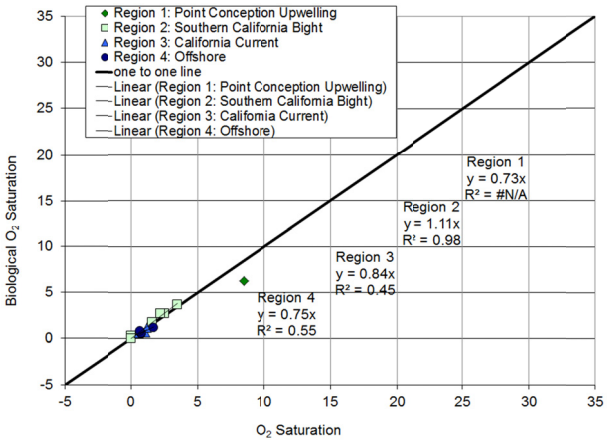

January 2007

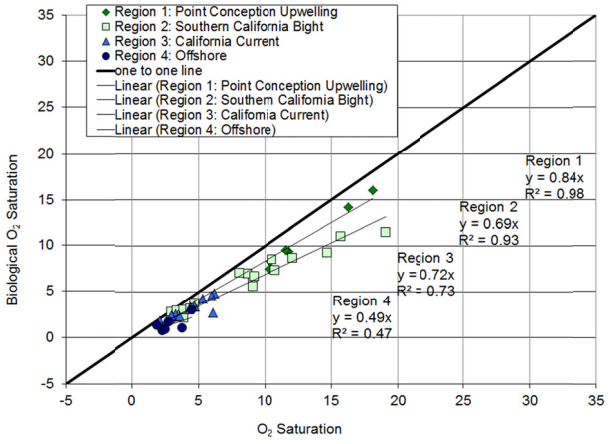

August 2008

Figure 3.2. Relationship between mixed layer O_2 saturation and mixed layer biological O_2 saturation $[(O_2{:}Ar)_{meas} / (O_2{:}Ar)_{sat}]$ for five CalCOFI cruises.

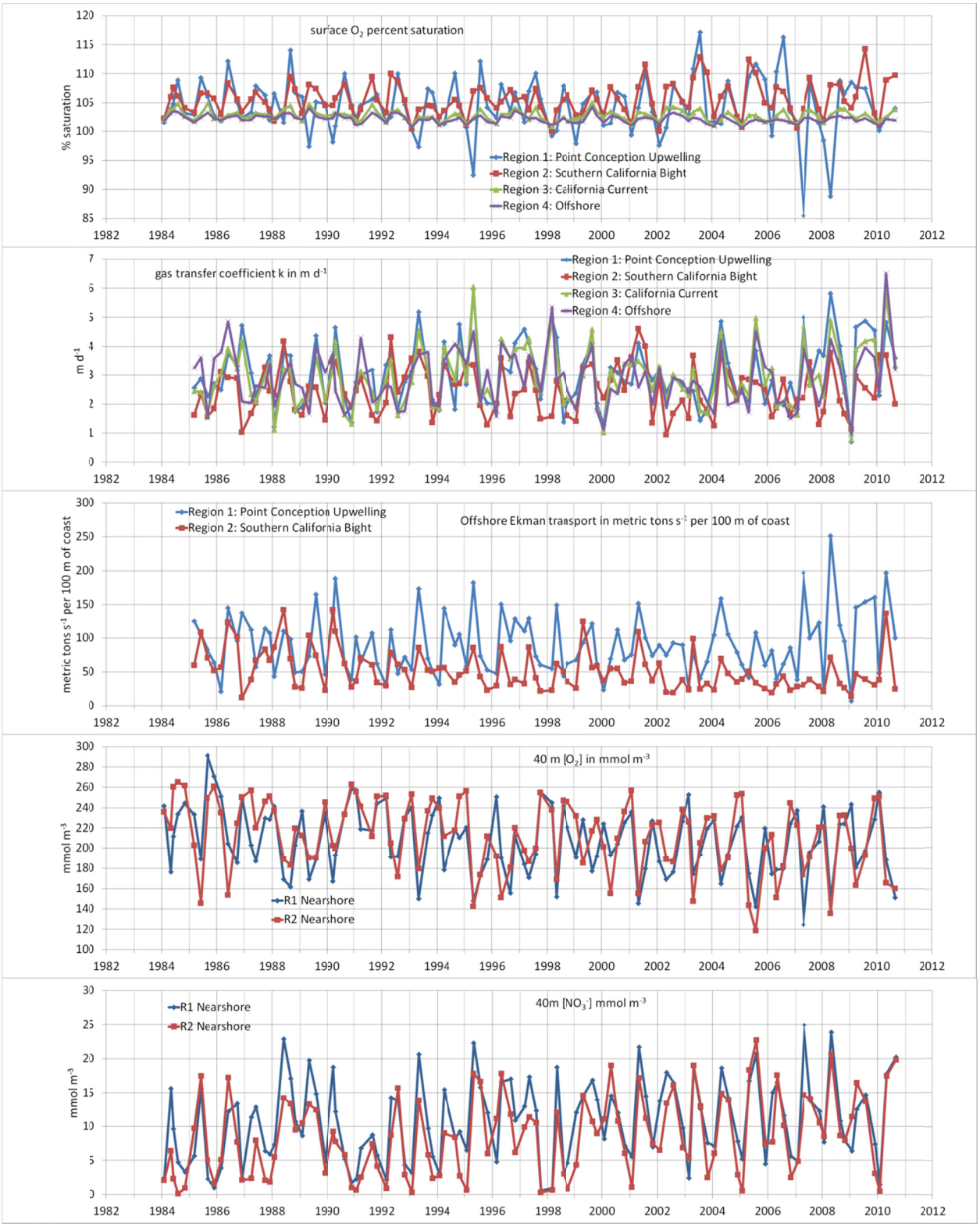

Figure 3.3. Record of (A) surface O_2 percent saturations, (B) gas exchange coefficients, (C) offshore Ekman transport, (D) 40 m O_2 percent saturations for the nearshore zones (i.e., within 25 km or one Rossby radius of the coast) of Regions 1 and 2, (E) and 40 m nitrate concentrations for the nearshore zones of Regions 1 and 2.

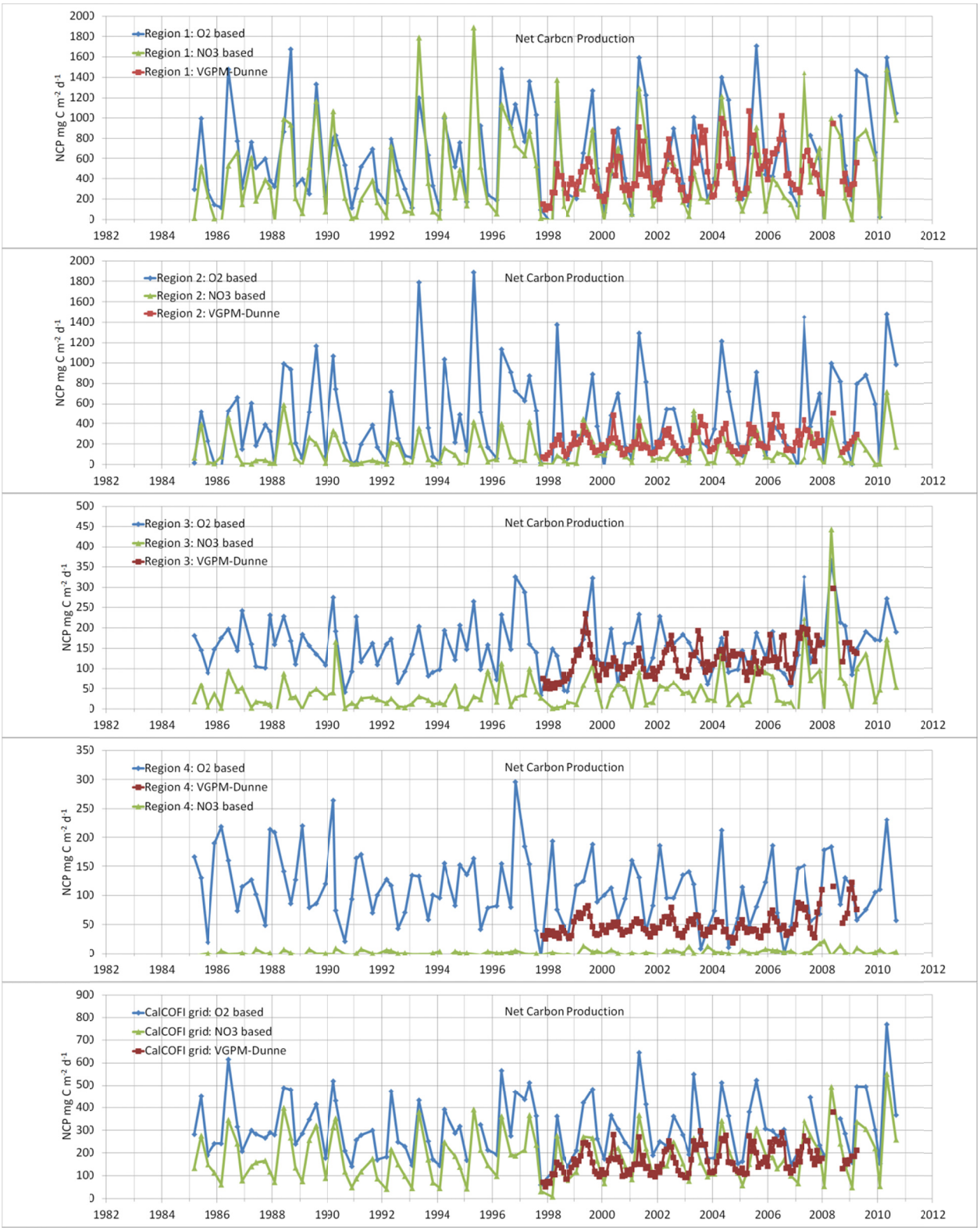

Figure 3.4. Net carbon production calculated using the O_2-based method, nitrate-based method, and NCP07 (VGPMxDunne07) algorithm for (A) Region 1, (B) Region 2, (C) Region 3, (D) Region 4, and (E) the entire CalCOFI grid.

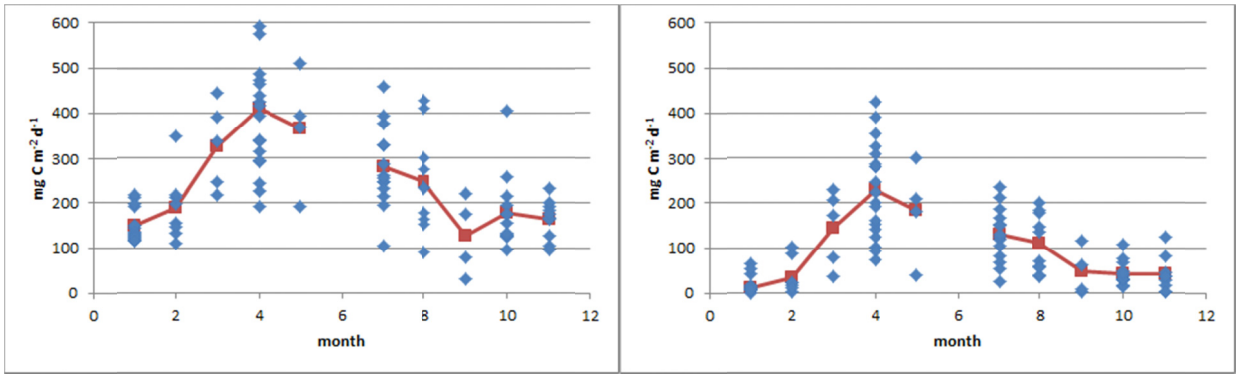

O_2-NCP nitrate-NCP

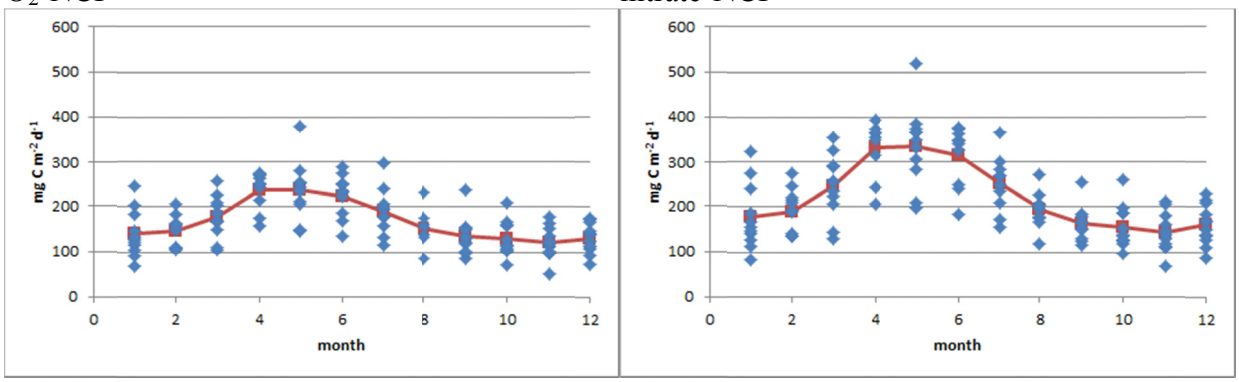

NCP07 NCP00

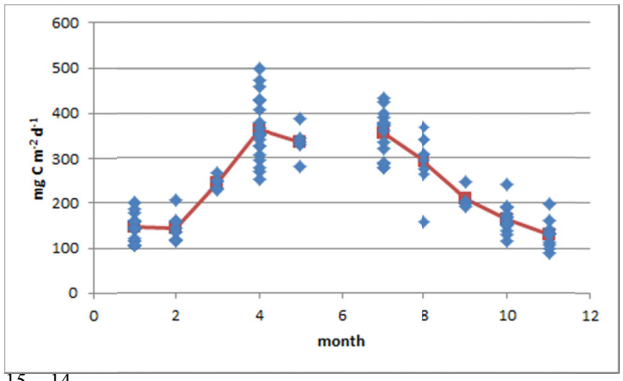

$^{15}N^{14}C$-NCP

Figure 3.5. Seasonality of NCP estimates. Red line indicates time series mean for each month.

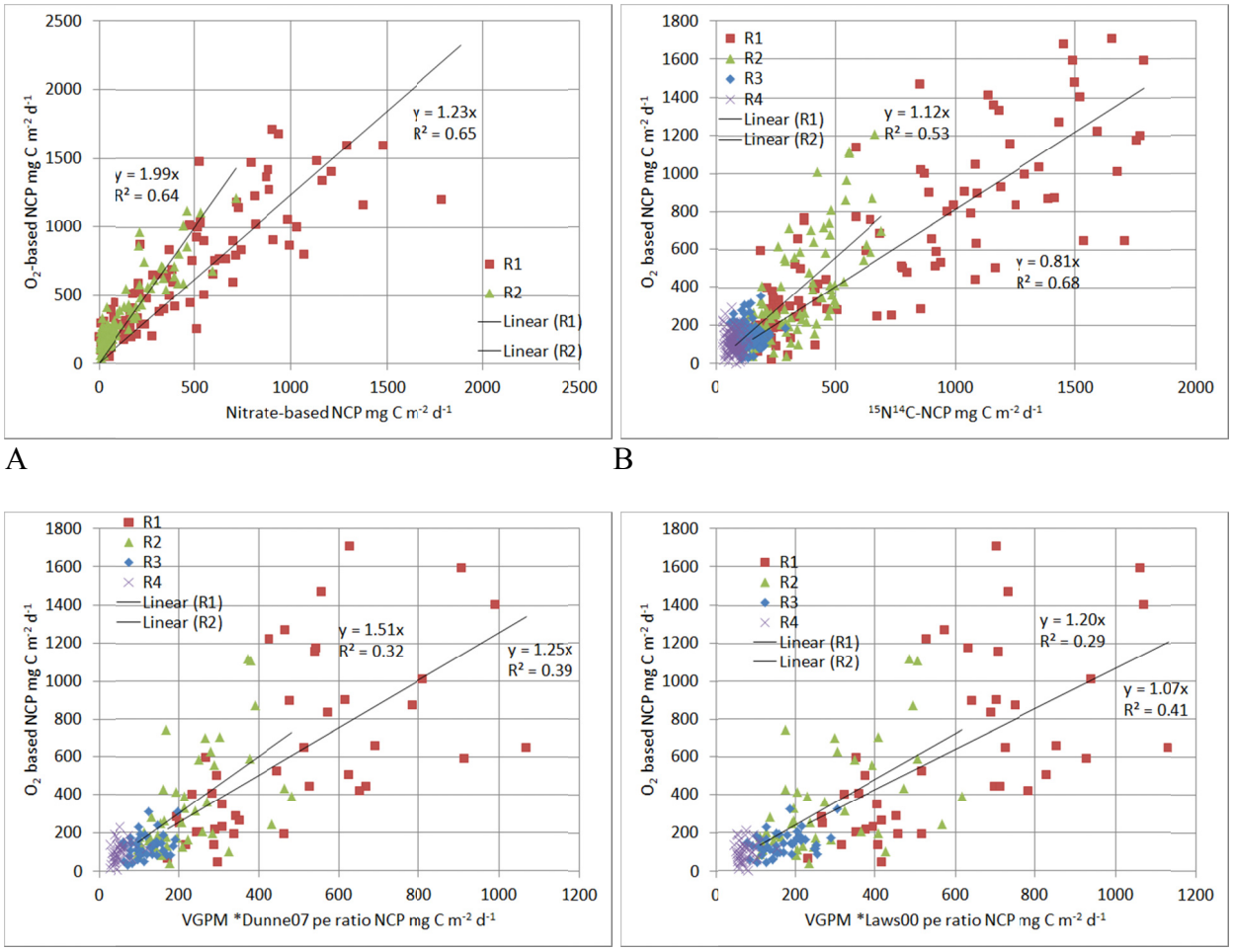

Figure 3.6. The relationship between O_2-based net carbon production (NCP) and (A) nitrate-NCP, (B) $^{15}N^{14}C$-NCP, (C) NCP07, and (D) NCP00.

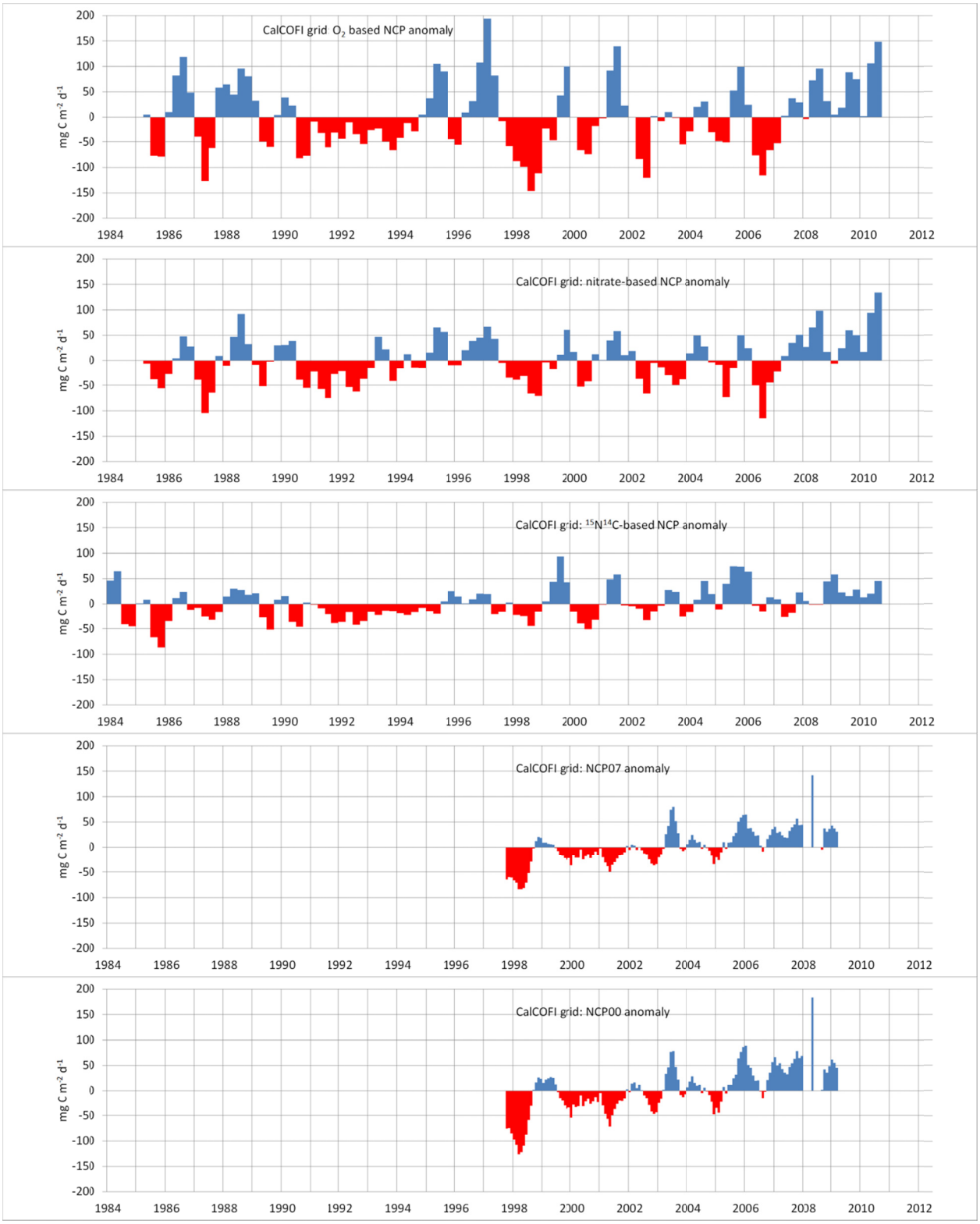

Figure 3.7. Interannual variability of NCP estimates; NCP anomalies for the CalCOFI grid calculated by differencing cruise estimate from the monthly time series mean and smoothing with a two-point running mean.

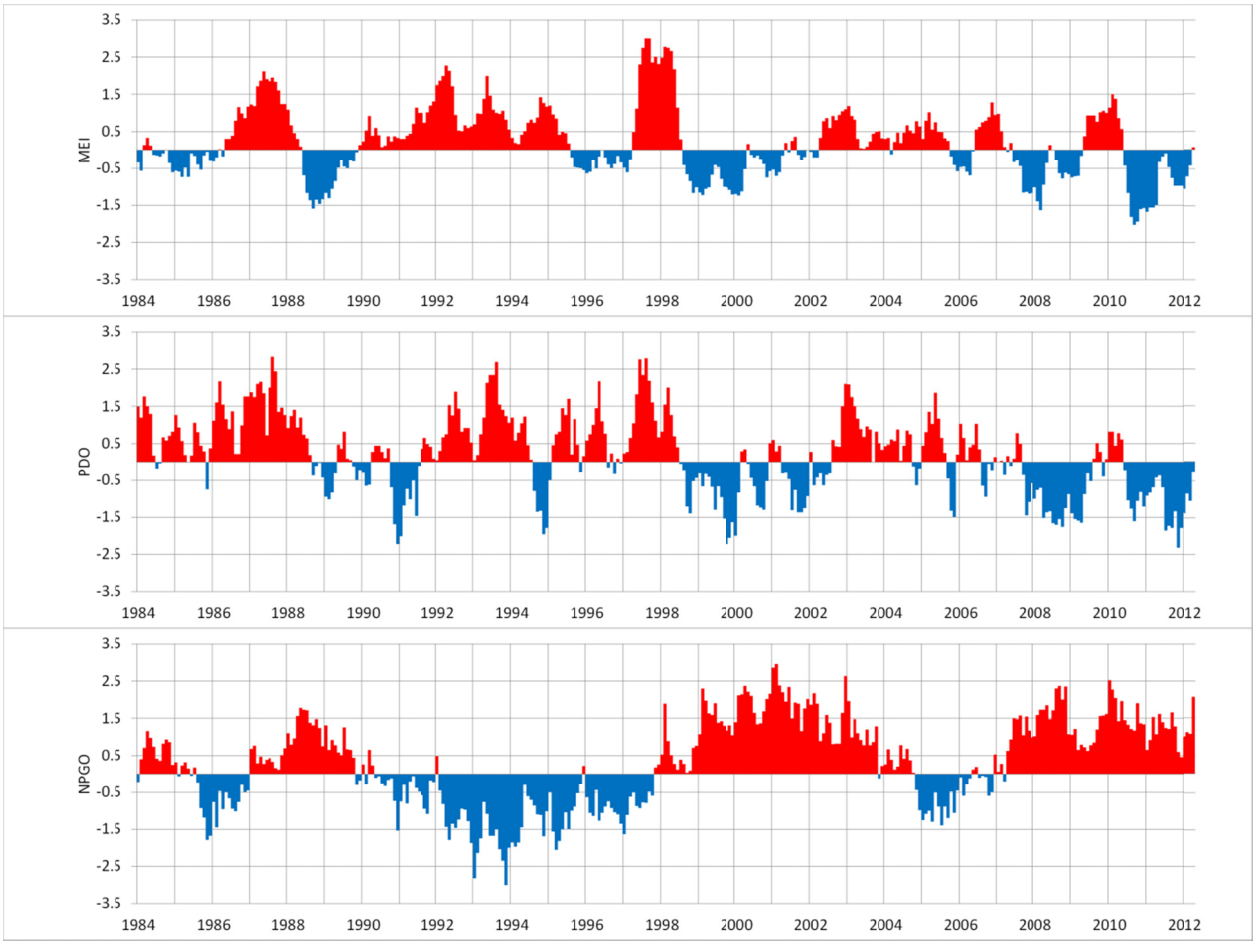

Figure 3.8. Time series of climate indices for the interval from 1984-2012 including (A) the Multivariate ENSO Index (MEI) downloaded from http://www.esrl.noaa.gov/psd/people/klaus.wolter/MEI/table.html; (B) the Pacific Decadal Oscillation (PDO) downloaded from http://jisao.washington.edu/pdo/PDO.latest ; and (C) the North Pacific Gyre Oscillation (NPGO) downloaded from http://www.o3d.org/npgo/data/NPGO.txt).

Chapter 4: Application of $^{17}\Delta$ and O_2:Ar methods in the coastal ocean: What has been learned and opportunities for future research

4.1 Advantages and limitations of the $^{17}\Delta$ and O_2:Ar approaches in the coastal ocean

The $^{17}\Delta$ and O_2:Ar methods for estimating gross and net O_2 production (GOP and NOP) have provided significant insights into spatial and seasonal variability of biological production rates within the southern California Current System (CCS). The advantages of these in situ approaches in comparison to traditional approaches for estimating primary production (PP) rates include the ability collect samples at much greater spatial and temporal resolution than possible with traditional incubation approaches and the fact that the $^{17}\Delta$ and O_2:Ar approaches are in situ measurements rather than bottle-based experiments thus avoiding the assumption that rates measured in a bottle are equivalent to rates in nature. Also, both $^{17}\Delta$-GOP and O_2:Ar-NOP integrate over the residence time of O_2 in the mixed layer which in the coastal ocean is generally around seven days, a time frame which integrates temporally over short duration events and spatially over small scale variations; this time interval is closer to the typical integration time represented by satellite-based approaches than incubation experiments which are typically conducted over the course of several hours. In comparison to nutrient budget approaches for estimation of new and/or export production, the O_2:Ar-NOP approach has a significant advantage in that the gas exchange term is dominant for most regions with the exception of the more productive upwelling regions (i.e., Region 1 in Chapters 2 and 3). Because upwelling terms in nutrient (and O_2) budgets come with significant uncertainty regarding both the estimated rate and depth of water upwelled into the surface ocean and sources of nitrate to the mixed layer are difficult to quantify in oligotrophic regions (Johnson et al. 2010), the addition of the better-

constrained gas exchange term makes O_2-based net community production (NCP) estimates inherently more accurate than nutrient budget-based NCP for many regions.

An important advantage to application of $^{17}\Delta$ and O_2:Ar methods in the coastal ocean relative to the open ocean is that natural spatial and temporal variability in PP and NCP is much greater than in the oligotrophic ocean and thus more important to detect to accurately determine mean conditions. The enhanced spatial resolution in PP determined during CalCOFI cruises using the $^{17}\Delta$-GOP approach compared to incubation-based ^{14}C-PP is apparent in productive regions such as Region 1 in Chapters 2 and 3. Also, the uncertainty due to measurement precision decreases with increasing $^{17}\Delta$ and O_2:Ar (i.e., moving away from the atmospheric equilibrium $^{17}\Delta$ and O_2:Ar values) such that measurement error based uncertainty decreases in importance in eutrophic regions relative to the uncertainty of the gas exchange parameterization and other terms in the $^{17}\Delta$ and O_2:Ar budgets. For example, the seasonal signal in $^{17}\Delta$-GOP was difficult to detect at the Hawaii Ocean Time series (HOT) in the oligotrophic North Pacific (Quay et al. 2010) where the annual $^{17}\Delta$ of the mixed layer (33±2 per meg) was less than half that in Region 1 at CalCOFI (~90 per meg) and significantly closer to the atmospheric equilibrium value of 8 to 16 (Luz and Barkan 2009).

There are limitations when utilizing the $^{17}\Delta$ and O_2:Ar approaches to estimate GOP and NCP in the coastal ocean. Both methods integrate through the mixed layer rather than the photic zone such that a significant fraction of productivity is missed when mixed layer depths are significantly shallower than photic zone depths. Although this condition occurs often in the CalCOFI grid, it is most pronounced in less productive regions including the Southern California Bight and the oligotrophic North Pacific (Region 4) where mean photic zone depths (~80 m) are typically twice the depth of the mixed layer (~40 m). ^{14}C-primary productivity (^{14}C-PP)

experiments help to alleviate some of this uncertainty by providing an estimate of the mixed layer versus photic zone integrated PP. Based on ^{14}C-PP depth profiles, ~30% of depth-integrated photic NPP occurred below the mixed layer in the two offshore regions at CalCOFI.

In productive regions inshore of the California Current the uncertainty associated with the coastal upwelling term adds significantly to the uncertainty of individual $^{17}\Delta$-GOP and O_2:Ar-NOP estimates, particularly for the latter due to sharp vertical gradients in O_2 concentration and percent saturation below the photic mixed layer (Chapter 3). In comparison, vertical $^{17}\Delta$ gradients are typically small in coastal upwelling regions leading to relatively small upwelling corrections even when upwelling rates are high. Significant horizontal and vertical gradients, high rates of horizontal and vertical advection, and relatively long residence times for mixed layer O_2 cause high uncertainty for individual estimates based on single $^{17}\Delta$ and O_2:Ar measurements (and all budget based approaches); as a result, variability over small spatial scales (within 10 km) is difficult to resolve. Spatial averaging such as the regional averaging scheme utilized in this study (see Fig. 2.1 or 3.1 in Chapters 2 and 3) reduces uncertainty while still allowing identification of significant spatial and temporal patterns.

Another issue when applying the $^{17}\Delta$-GOP and O_2-Ar approaches in a dynamic region such as that at CalCOFI is the assumption of steady state. At CalCOFI we determined that the steady state assumption was not valid for individual stations within the productive upwelling regions inshore of the California Current (i.e., Regions 1 and 2 in Chapters 2 and 3) due to the dominance and error associated with upwelling terms in budgets of $^{17}\Delta$ and O_2:Ar. The steady state assumption is valid, however, when we average observations over significant spatial scales as done for the regional analysis described in Chapters 2 and 3. The appropriateness of the steady state assumption for the four CalCOFI regions was tested by comparing residence times for O_2 in

the mixed layer with residence times for water in each region. For each region, residence times of water were at least 2 to 3x greater than residence times for O_2 even for inshore regions. An alternative approach to estimation of $^{17}\Delta$-GOP and O_2:Ar-NOP in dynamic coastal regions which was not possible at CalCOFI would be to conduct Lagrangian experiments where repeated observations would be made within the same water mass over a number of days to estimate the time rate of change term and alleviate the need for a steady state assumption. Furthermore, during a Lagrangian experiment it would be possible to collect repeat depth profiles which would provide an estimate of full photic zone productivity rates and avoid the potential bias to mixed layer productivity estimates due to entrainment of sub-mixed layer waters.

4.2 Conclusions from application of $^{17}\Delta$ and O_2:Ar methods at CalCOFI

Major conclusions from estimates based on $^{17}\Delta$ and O_2:Ar measurements at CalCOFI include the following.

1. Annual primary production rates as estimated by three independent methods ($^{17}\Delta$-GOP, ^{14}C-PP, and VGPM-PP) increase by a factor of four from the oligotrophic offshore region to the coastal upwelling regions inshore of the California Current within the CalCOFI grid.

2. The ratio of mixed layer $^{17}\Delta$-GOP:^{14}C-PP at CalCOFI (~5 to 7) is twice the value expected based on previous comparisons of ^{18}O-GOP:^{14}C-PP (2.7) (Marra 2002) which may result from methodological biases in the ^{14}C-PP experiments at CalCOFI or from variability in O_2:C production within the mixed layer.

3. The spatially-averaged e-ratio (NOP:GOP) in O_2 production units for the CalCOFI grid of 0.16 is surprisingly similar to ratios determined using similar methodology in the subtropical North Pacific at HOT (Quay et al. 2010), subtropical North Atlantic at BATS (Luz et al. 2009), subarctic North Pacific (Juranek et al. 2012), Equatorial Pacific (Hendricks et al. 2005; Stanley et al. 2010), and Southern Ocean (Reuer et al. 2007; Hamme et al. 2012).

4. Similarity of surface layer O_2:Ar-based NCP results with water column integrated nitrate budget based NCP estimates of Roemmich (1989) and Bograd et al. (2001) suggest either that most export production from the surface layer within the CalCOFI grid is not remineralized within the water column or there are sufficient methodological biases in the two NCP approaches that they cannot be accurately compared (e.g., that the nutrient estimates of Roemmich (1989) and Bograd et al. (2001) could be biased high or that O_2:Ar-based NCP results could be biased low).

5. Annual NCP determined by several methods (i.e., O_2:Ar, nitrate budget, ^{15}N incubations, satellite NPP) increases by 5-10x from the offshore oligotrophic region to the coastal upwelling region inshore of the California Current within the CalCOFI grid.

6. Seasonality of all PP and NCP estimates is greatest in regions inshore of the California Current. Spatially-averaged $^{17}\Delta$-GOP and O_2:Ar-NCP for the entire CalCOFI grid increases by 1.5x and 2x, respectively, between winter and spring.

7. Measured surface O_2 saturation state and surface layer O_2 budget estimates of NCP from 1984-2010 indicate that the CalCOFI grid is autotrophic year round with no significant regions of net heterotrophy observed during the time series.

8. The time series of NCP estimates from 1984-2010 show negative NCP anomalies in response to strong El Niño events (e.g., 1987, 1991-92, and 1998) and yet, no significant response to weak El Niño and La Niña events.

9. Since 2007, positive NCP anomalies have been observed at CalCOFI based on several NCP estimates (i.e., O_2:Ar, nitrate budget, ^{15}N incubation and satellite NPP); positive NCP anomalies coincide with cool conditions in the northeast Pacific and stronger than normal equatorward transport in the California Current.

4.3 Future Work

Future studies utilizing the $^{17}\Delta$ and O_2:Ar methods in the coastal ocean will undoubtedly have an impact on our understanding of coastal carbon cycling and hopefully prove useful in closing carbon budgets in continental margin systems around the world. An enormous advantage of the $^{17}\Delta$-GOP and O_2:Ar methods is that any ship is a potential sampling platform as mentioned above and demonstrated by Juranek et al. (2010) and Quay et al (2012). This greatly expands the potential spatial and temporal resolution achievable with significantly less effort compared to time-intensive bottle incubation experiments. Most coastal margin systems are undersampled and border underdeveloped and in some cases politically unstable regions. The relative simplicity of $^{17}\Delta$ and O_2:Ar sample collection procedure provides a significant advantage in conducting

productivity studies in regions where resource intensive incubation experiments might prove infeasible.

We have performed exploratory $^{17}\Delta$ and O_2:Ar sampling in three coastal regions in addition to CalCOFI. A description of preliminary results and conclusions follows.

Canary Current System off Mauritania, West Africa – Samples for $^{17}\Delta$ and O_2:Ar were collected during a cruise in February 2008 to the coastal upwelling region off Mauritania and extending offshore to Cape Verde Islands. The significant observations were as follows. $^{17}\Delta$-GOP rates within 100 km of the coast were 3x rates measured from 100-300 km offshore. $^{17}\Delta$-GOP rates for the inshore region were comparable to rates measured in the North Inshore region at CalCOFI. O_2:Ar-NCP for the offshore region was similar to rates observed in the oligotrophic portion of the CalCOFI grid. However, O_2:Ar-NCP rates were not calculated for regions within 50 km of the coast due to steep vertical gradients in O_2 and surface O_2 undersaturation (i.e., widespread region at the surface with O_2 saturations <90%).

Central California Coast, MBARI time series – Samples for $^{17}\Delta$ and O_2:Ar were collected during four cruises from June 2010 to November 2010. A consistent offshore decrease in $^{17}\Delta$-GOP, O_2:Ar-NOP, and ^{14}C-PP was observed during all cruises. $^{17}\Delta$-GOP and O_2:Ar-NCP rates for the region inshore of the California Current (i.e., within 100 km of the coast) were 3x and 4x, respectively, rates for the offshore region and comparable to rates observed during summer and fall at CalCOFI for the inshore and offshore region with the exception that GOP rates for the inshore region for fall increased by a factor of 2x from summer. The NCP:GOP ratio in O_2 terms (~0.17) averaged for the inshore and offshore region from summer to fall was nearly identical to

that observed at CalCOFI (~0.16) with a lack of seasonal variability for both the inshore and offshore region. Spatially, the NCP:GOP ratios for the inshore region were indistinguishable from the offshore region similar to observed spatial variability at CalCOFI. The $^{17}\Delta$-GOP:^{14}C-PP ratio calculated for the mixed layer was 2.7±1.3 and 2.2±1.0 for the inshore and offshore regions, respectively, which is essentially indistinguishable from the ^{18}O-GOP:^{14}C-PP ratio of 2.7 determined during JGOFS (Marra 2002) and significantly different from ratios observed at CalCOFI. This result lends support to the hypothesis that ^{14}C-PP at CalCOFI underestimates NPP due to methodological biases (i.e., presented in the discussion of Chapter 2).

Mid Atlantic Bight, Georges Bank, and Gulf of Maine – Samples for $^{17}\Delta$ and O_2:Ar were collected during four cruises to the Mid Atlantic Bight (MAB), Georges Bank (GB), and Gulf of Maine from August 2009 to May 2010. $^{17}\Delta$-GOP and O_2:Ar-NOP estimates were complicated by very shallow mixed layers in spring and summer (<5 m) which implies that most of the productivity occurred below the mixed layer and significantly limited the usefulness of $^{17}\Delta$ and O_2:Ar methods (i.e., GPP and NCP could be determined at only 25% of stations during the spring and summer cruises). At the stations where the $^{17}\Delta$ and O_2:Ar method were applicable, the $^{17}\Delta$-GOP:VGPM ratio (i.e., mixed layer GOP : photic zone VGPM) for all cruises (~1) was significantly lower than observed at CalCOFI (~2-3) which could be a result of a greater fraction of PP occurred in the photic zone beneath the mixed layer in the MAB compared to CalCOFI. NCP:GPP (in O_2 production units) was estimated during the May 2010 cruise and yielded a mean of 0.2±0.1 which is similar to the ratio of 0.2±0.1 measured inshore of the California Current during spring and summer. In contrast to CalCOFI, biological O_2 saturation based on

surface O_2:Ar measurements for the MAB cruise in November 2009 cruise indicated widespread regions of net heterotrophy over the continental shelf.

Comparison of Sites – Future work involves a comparison of GOP and NCP at the three Eastern Boundary Current (EBC) settings focusing on the following objectives and questions:

1. Compare estimates of satellite PP and estimates of NCP derived from satellite PP coupled with common export models (e.g., Dunne et al. 2007; Laws et al. 2000) to $^{17}\Delta$-GOP and O_2:Ar-NCP. Do comparisons of GOP and NCP indicate that the Canary Current System is significantly more productive than the California Current System as suggested by satellite PP studies (Carr 2002) and nutrient budget (Messié et al. 2009) comparisons of EBC systems?

2. Is there a relationship between PP, NCP, and the e-ratio (i.e., both as estimated using the NCP:GOP ratio and using common algorithms including those of Dunne et al. (2007) and Laws et al. (2000)) and upwelling intensity?

3. Is offshore variability in PP and NCP similar between sites and related to upwelling intensity and/or the offshore gradient in nitrate?

In addition, incubation-based PP data (i.e., ^{13}C-PP) from the MAB cruises has recently become available and provides an opportunity to compare bottle based and in situ PP rates at three coastal sites, the CalCOFI grid in the Southern California Current System, off the Central California coast, and off the East Coast of the United States. The goal is to determine the

similarities of the magnitude and efficiency of the biological pump in the three coastal upwelling systems and compare our in situ based estimates to those derived from satellite based estimates of primary production and organic carbon export.

References

Angert, A., S. Rachmilevitch, E. Barkan, and B. Luz. 2003. Effects of photorespiration, the cytochrome pathway, and the alternative pathway on the triple isotopic composition of atmospheric O_2. Global Biogeochem. Cycles **17**: 1030, doi:10.1029/2002GB001933

Bakun, A. 1990. Global climate change and intensification of coastal ocean upwelling. Science **247**: 198–201.

Behrenfeld, M. J., and P. G. Falkowski. 1997. Photosynthetic rates derived from satellite-based chlorophyll concentration. Limnol. Oceanogr. **42**: 1–20.

Benitez-Nelson, C., K. O. Buesseler, D. M. Karl, and J. Andrews. 2001. A time-series study of particulate matter export in the North Pacific Subtropical Gyre based on ^{234}Th:^{238}U disequilibrium, Deep-Sea Res. I **48**: 2595–2611.

Bjorkstedt, E. P., R. Goericke, S. McClatchie, E. Weber, W. Watson, N. Lo, W. T. Peterson, R. L. Emmett, R. D. Brodeur, J. Peterson, M. Litz, J. Gómez-Valdés, G. Gaxiola-Castro, B. Lavaniegos, F. P. Chavez, C. A. Collins, J. Field, K. Sakuma, S. J. Bograd, F. B. Schwing, P. Warzybok, R. Bradley, J. Jahncke, G. S. Campbell, J. A. Hildebrand, W. J. Sydeman, S. A. Thompson, J. L. Largier, C. Halle, S. Y. Kim, and J. Abell. 2011. State of the California Current 2010–2011: Regionally variable responses to a strong (but fleeting?) La Niña. Calif. Coop. Ocean. Fish. Invest. Rep. **52**: 36–68.

Bograd, S. J., T. K. Chereskina, and D. Roemmich. 2001. Transport of mass, heat, salt, and nutrients in the southern California Current System: Annual cycle and interannual variability. J. Geophys. Res. **106**: 9255–9275.

Bograd, S. J., C. G. Castro, E. Di Lorenzo, D. M. Palacios, H. Bailey, W. Gilly, and F. P. Chavez. 2008. Oxygen declines and the shoaling of the hypoxic boundary in the California Current. Geophys. Res. Lett. **35**: L12607, doi:10.1029/2008GL034185

Boyce, D. G., M. R. Lewis, and B. Worm. 2010. Global phytoplankton decline over the past century. Nature **466**: 591–596, doi:10.1038/nature09268

Cai, W-J., M. Dai, and Y. Wang. 2006. Air-sea exchange of carbon dioxide in ocean margins: A province-based synthesis, Geophys. Res. Lett. **33**: L12603, doi:10.1029/2006GL026219

Carpenter, J. H. 1965. The Chesapeake Bay Institute technique for the Winkler dissolved oxygen method. Limnol. and Oceanogr. **10**: 141–143.

Carr, M-E., 2002. Estimation of potential productivity in Eastern Boundary Currents using remote sensing. Deep Sea Res. Part II **49**: 59–80.

Carr, M-E., M. A. M. Friedrichs, M. Schmeltz, M. N. Aita, D. Antoine, K. R. Arrigo, I. Asanuma, O. Aumont, R. Barber, M. Behrenfeld, R. Bidigare, E. T. Buitenhuis J. Campbell,

A. Ciotti, H. Dierssen, M. Dowell, J. Dunne, W. Esaias, B. Gentili, W. Gregg, S. Groom, N. Hoepffner, J. Ishizaka, T. Kameda, C. Le Quéré, S. Lohrenz, J. Marra, F. Mélin, K. Moore, A. Morel, T. E. Reddy, J. Ryan, M. Scardi, T. Smyth, K. Turpie, G. Tilstone, K. Waters, and Y. Yamanaka, 2006. A comparison of global estimates of marine primary production from ocean color, Deep Sea Res. II **53**: 741–770, doi:10.1016/j.dsr2.2006.01.028

Chavez, F. P., and J. R. Toggweiler. 1995. Physical estimates of global new production: the upwelling contribution, p. 313–320. *In* C. P. Summerhayes, K. C. Emeis, M. V. Angel, R. L. Smith, and B. Zeitzschel [eds.] Upwelling in the ocean: Modern processes and ancient records. J. Wiley & Sons.

Chavez, F. P., and Messié, M., 2009. A comparative analysis of eastern boundary upwelling ecosystems. Prog. Oceanogr. **83**: 80–96, doi:10.1016/j.pocean.2009.07.032

Chavez, F. P., J. Ryan, S. E. Lluch-Cota, and M. Ñiquen. 2003. From anchovies to sardines and back: Multidecadal change in the Pacific Ocean. Science **299**: 217–221.

Chavez, F. P., M. Messié, and J. T. Pennington. 2011. Marine primary production in relation to climate variability and change. Annu. Rev. Mar. Sci. **3**: 227–260, doi:10.1146/annurev.marine.010908.163917

Checkley, D. M., and J. A. Barth. 2009. Patterns and processes in the California Current System. Prog. Oceanogr. **83**: 49–64, doi:10.1016/j.pocean.2009.07.028

Chhak, K., and E. Di Lorenzo. 2007. Decadal variations in the California Current upwelling cells. Geophys. Res. Lett. **34**: L14604, doi:10.1029/2007GL030203

Craig, H., and T. L. Hayward. 1987. Oxygen supersaturation in the ocean: Biological vs. physical contributions. Science **235**: 199–202.

Deutsch, C., H. Brix, T. Ito, H. Frenzel, and L. Thompson. 2011. Climate-forced variability of ocean hypoxia. Science **333**: 336–339, doi:10.1126/science.1202422

Di Lorenzo, E., A. J. Miller, N. Schneider, and J. C. McWilliams. 2005. The warming of the California Current: Dynamics and ecosystem implications. J. Phys. Oceanogr. **35**: 336–362, doi:10.1175/JPO-2690.1

Di Lorenzo, E., N. Schneider, K. M. Cobb, K. Chhak, P. J. S. Franks, A. J. Miller, J. C. McWilliams, S. J. Bograd, H. Arango, E. Curchister, T. M. Powell, and P. Rivere. 2008. North Pacific Gyre Oscillation links ocean climate and ecosystem change. Geophys. Res. Lett. **35**: L08607, doi:10.1029/2007GL032838

Dugdale R., and F. Wilkerson. 1992. Nutrient limitation of new production in the sea, p. 107–122. *In* P. G. Falkowski [ed.] Primary productivity and biogeochemical cycles in the sea. Plenum Press.

Dunne, J. P., J. L. Sarmiento, and A. Gnanadesikan. 2007. A synthesis of global particle export from the surface ocean and cycling through the ocean interior and on the seafloor. Global Biogeochem. Cycles **21**: GB4006, doi:10.1029/2006GB002907

Emerson, S., P. Quay, D. Karl, C. Winn, L. Tupas, and M. Landry. 1997. Experimental determination of the organic carbon flux from open-ocean surface waters. Nature **389**: 951–954.

Emerson, S., C. Stump, and D. Nicholson. 2008. Net biological oxygen production in the ocean: Remote in situ measurements of O_2 and N_2 in surface waters, Global Biogeochem. Cycles **22**: GB3023, doi:10.1029/2007GB003095.

Eppley, R. W. 1992. Chlorophyll, photosynthesis, and new production in the Southern California Bight. Prog. Oceanogr. **30**: 117–150.

Eppley, R., E. Renger, and W. Harrison. 1979. Nitrate and phytoplankton production in southern California coastal waters. Limnol. Oceanogr. **24**: 483–494.

Friederich, G. E., P. M. Walz, M. G. Burczynski, and F. P. Chavez. 2002. Inorganic carbon in the central California upwelling system during the 1997–1999 El Niño–La Niña event. Prog. Oceanogr. **54**: 185–203.

Garcia, H. E., and L. I. Gordon. 1992. Oxygen solubility in seawater: Better fitting equations, Limnol. Oceanogr. **37**: 1307–1312.

Grande, K. D., P. J. Williams, J. Marra, D. A. Purdie, K. Heinemann, R. W. Eppley, and M. L. Bender. 1989. Primary production in the North Pacific gyre: A comparison of rates determined by the ^{14}C, O_2 concentration, and ^{18}O methods. Deep Sea Res. **36**: 1621–1634.

Hales, B., T. Takahashi, and L. Bandstra. 2005. Atmospheric CO_2 uptake by a coastal upwelling system, Global Biogeochem. Cycles **19**: GB1009, doi:10.1029/2004GB002295

Hales, B., W.-J. Cai, B. G. Mitchell, C. L. Sabine, and O. Schofield. 2008. Introduction and background, p. 3–13. *In* B. Hales, W.-J. Cai, B. G. Mitchell, C. L. Sabine, and O. Schofield [eds.] North American continental margins: A synthesis and planning workshop. Report of the North American continental margins working group for the U. S. Carbon Cycle Scientific Steering Group and Interagency Working Group. U. S. Carbon Cycle Science Program.

Hamme, R. C., and S. E. Emerson. 2004. The solubility of neon, nitrogen and argon in distilled water and seawater. Deep Sea Res. I **51**: 1517–1528, doi:10.1016/j.dsr.2004.06.009

Hamme, R. C., N. Cassar, V. P. Lance, R. D. Vaillancourt, M. L. Bender, P. G. Strutton, T. S. Moore, M. D. DeGrandpre, C. L. Sabine, D. T. Ho, and B. R. Hargreaves. 2012. Dissolved O_2/Ar and other methods reveal rapid changes in productivity during a Lagrangian experiment in the Southern Ocean. J. Geophys. Res. **117**: C00F12,

doi:10.1029/2011JC007046.

Hansell, D. A., and C. A. Carlson. 1998. Net community production of dissolved organic carbon. Global Biogeochem. Cycles **12**: 443–453.

Harris, G. P. 1984. Phytoplankton productivity and growth measurements: Past, present and future. J. Plankton Res. **6**: 219–237.

Hendricks, M. B., M. L. Bender, and B. A. Barnett. 2004. Net and gross O_2 production in the Southern Ocean from measurements of biological O_2 saturation and its triple isotope composition. Deep Sea Res. I **51**: 1541–1561, doi:10.1016/j.dsr.2004.06.006

Hendricks, M. B., M. L. Bender, B. A. Barnett, P. Strutton, and F. P. Chavez. 2005. Triple oxygen isotope composition of dissolved O_2 in the equatorial Pacific: A tracer of mixing, production, and respiration. J. Geophys. Res. **110**: C12021, doi:10.1029/2004JC002735

Hickey, B. M., and N. S. Banas. 2008. Why is the northern end of the California Current System so productive? Oceanography **21**: 90–107.

Ho, D. T., C. S. Law, M. J. Smith, P. Schlosser, M. Harvey, and P. Hill. 2006. Measurements of air-sea gas exchange at high wind speeds in the Southern Ocean: Implications for global parameterizations. Geophys. Res. Lett. **33**: L16611, doi:10.1029/2006GL026817

Huh, C-A., and T. M. Beasley. 1987. Profiles of dissolved and particulate thorium isotopes in the water column of coastal Southern California. Earth Planet. Sci. Lett. **85**: 1–10.

Ianson, D., and S. E. Allen. 2002. A two-dimensional nitrogen and carbon flux model in a coastal upwelling region. Global Biogeochem. Cycles **16**: doi:10.1029/2001GB001451

Johnson, K. S., S. C. Riser, and D. M. Karl. 2010. Nitrate supply to near-surface waters of the North Pacific subtropical gyre. Nature **465**:1062–65, doi:10.1038/nature09170.

Juranek, L. W., and P. D. Quay. 2005. In vitro and in situ gross primary and net community production in the North Pacific Subtropical Gyre using labeled and natural abundance isotopes of dissolved O_2. Global Biogeochem. Cycles **19**: GB3009, doi:10.1029/2004GB002384

Juranek, L. W., and P. D. Quay. 2010. Basin-wide photosynthetic production rates in the subtropical and tropical Pacific Ocean determined from dissolved oxygen isotope ratio measurements. Global Biogeochem. Cycles **24**: GB2006, doi:10.1029/2009GB003492

Juranek, L. W., and P. D. Quay. 2013. Using triple isotopes of dissolved oxygen to evaluate global marine productivity. Annu. Rev. Mar. Sci. **5**: 10.1–10.22, doi:10.1146/annurev-marine-121211-172430

Juranek, L. W., P. D. Quay, R. A. Feely, D. Lockwood, D. M. Karl, and M. J. Church. 2012.

Biological production in the NE Pacific and its influence on air-sea CO_2 flux: Evidence from dissolved oxygen isotopes and O_2 /Ar. J. Geophys. Res. **117**: C05022, doi:10.1029/2011JC007450

Kahru, M., and B. G. Mitchell. 2002. Influence of the El Niño-La Niña cycle on satellite-derived primary production in the California Current. Geophys. Res. Lett. **29**: 1846, doi:10.1029/2002GL014963

Kahru, M., and B. G. Mitchell. 2008. Ocean color reveals increased blooms in various parts of the World. Eos Trans. AGU. **89**: 170, doi:10.1029/2008EO180002

Kahru, M., R. Kudela, M. Manzano-Sarabia, and B. G. Mitchell. 2009. Trends in primary production in the California Current detected with satellite data. J. Geophys. Res. **114**: C02004, doi:10.1029/2008JC004979

Karl, D. M., J. R. Christian, J. E. Dore, D. V. Hebel, R. M. Letelier, L. M. Tupas, and C. D. Winn. 1996. Seasonal and interannual variability in primary production and particle flux at Station ALOHA. Deep Sea Res. II **43**: 539–568

Karl, D. M., D. V. Hebel, K. Björkman, and R. M. Letelier. 1998. The role of dissolved organic matter release in the productivity of the oligotrophic North Pacific Ocean. Limnol. Oceanogr. **43**: 1270–1286.

Knauer, G., and J. Martin. 1981. Primary production and carbon-nitrogen fluxes in the upper 1500 m of the northeast Pacific, Limnol. Oceanogr. **26**: 181–186.

Kudela, R. M., N. S. Banas, J. A. Barth, E. R. Frame, D. A. Jay, J. L. Largier, E. J. Lessard, T. D. Peterson, and A. J. Vander Woude. 2008. New insights into the controls and mechanisms of plankton productivity in coastal upwelling waters of the northern California Current System. Oceanography **21**: 46–59.

Landry, M. R., W. K. Peterson, and C. C. Andrews. 1992. Particulate flux in the water column overlying Santa Monica Basin. Prog. Oceanogr. **30**: 117–150.

Large, W. G., J. C. McWilliams, and S. C. Doney. 1994. Oceanic vertical mixing: A review and a model with a nonlocal boundary-layer parameterization. Rev. Geophys. **32**: 363–403.

Laws, E. A. 1991. Photosynthetic quotients, new production and net community production in the open ocean. Deep Sea Res. **38**: 143–167.

Laws, E. A., P. G. Falkowski, W. O. Smith, H. Ducklow, and J. J. McCarthy. 2000. Temperature effects on export production in the open ocean. Global Biogeochem. Cycles **14**: 1231–1246.

Letelier, R. M., J. E. Dore, C. D. Winn, and D. M. Karl. 1996. Seasonal and interannual variations in phytosynthetic carbon assimilation at Station ALOHA. Deep-Sea Res. II

43:467–90.

Liss, P. S., and L. Merlivat. 1986. Air-sea exchange rates: Introduction and synthesis. p. 113–127. *In* P. Buat-Ménard [ed.] The role of air-sea exchange in geochemical cycling. Springer.

Luz, B., and E. Barkan. 2000. Assessment of oceanic productivity with the triple-isotope composition of dissolved oxygen. Science **288**: 2028–2031.

Luz, B., and E. Barkan. 2005. The isotopic ratios $^{17}O/^{16}O$ and $^{18}O/^{16}O$ in molecular oxygen and their significance in biogeochemistry. Geochim. Cosmochim. Acta. **69**: 1099–1110, doi:10.1016/j.gca.2004.09.001

Luz, B., and E. Barkan. 2009. Net and gross oxygen production from O_2/Ar, $^{17}O/^{16}O$ and $^{18}O/^{16}O$ ratios. Aquat. Microb. Ecol. **56**: 133–145, doi:10.3354/ame01296

Luz, B., and E. Barkan. 2011. Proper estimation of marine gross O_2 production with $^{17}O/^{16}O$ and $^{18}O/^{16}O$ ratios of dissolved O_2. Geophys. Res. Lett. **38**: L19606, doi:10.1029/2011GL049138

Luz, B., E. Barkan, Y. Sagi, and Y. Z. Yacobi. 2002. Evaluation of community respiratory mechanisms with oxygen isotopes: a case study in Lake Kinneret. Limnol. Oceanogr. **47**: 33–42.

Mantua, N. J., S. R. Hare, Y. Zhang, J. M. Wallace, and R. C. Francis. 1997. A Pacific interdecadal climate oscillation with impacts on salmon production. Bull. Am. Meteorol. Soc. **78**: 1069–1079.

Mantyla, A. W., E. L. Venrick, and T. L. Hayward. 1995. Primary production and chlorophyll relationships, derived from ten years of CalCOFI measurements. Calif. Coop. Ocean. Fish. Invest. Rep. **36**: 159–166.

Mantyla, A. W., S. J. Bograd, and E. L. Venrick. 2008. Patterns and controls of chlorophyll-*a* and primary productivity cycles in the Southern California Bight. J. Mar. Syst. **36**: 48–60, doi:10.1016/j.jmarsys.2007.08.001

Marra, J. 1980. Vertical mixing and primary production, p. 121–137. *In* P. G. Falkowski [ed.] Primary productivity in the sea. Plenum Press.

Marra, J. 2002. Approaches to the measurement of plankton production, p. 78–108. *In* P. J. l. B. Williams, D. N. Thomas, and C. S. Reynolds [eds.] Phytoplankton productivity: Carbon assimilation in marine and freshwater ecosystems. Blackwell.

McClatchie, S., R. Goericke, R. Cosgrove, G. Auad, and R. Vetter. 2010. Oxygen in the Southern California Bight: Multidecadal trends and implications for demersal fisheries. Geophys. Res. Lett. **37**: L19602, doi:10.1029/2010GL044497

McGillicuddy, D. J., L. A. Anderson, N. R. Bates, T. Bibby, K. O. Buesseler, C. A. Carlson, C.

S. Davis, C. Ewart, P. G. Falkowski, S. A. Goldthwait, D. A. Hansell, W. J. Jenkins, R. Johnson, V. K. Kosnyrev, J. R. Ledwell, Q. P. Li, D. A. Siegel, and D. K. Steinberg. 2007. Eddy/wind interaction stimulated extraordinary mid-ocean plankton blooms. Science **316**: 1021–27, doi:10.1126/science.1136256

Messié, M., J. Ledesma, D. D. Kolber, R. P. Michisaki, D. G. Foley, and F. P. Chavez. 2009. Potential new production estimates in four eastern boundary upwelling ecosystems. Prog. Oceanogr. **83**: 151–158, doi:10.1016/j.pocean.2009.07.018

Miller, M. F. 2002. Isotopic fractionation and the quantification of ^{17}O anomalies in the oxygen three-isotope system: An appraisal and geochemical significance, Geochim. Cosmochim. Acta. **66**: 1881–1889.

Mitchell, B. G., and M. Kahru. 1998. SeaWiFS algorithms developed with CalCOFI bio-optical data, Coop. Ocean. Fish. Rep. **39**: 133–147.

Muller-Karger, F. E., R. Varela, R. Thunell, R. Luerssen, C. Hu, and J. J. Walsh. 2005. The importance of continental margins in the global carbon cycle. Geophys. Res. Lett. **32**: L01602, doi:10.1029/2004GL021346

Nicholson, D. P., R. H. R. Stanley, E. Barkan, D. M. Karl, B. Luz, P. D. Quay, and S. C. Doney. 2012. Evaluating triple oxygen isotope estimates of gross primary production at the Hawaii Ocean Time-series and Bermuda Atlantic Time-series study sites, J. Geophys. Res. **117**: C05012, doi:10.1029/2010JC006856

Nightingale, P. D., G. Malin, C. S. Law, A. J. Watson, P. S. Liss, M. I. Liddicoat, J. Boutin, and R. C. Upstill-Goddard. 2000. In situ evaluation of air-sea exchange parameterizations using novel conservative and volatile tracers, Global Biogeochem. Cycles **14**: 373–387.

Olivieri, R. A., and F. P. Chavez. 2000. A model of plankton dynamics for the coastal upwelling system of Monterey Bay, California. Deep-Sea Res. II **47**: 1077–1106.

Pennington, J. T., G. E. Friederich, C. G. Castro, C. A. Collins, W. W. Evans, and F. P. Chavez. 2010. A carbon budget for the northern and central California coastal upwelling system. Continental Margins Task Team, The Synthesis Book. Springer-Verlag.

Pickett, M. H., and F. B. Schwing. 2006. Evaluating upwelling estimates off the west coasts of North and South America. Fish. Oceanogr. **15**: 256–259, doi:10.1111/j.1365-2419.2005.00400.x

Prokopenko, M. G., O. M. Pauluis, J. Granger, and L. Y. Yeung. 2011. Exact evaluation of gross photosynthetic production from the oxygen triple-isotope composition of O_2: Implications for the net-to-gross primary production ratios. Geophys. Res. Lett. **38**: L14603, doi:10.1029/2011GL047652

Quay, P. D., J. Stutsman, R. A. Feely, and L. W. Juranek. 2009. Net community production rates

across the subtropical and equatorial Pacific Ocean estimated from air-sea $\delta^{13}C$ disequilibrium. Global Biogeochem. Cycles **23**: GB2006, doi:10.1029/2008GB003193

Quay, P. D., C. Peacock, K. Björkman, and D. M. Karl. 2010. Measuring primary production rates in the ocean: Enigmatic results between incubation and non-incubation methods at Station ALOHA. Global Biogeochem. Cycles **24**: GB3014, doi:10.1029/2009GB003665

Quay, P. D., J. Stutsman, and T. Steinhoff. 2012. Primary production and carbon export rates across the subpolar N. Atlantic Ocean basin based on triple oxygen isotope and dissolved O_2 and Ar gas measurements. Global Biogeochem. Cycles. **26**: GB2003, doi:10.1029/2010GB004003

Reid, J. L., and A. W. Mantyla. 1976. The effect of the geostrophic flow upon coastal sea elevations in the northern north Pacific ocean. J. Geophys. Res. **81**: 3100–3110.

Reuer, M. K., B. A. Barnett, M. L. Bender, P. G. Falkowski, and M. B. Hendricks. 2007. New estimates of southern ocean biological production rates from O_2/Ar ratios and triple isotope composition of O_2. Deep Sea Res. I **54**: 951–974, doi:10.1016/j.dsr.2007.02.007

Robinson, C., G. H. Tilstone, A. P. Rees, T. J. Smyth, J. R. Fishwick, G. A. Tarran, B. Luz, E. Barkan, and E. David. 2009. Comparison of in vitro and in situ plankton production determinations. Aquat. Microb. Ecol. **54**: 13–34, doi:10.3354/ame01250

Roemmich, D. 1989. Mean transport of mass, heat, salt and nutrients in southern California coastal waters: Implications for primary production and nutrient cycling. Deep Sea Res. I **36**: 1359–1378.

Rykaczewski, R. R., and D. M. Checkley. 2008. Influence of ocean winds on the pelagic ecosystem in upwelling regions. Proc. Natl. Acad. Sci. USA. **105**: 1965–1970, doi:10.1073/pnas.0711777105

Sarma, V. V. S. S., O. Abe, S. Hashimoto, A. Hinuma, and T. Saino. 2005. Seasonal variations in triple oxygen isotopes and gross oxygen production in the Sagami Bay, central Japan. Limnolog. Oceanogr. **50**: 544–552 .

Sarma, V. V. S. S., O. Abe, A. Hinuma, and T. Saino. 2006. Short-term variation of triple oxygen isotopes and gross oxygen production in the Sagami Bay, central Japan, Limnol. Oceanogr. **51**: 1432–1442.

Sarma, V. V. S. S., O. Abe, and T. Saino. 2008. Spatial variations in time-integrated plankton metabolic rates in Sagami Bay using triple oxygen isotopes and O_2 : Ar ratios, Limnol. Oceanogr. **53**: 1776–1783, doi:10.4319/lo.2008.53.5.1776

Snyder, M. A., L. C. Sloan, N. S. Diffenbaugh, and J. L. Bell. 2003. Future climate change and upwelling in the California Current, Geophys. Res. Lett. **30**: 1823, doi:10.1029/2003GL017647

Stanley, R. H. R., J. B. Kirkpatrick, N. Cassar, B. A. Barnett, and M. L. Bender. 2010. Net community production and gross primary production rates in the western equatorial Pacific. Global Biogeochem. Cycles. **24**: GB4001, doi:10.1029/2009GB003651

Steemann Nielsen, E. 1952. The use of radioactive carbon (C^{14}) for measuring organic production in the sea. J. Cons. Int. Explor. Mer. **18**: 117–140.

Stukel, M. R., M. R. Landry, C. R. Benitez-Nelson, and R. Goericke. 2011. Trophic cycling and carbon export relationships in the California Current Ecosystem. Limnol. Oceanogr. **56**: 1866–1878, doi:10.4319/lo.2011.56.5.1866

Thomas, H., Y. Bozec, K. Elkalay, and H. J. W. de Baar. 2004. Enhanced open ocean storage of CO_2 from shelf sea pumping. Science **304**: 1005–1008, doi:10.1126/science.1095491

Thunell, R. C. 1998. Particle fluxes in a coastal upwelling zone: sediment trap results from Santa Barbara Basin, California. Deep Sea Res. II **45**: 1863–1884.

Wanninkhof, R. 1992. Relationship between wind speed and gas exchange over the ocean. J. Geophys. Res. **97**: 7373–7382.

Westberry, T., M. Behrenfeld, D. Siegel, and E. Boss. 2008. Carbon-based primary productivity modeling with vertically resolved photoacclimation, Global Biogeochem. Cycles **22**: GB2024, doi:10.1029/2007GB003078

Wolter, K., and M. S. Timlin. 1998. Measuring the strength of ENSO events - how does 1997/98 rank? Weather **53**: 315–324.

Zehr J. P., and H. W. Paerl. 2008. Molecular ecological aspects of nitrogen fixation in the marine nvironment, p. 481–523. *In* D. L. Kirchman [ed.] Microbial Ecology of the Oceans. Wiley-Liss.

Zehr, J. P., and R. M. Kudela. 2009. Photosynthesis in the open ocean. Science **326**: 945–246, doi:10.1126/science.1181277

Curriculum Vitae
David Munro

School of Oceanography
University of Washington
Box 357940
Seattle, WA 98195-7940

phone: 206.221.6740
dmunro@uw.edu

EDUCATION

Ph.D., University of Washington, Chemical Oceanography, October 2012
Biological Production Rates in the Southern California Current System
Advisor: Paul D. Quay

M.S., Stanford University, Earth Systems, March 2004
Stable isotope composition of dissolved inorganic carbon and particulate organic carbon as tracers of biogeochemical processes in Antarctic sea ice
Advisor: Robert B. Dunbar

B.S., Stanford University, Earth Systems, June 2000

RESEARCH

-Research Assistant, Quay Stable Isotope Lab, 2005 to present
School of Oceanography, Seattle, WA

-Research Assistant, Dunbar Stable Isotope Lab, 2002 to 2004
Geological and Environmental Sciences, Stanford, CA

TEACHING

- Teaching Assistant for Introduction to Oceanography – Ocean 200 at U. Washington, Spring 2012
- Teaching Assistant for Deep Sea Exploration – Ocean 121at U. Washington, Winter 2012
- Teaching Assistant for Ocean Circulation – Ocean 210 at U. Washington, Autumn 2011, 2010 and 2009
- Teaching Assistant for Chemical Oceanography – Ocean 400 at U. Washington, Winter 2010
- Teaching Assistant for Chemical Oceanography – Ocean 520 at U. Washington, Autumn 2008
- Tutor for Big Step, Milwaukee, WI, 2004 to 2005
- Grader for Earth Systems 10, Stanford, CA, Winter 2004
- Teaching Assistant for Earth Systems 10, Stanford, CA, Winter 2003
- Teaching Assistant for Stanford at SEA (Sea Education Association), Pacific Grove, CA; Pacific Ocean, Spring 2003
- SCA New Hampshire Parks Americorps Volunteer, Allenstown, NH, 2000 to 2001

PUBLICATIONS

Munro, D. R., R. B. Dunbar, D. A. Mucciarone, K. R. Arrigo, and M. C. Long (2010), Stable Isotope Composition of Dissolved Inorganic Carbon and Particulate Organic Carbon in Sea Ice from the Ross Sea, Antarctica, *J. Geophys. Res.,* doi:10.1029/2009JC005661.

Manuscript submitted for publication:

Munro, D. R., P. D. Quay, L.W. Juranek, and R. Goericke, Biological production rates off the Southern California coast estimated from triple O_2 isotopes and O_2:Ar gas ratios, *Limnology and Oceanography.*

Manuscripts in preparation:

Munro, D. R., P. D. Quay, Multi-decadal records of net biological production rates in the southern California Current System based on dissolved oxygen and nitrate budgets, target journal: *Limnology and Oceanography.*

Munro, D. R., P. D. Quay, and A. Kortzinger, Application of natural abundance isotopes of dissolved oxygen and the O_2:Ar Ratio to estimate gross and net production in eastern boundary current systems, target journal: *Geophysical Research Letters.*

Munro, D. R., P. D. Quay, J. Stutsman, M. Haught, and A. Mannino, Biological production rates in the Mid-Atlantic Bight estimated from triple O_2 isotopes and O_2:Ar gas ratios, target journal: *Limnology and Oceanography.*

SELECTED PRESENTATIONS

Munro, D. R., and P. D. Quay (2012), Multi-decadal record of net biological production in the Southern California Current based on O_2 and nitrate budgets, ASLO Ocean Sciences, Salt Lake City, UT.

Munro, D. R. and P. D. Quay (2010), Gross and Net Production Estimates in the California Current System from Oxygen Triple Isotopes and the O_2/Ar Ratio, AGU Fall Meeting, San Francisco, CA.

Munro, D. R. (2010), Estimates of Primary Production and Net Community Production in the Coastal Ocean: Application of the ^{17}O-GOP and O_2/Ar NOP Methods to Three Distinct Continental Margin Settings, Dissertations in Chemical Oceanography Symposium, Honolulu, HI.

Munro, D. R., P. D. Quay, and G. E. Friederich (2010), Gross and Net Production Estimates in the Coastal Ocean from Oxygen Triple Isotopes and the O_2/Ar Ratio, ASLO Ocean Sciences, Portland, OR.

Munro, D. R., P. D. Quay, and G. E. Friederich (2009), Application of Natural Abundance Isotopes of Dissolved Oxygen and the O_2/Ar Ratio to Estimate Gross and Net Production in Eastern Boundary Current Systems, Gordon Research Conference – Chemical Oceanography, Tilton, NH.

Munro, D. R. (2009), Estimates of Primary Production and Carbon Export in the Southern California Bight, University of Washington Chemical Oceanography Seminar, Seattle, WA.

Juranek, L., P. Quay, D. Munro, and C. Peacock (2008), Validation of Satellite Primary Productivity Estimates Using Measurements of the Oxygen Isotope Composition of Dissolved O_2, NASA Conference, Greenbelt, MD.

Munro, D. R., and P. D. Quay (2008), Implications of Oxygen Isotope-Based Gross Primary Production Rates to Carbon Cycling off the Coast of Southern California, ASLO Ocean Sciences, Orlando, FL.

Munro, D. R. (2007), In Situ Measurements of Primary Production in the Coastal Ocean, University of Washington Chemical Oceanography Seminar, Seattle, WA.

Munro, D. R., P. D. Quay, and L. W. Juranek (2006) Comparison of Gross Primary Production from $^{17}\Delta$ of Dissolved O_2 with CalCOFI ^{14}C Primary Production, CalCOFI Conference, Asilomar, CA.

Munro, D. R., R. B. Dunbar, D. A. Mucciarone, K. R. Arrigo, and M. Lizotte (2000), Nutrient Concentrations and Isotopic Composition of Inorganic Carbon and Particulate Organic Material in Sea Ice Brine from the Ross Sea, Antarctica, ASLO Ocean Sciences, San Antonio, TX.

HONORS, AWARDS, AND FELLOWSHIPS

- NASA Space Grant Graduate Fellowship, 2010
- National Defense Science and Engineering Graduate Fellowship (NDSEG), 2006-2009
- Program on Climate Change Graduate Fellowship, University of Washington, 2005-2006
- Excellence in Undergraduate Research Award, Earth Systems Program, Stanford University, 2000
- Antarctic Service Medal, awarded by the National Science Foundation with authorization from U.S. Congress, 2000
- Stanford Scholar Athlete, Golf, 1997

PROFESSIONAL ORGANIZATIONS

- American Geophysical Union
- American Society of Limnology and Oceanography

OCEANOGRAPHIC CRUISES

November 2009 Mid-Atlantic Bight/Gulf of Maine; R/V Delaware II; collected O_2 isotope, O_2/Ar, and DI^{13}C samples

August 2008 CalCOFI – Southern California Bight; R/V New Horizon; collected O_2 isotope, O_2/Ar, and DI^{13}C samples; assisted with standard CalCOFI measurements including chlorophyll, POC, and HPLC samples

February 2008 Dakar, Senegal to Cape Verde Islands; R/V Atalante; collected O_2 isotope, O_2/Ar, and DI^{13}C samples

March 2007 Transit Cruise Seattle-San Diego; R/V Thomas G. Thompson; collected O_2 isotope, O_2/Ar, and DI^{13}C samples

July 2006 CalCOFI – Southern California Bight; R/V New Horizon; collected O_2 isotope, O_2/Ar, and DI^{13}C samples; assisted with standard CalCOFI measurements including chlorophyll, POC, and HPLC samples

April 2006 CalCOFI – Southern California Bight; R/V New Horizon; collected O_2 isotope, O_2/Ar, and DI^{13}C samples; assisted with standard CalCOFI measurements including chlorophyll, POC, and HPLC samples

November 2005 CalCOFI – Southern California Bight; R/V New Horizon; collected O_2 isotope, O_2/Ar, and DI^{13}C samples; assisted with standard CalCOFI measurements including chlorophyll, POC, and HPLC samples

May 2003 Honolulu, HI to Line Islands and back; SSV Robert C. Seamans; assisted undergraduates with research projects; collected gravity core at Palmyra Atoll

November – December 1998 Ross Sea, Antarctica; RV/IB Nathaniel B. Palmer; assisted in the collection of DIC and DI^{13}C samples; conducted an individual research project on the chemical composition of sea ice brines extracted from pack ice